STUDY OF CANOPY VARIABILITY AND IRRIGABLE POTENTIAL OF REHABILITATED AND VIRGIN MINE LANDS BY MEANS OF REMOTE SENSING AND SPATIAL ANALYSIS

By

GIOVANNI NARCISO

SUBMITTED IN PARTIAL FULFILMENT OF THE REQUIREMENTS OF MSC AGRONOMY

DEPARTMENT: Plant Production and Soil Science

In the

FACULTY OF NATURAL AND AGRICULTURAL SCIENCES
UNIVERSITY OF PRETORIA
PRETORIA

Supervisor Prof. J. G. Annandale

Co-Supervisor Dr. N. Z. Jovanovic

INDEX

ABSTRACT 5
1. INTRODUCTION 8
2. REMOTE SENSING TECHNOLOGY AND GEOGRAPHIC INFORMATION SYSTEMS APPLIED TO AGRICULTURE 11
3. METHODOLOGY 16
4. DATA ACQUISITION 19
4.1. Image acquisition 19
4.1.1. The airborne platform 19
4.1.2. The Digital Multi-Spectral Video System (STS-DMSV) 20
4.1.3. Flight planning 24
4.1.4. Remote imaging of the pivots 25
4.2. Data collection 28
4.2.1. Stratification and sampling plan 28
4.2.2. Soil and crop survey 30
4.2.3. Harvester data logging 34
5. PROCESSING OF THE REMOTELY SENSED DATA 35
5.1. Image processing 35
5.1.1. Image pre-processing 36
5.1.2. Radiometric corrections 36
5.1.3. Calibration 38
5.1.4. Geometric correction 39
5.2. Image enhancement 40
5.2.1. Band values 42
5.2.2. Vegetation indices 42
5.2.3. Principal components 46
5.2.4. Classification 47
6. THE SPATIAL DATABASE 48
6.1. Point data interpolation procedure 51
6.1.1. Surface DEM 52
6.1.2. Depth to spoil or impermeable layer maps 53

ACKNOWLEDGEMENTS

I am greatly indebted to my supervisor Prof. J. G. Annandale and co-supervisor Dr. Nebo Jovanovic for their guidance and support.

The other participants of the Project: Dr. Simon Lorentz, the late Prof. Mike Johnston and Prof. Andries Claassens for their collaboration, insight and sharing of raw data.

The technical staff in charge of pre-processing of DMSV data, especially Mr. J.P. Roussow

The THRIP, COM and WRC funding of the project is also appreciated.

ABSTRACT

The Department of Plant Production and Soil Science of the University of Pretoria has undertaken to study the use of mine waste water for the irrigation of crops grown on rehabilitated mine lands and previously un-mined landscapes. The main objective of the research project is to recommend sustainable cropping and irrigation management practices for these conditions.

Within this framework, Mr. Giovanni Narciso and the Institute for Soil, Climate and Water of the Agricultural Research Council (ARC-ISCW) were appointed to carry out a study on the cause/effect relationships of soil spatial variability on crop canopies irrigated with mine water on virgin and rehabilitated landscapes. The study concentrated on two pivots within the boundaries of the Kleinkopjé Colliery and it was conducted making use of remote sensing technology and geographic information systems (GIS).

The two centre pivots, named 'Major' and 'Tweefontein' are both irrigated with gypsiferous mine water. Tweefontein is a rehabilitated opencast mine section, while Major has been undermined but has a 'virgin' soil profile.

For Pivot Tweefontein, the variability in the crop canopy can be broadly attributed to the non-uniform preparation of the soil sub-stratum when the land was reclaimed and the resulting drainage problems that ensued. For the Major pivot, on the other hand, the variability in the development of the crop canopy may be explained by the presence of an impermeable layer of varying depth in certain portions of the field. The capacity to identify and map these occurrences as well as to relate them to the final productive outcome of the cultivated crops was the main scope of this project that was structured in the following phases:

- Acquisition of aerial imagery and other available information.
- Field surveys and measurements.
- Data processing and the creation of a database for static and dynamic

variables. These data gave origin to maps that were integrated in a GIS

- Data analysis and interpretation

Four aerial images were acquired for each of the two pivots, over two growing seasons (1998 and 1999). These images were acquired using the STS-DMSV (SpecTerra Systems-Digital Multi-Spectral Video) sensor carried in flight by a Jabiru micro-light aeroplane. Additional data sets were acquired from other research projects being conducted simultaneously on the same sites.

A soil survey was carried out during the 1999 season, when both pivots were cropped to wheat and the crop was in an early stage of development. When harvest time came, in spring 1999, a harvester specifically equipped with a GPS and a data-logging device recorded the yield and its spatial distribution over the pivot areas. This and all the other information considered relevant to the study went through specific processing in order to be transformed into maps that were analysed in a GIS environment. This operation can also be described as the assembling of a 'spatial database'.

The first task of the analysis was to identify a gauging tool and a spatial measure for performance and variability. Indicators derived from the spectral values[1] of the STS-DMSV sensor's bands provided these measures. Among the many possible indicators the analysis was restricted to the TVI (Transformed Vegetation Index) and the First Principal Component (PC1). Both performance and spatial homogeneity of the cultivated crops is expected to differ between 'virgin' Major and rehabilitated Tweefontein, due to the differing natures of the substratum, and, specifically for Tweefontein, the different depths of spoil material and the differing levels of compaction resulting from the rehabilitation works. On this basis, the analysis addressed the detection of possible differences in crop canopy

[1] **Spectral values**: For any given material, the amount of solar radiation that reflects, absorbs, or transmits varies with wavelength. This property of matter makes it possible to identify different substances or classes and separate them by their spectral signatures (spectral curves).

growth of the two pivots within the same season and over different seasons. Once these differences were detected, the analysis aimed at explaining the possible causes of both the spatial and performance variability between the two pivots. The following analysis procedures were implemented:

- A statistical correlation analysis between indicators derived from remotely sensed images and the various maps derived from data collected on the ground, referring to both permanent (static, e.g. soil properties) and variable (dynamic, e.g. crop growth) features.
- A focal, correlation analysis carried out in an attempt to represent the statistical correspondence between remotely sensed indicators and ground data, in the form of a map.
- An analysis of variability between the two pivots and within the same pivot, across two seasons and different crops. This was done by extracting both statistics from the images and by plotting diagrams of the distribution of the vegetation indices.

The analyses yielded the following results:

- The performance and productive outcome of the crops cultivated on Major and Tweefontein pivots showed distinct differences from one another over the period of the experiment (1998-1999). Furthermore, within each pivot a marked variability was evident.

- These outcomes showed better performance and less variability for winter crops than for summer crops, especially over the rehabilitated pivot, with the possible conclusion that rehabilitated pivots can be irrigated successfully in winter while they can take only supplemental irrigation in summer (otherwise water logging may result and drainage systems may be required for excess rain).

The biggest achievement of this work, however, was the design and implementation of a system for the analysis of spatial variability of cultivated fields. Such a system has the potential of evolving into an innovative crop management tool.

1. INTRODUCTION

The Department of Plant Production and Soil Science of the University of Pretoria has been conducting extensive research on the use of mine water for irrigation of agricultural crops. As part of this research, the Department has also undertaken to study the use of mine water for the irrigation of crops grown on rehabilitated mine surfaces.

A pilot trial to irrigate virgin and rehabilitated land *(Annandale et al., 2000)* was conducted at Kleinkopjé Colliery, Witbank, South Africa. Three centre pivots, identified as Major, Jacuzzi and Tweefontein, within the colliery boundaries, irrigated different tracts of land. Of these, Jacuzzi and Tweefontein were set up on rehabilitated mine dumps whilst Major is on virgin land.

The Kleinkopjé Colliery, belonging to Anglo Coal, is located close to Witbank, in Mpumalanga (26 00' S, 29 21' E, altitude 1570 m), in the summer rainfall region, with an average rainfall of about 690 mm a^{-1}. The soils irrigated by the pivots are predominantly, a medium-textured Ferralsol (FAO, 1998). For Major, an underlying layer of weathered sandstone limits free percolation of water with occasional plinthic formations (generally at 1.1 m depth). Contouring and building of waterways was therefore indispensable, to facilitate drainage of excess surface water.

The effluent generated by this mine has high concentrations of Ca^{2+} and SO_4^{2-} associated with a moderate to high presence of Mg^{2+}. The water used to irrigate at Pivot Major originates in old underground workings and needs to be pumped to the surface and utilised in order to enable mining operations to continue. The water used to irrigate at Pivot Jacuzzi and Tweefontein is predominantly runoff water. The effects of the chemistry of the mine water can be masked or even enhanced by the condition of the soil and of the sub-soil. These specific conditions can range from irregular compaction across the field, resulting in an uneven depth to spoil, up to a marked variability in the characteristics of the soils themselves because of

the irregular mixing of the dumped heaps that are later flattened. Slumping of spoil layers can also take place.

The study concentrated on two of the centre pivots, specifically Major and Tweefontein. Both are irrigated with mine water, but, as stated above, Pivot Major, has been undermined, but has a virgin soil profile, whilst Tweefontein is a rehabilitated open cast section.

The object of this study was to observe, measure, analyse this variability with an emphasis on the tools and instruments that can be used for such a process. It is crucial to the whole methodology of the study that all matters causing spatial variability are taken into consideration and, conscious of this, the Department of Plant Production and Soil Science decided to explore and apply remote sensing and GIS technology to their studies.

In this framework, Mr. Giovanni Narciso, the experiment researcher with the Institute for Soil, Climate and Water of the Agricultural Research Council (ARC-ISCW), was appointed to carry out a study on the determination of the cause/effect relationships of spatial variability on crop canopies irrigated with mine water on virgin and rehabilitated landscapes using remote sensing.

In the course of normal everyday farm management practices, the eye of the farmer and his experience are the most used, and at times, the best available 'instrument' for gauging crop conditions. However, electronic instrumentation and various other technical devices are increasingly enhancing our observation capacity. Nevertheless, the ground level observation of crops, whether 'human' or 'electronic', provides a spatially distorted observation point of the fields and the awareness of any spatial alteration is limited.

A vertical, downward view allows a more effective examination of the spatial variability of a cultivated field and the identification of the correct significance, size and shape of anomalies over the crop canopy. This is the

basic requirement addressed by remote sensing technology, which literally means collecting information from a distance and possibly, vertically, from above.

Just as relevant as the assessment of crop conditions though, is the study of farming systems, which calls for a detailed analysis of the complex interactions between crop, soil and management practices. Remote sensing technology and Geographic Information Systems (GIS) can play a significant role also in these studies *(Goddard et al, 1996).*

The use of remote sensing and GIS addresses the observation and measurement component of the study. The analysis, also conducted utilising GIS technology, focuses on the links between soil variability and crop performance (as well as the different suitability of crops to irrigation with mine water). The aim is ultimately, to explain the reason for the existence of the poorer-performing parts of the two fields. Furthermore, knowing that the comparison is carried out between a 'virgin' and a rehabilitated site, the study also aims at understanding why they differ, and to provide helpful hints to further studies on how rehabilitation works and land preparation over former open cast sites should be carried out.

Finally, the main objective of the research is to contribute to the specific knowledge addressed at recommending sustainable cropping and irrigation management practices in the specific environment of the mines using wastewaters on virgin and rehabilitated sites.

2. REMOTE SENSING TECHNOLOGY AND GEOGRAPHIC INFORMATION SYSTEMS APPLIED TO AGRICULTURE

Remote sensing broadly refers to measuring reflected electromagnetic energy using specific analog or digital sensors. The application of this technology in agriculture makes use of a wide range of instruments mounted on various platforms. These range from hand-held radiometers on the ground, aerial cameras, to optical and radar sensors mounted on satellites orbiting the earth.

The first experiments using hand-held radiometers for the measure of crop canopy electromagnetic reflectance and temperature, were conducted in the early sixties. The variables measured by these instruments were considered possible indicators of stress to be used for irrigation scheduling and this can be considered the beginning of remote sensing being applied to agricultural management. *(Nieuwenhuis et al., 1990)*

A decade later, the first satellite for the study of natural resources was launched with the goal, amongst others, of providing operational remote sensing information on crops to the farming community. Satellite remote sensing technology, just as traditional aerial photography, held great promise for the development of new approaches to farming. Decision-making would no longer be based exclusively on the farmer's experience of the complex interaction of crop, soil and climate or on complicated modelling procedures, but more simply on the encompassing and objective observation of crop performance in the field and on early warning tools *(Morgan, M. et Ess, D.)*.

Soon enough, however, some basic shortcomings became evident. Resolutions in the order of 80, 30 or even 20 m for the first generation satellites proved inadequate for some crops *(Moody A.,* http://www.unc.edu/~aaronm/RSCC/.). Besides this, the uncertain availability of images due to cloud cover, the sometimes excessive time lag

between acquisition and delivery of the imagery and, finally, cost, made satellite remote sensing virtually unavailable for farm management. All the same, agriculture benefited from this new technology for climate monitoring, food security, regional crop statistics, modelling, resource inventories, land cover mapping, etc.

In the nineties further development of instrument technology and the availability of digital airborne video and cameras provided new impetus to the application of remote sensing technology in everyday farming. *(Goddard et al., 1996)*

It is possible today to fly a digital camera or video, record very detailed images of fields, process and make them available to the farm manager within hours of acquisition, and, all this, at an affordable cost. This technology stemming from traditional aerial photography, plugs into all the expertise and applications built on and around satellite remote sensing, bringing with it the advantages of digital technology as far as ease of data handling is concerned.

Additional benefits of airborne digital remote sensing are a much wider flexibility in operations with respect to orbiting sensors. Survey instruments can be operated from airborne platforms with the ability to customise the acquisition process to the specific requirements of the end-user in terms of target selection, timing and resolution. It is, by all means, a transition technology, because the future will see satellite sensors overcome the present limitations in terms of resolution and data availability. There will, most probably be constellations of satellites that will guarantee the constant imaging of any point on the earth at any given time and at a high resolution. This technology however is not yet available, and will not be for some time to come. *(http://www.space.edu/projects/book/chapter27.html).*

Returning to the present, however, the images and data provided by airborne digital sensors can be used for resource evaluation and in the development and operation of a wide range of other applications that will

maintain a technical livelihood in future satellite technology.

These applications, as far as the agricultural sector is concerned, are commonly based on the 'imaging' of the crop or of the soil. The images that are collected can be either black and white, colour or multi-spectral, according to the type of instrument that is used. For black and white or colour images, the retrieval of the information relies on the ability of the expert to interpret shapes and colours.

In the case of multi-spectral and hyper–spectral imaging, information can also be obtained by measuring the intensity and variations that the reflected electromagnetic energy can assume within specific ranges (bands), some of which are outside the normal spectral range to which the human eye is sensitive.

Each band of information contains important and unique data, and the different wavelengths of incident electromagnetic energy are affected differently by the characteristics of the surface. These can be absorbed, reflected or transmitted in different proportions. Knowing the central wavelength positions for each band, these proportions of reflected energy can be measured to identify vegetation types, growth stage and health. Over time, these bands can monitor changes in these conditions. The combination of various reflected wavelengths provides a 'spectral signature' for the specific crop canopy and/or soil surface *(Price J. C., 1994)*.

The agricultural sector will derive great benefits from these new capabilities in operations such as irrigation scheduling, integrated pest control or precision farming techniques. These last applications in particular, imply the identification of within-field soil and vegetation anomalies, and variability in the quest to calibrate and optimise inputs to requirements and maximise cultivation efficiency[2].

---

[2] (***http://www.cnn.com/NATURE/9911/15/remote.sensing.enn***)

However, while instrument technology, driven by the commercial interests of manufacturers, is rapidly progressing, the development of suitably advanced applications is lagging behind. This is largely due to costs, a certain technological delay in the agricultural research sector, and the fact that every-day crop management is still actively carried out according to 'traditional' lines. New technologies have to face some inertia, if not opposition, in proving their effectiveness. There is consequently a wide range of opportunities to analyse the information that images can provide. The detailed resolution and the capacity to discriminate and gauge physiological conditions of crops is extremely important in supporting farm management decisions, thus allowing a significant optimisation of cultivation practices and technical inputs.

Similarly to the empowerment brought about by remote sensing in the capacity of 'looking' at fields and crops, GIS technology has completely changed and enormously increased the capacity to analyse spatial data. GIS is a fast moving, continuously developing field, and the definitions of a few years ago may no longer be appropriate to current technology:

'A Geographic Information System is a group of procedures that provide data input, storage and retrieval, mapping and spatial analysis for both spatial and attributes data, to support the decision making activities of....' (Grimashaw, 1994)

Digital data in a GIS represents the world on a computer in a similar way that conventional maps represent the world on paper. GIS technology offers quick access to data and a lot more spatial information referred to the same location can be stored at the same time.

In the GIS environment, data can be attained in two different formats, namely, raster and vector data. Vector data represent geographic features as point, line or polygon objects that specify locations or boundaries. Raster data represent geographical features by dividing the represented surfaces

into discrete cells called pixels[3], for each of which a 'describing value' is stored. An image is the simplest form of raster data.

In South Africa, airborne digital imaging as well as GIS technology for agriculture has over time, been tested by the Agricultural Research Council (ARC), the Council for Science and Industrial Research (CSIR) and a number of Universities.

At the end of 1996, the ISCW conducted a number of test flights using an Australian instrument, the STS-DMSV (SpecTerra Systems - Digital Multi Spectral Video). The tests were conducted over agricultural, forest and natural vegetation targets, and provided very encouraging results. The instrument was purchased in 1997 and a semi-operational development program was initiated.

The long-term goal of this program is the achievement of a cost effective and efficient service, providing near-to-real time management support information to farmers based on value adding to remotely sensed digital imagery.

[3] **Pixel**, short for picture element; One spot in a rectilinear grid of thousands of such spots that are individually "painted" to form an image produced on the screen by a computer or on paper by a printer. A pixel is the smallest element that display or print hardware and software can manipulate in creating letters, numbers, or graphics.

3. METHODOLOGY

The methodological framework given to the project is traditional, in the sense that it goes through the normal steps of data acquisition, analysis and conclusions. However, some of the data acquisition and manipulation procedures can be considered to be an innovative element in this particular field of research, as they make use of remote sensing and image processing, as well as structuring the data in a shared GIS environment.

Remote sensing and GIS were introduced in the project at a stage when relevant experience and information had already been acquired and there was already enough knowledge of the circumstances to formulate a number of hypotheses for the various anomalies in terms of development of the crops and production levels on the pivots. For example:

- The variability of the crop canopy at Pivot Tweefontein can be attributed to the non-uniform creation of the soil profile when the land was reclaimed after open cast mining and the dump heaps were levelled.

- The location of areas with different levels of soil compaction should be identified by the profile and reflected on the surface by the variability in the crop canopy.

- The variability of the crop canopy for Pivot Major may also be due to the presence of an impermeable plinthic layer, which in this case is not due to anthropogenic activity.

On the basis of all this, the following tasks were performed:

1. Data acquisition: This phase consisted of the following actions
    - Acquisition of aerial imagery which included:
        - The repeated aerial survey of the two pivots using the STS-DMSV sensor (See section 4.1.2).

- The pre-processing, processing and enhancement of the acquired data and the production of images.

- Acquisition of all available information describing the two pivots and collected by other participants to the project. These were:
    - Ground truth measurements for ground cover, top dry matter production and leaf area.
    - Penetrometer readings, by Dr. Simon Lorentz. (Un. of Natal, Faculty of Engineering and Environmental Hydrology)
    - Soil depth acquired through field 'augering' by Prof. Andries Claassens. (University of Pretoria, Dept. of Plant Production and Soil Science)
    - Data logging from the harvester for yield and crop moisture contents.

2. Data processing and management: The data collected by the other participants to the project were supplied in the most diverse formats and therefore had to be processed in order to be brought to a shared geographic reference scheme and to a common format (maps) for the ensuing analysis phases. Databases for static and dynamic data were then created and these databases were integrated in a GIS. Before embarking on the proper data analysis, it was also necessary to derive from the remotely sensed data, indicators of crop performance and variability that could guarantee consistency and repeatability. The preferred indicators were specific enhancements of the images of the fields as well as outputs of the data logger mounted on the harvester.

3. Data analysis: The analysis focused on highlighting possible differences in crop canopy over different seasons and, over the two pivots, within the same season. The effort was aimed at finding ways to graphically demonstrate the variability and, possibly by so doing, explaining the causes of difference and variability between the

'virgin' Major and the rehabilitated Tweefontein. The most important steps of this analysis can be summarized as follows:

- Compare the performance and variability of summer (maize/beans) and winter crops (wheat) within the same pivots.
- Compare the summer and winter crop variability and performance between the two pivots.

The flow chart of the methodology is shown in Fig. 1 and the various elements will be defined and explained in detail in the following chapters.

Fig. 1: Flow chart of the methodological approach

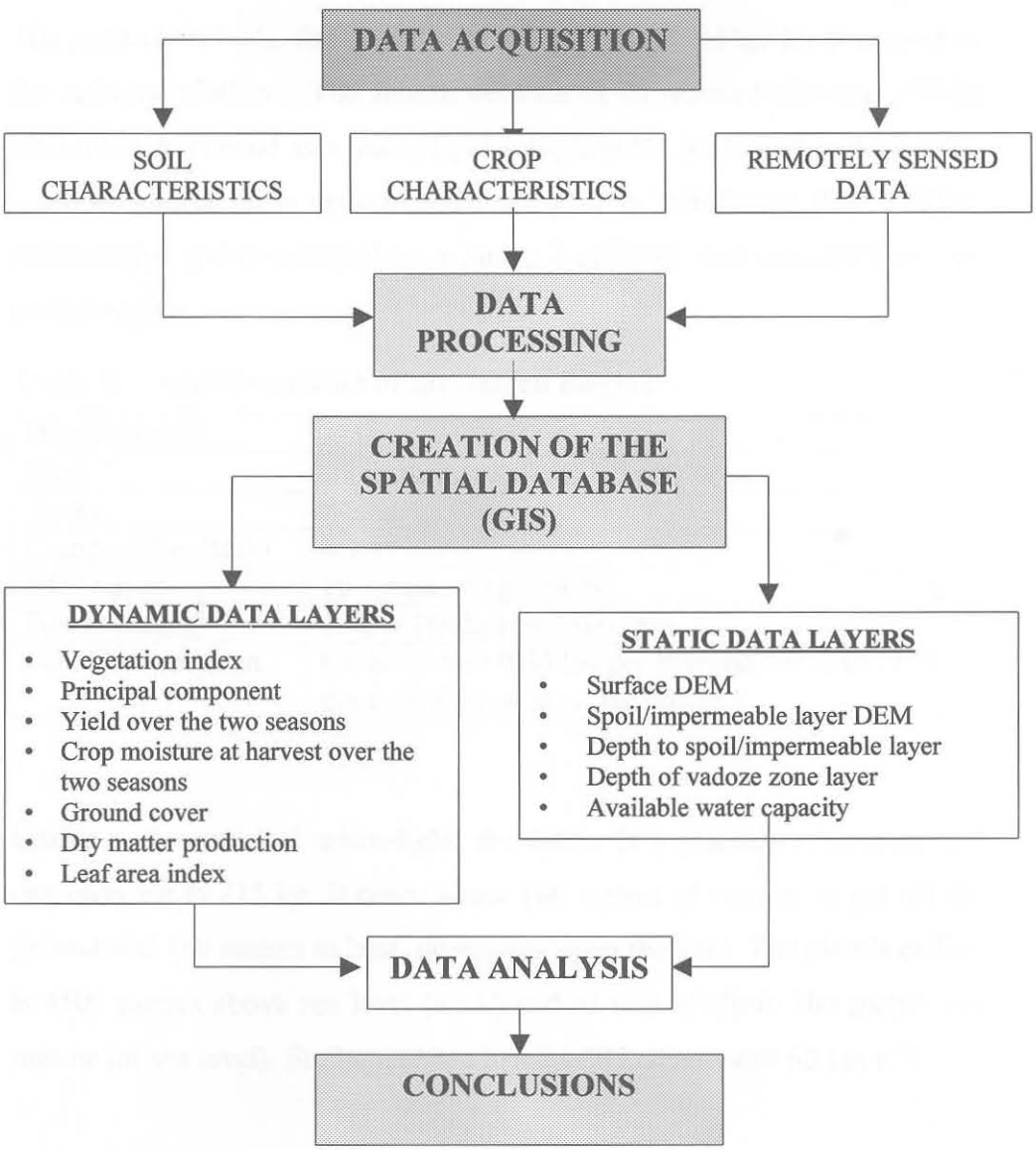

4. DATA ACQUISITION

4.1. Image acquisition

The images of the pivots were acquired by means of airborne remote sensing. The flights were conducted with a Jabiru micro-light aeroplane operating from the Witbank airport. For the imaging itself, the STS-DMSV sensor was utilized. A brief description of the platform and the sensor is provided below.

4.1.1. The airborne platform

The Australian-built, fixed-wing, Jabiru aircraft (See Fig. 2.) was used as the airborne platform. The Jabiru, because of its reduced size and 235 kg total mass, is classed as a micro-light aeroplane but looks and performs like a proper aircraft. It is manufactured using Fibre Reinforced Plastic (FRP) technologies and is powered by a Jabiru 4 cylinder, 4-stroke, 2200 cc, air-cooled engine.

Table 1: Characteristics of the Jabiru Engine

Displacement	2210 cc
Bore	97.5 mm
Stroke	74 mm
Compression Ratio	8.3:1
DC Output	10 Amps - single phase
Power Rating	60 kW (80 hp) @ 3300 rpm
Fuel Consumption	Cruise power 0.46 lbs per horsepower hour (274 grams/kW-hour at cruise power.)

Unlike a conventional micro-light, the Jabiru is a practical commuter and can carry up to 215 kg. It needs about 100 metres of runway to get off the ground and 160 metres to land, depending upon the load. The plane's ceiling is 4500 metres above sea level (a.s.l.) and its rate of climb 300 metres per minute (at sea level). Stall speed is a low 33-38 knots (about 60 km h^{-1}).

Fig. 2: The Jabiru micro-light aircraft

4.1.2. The Digital Multi-Spectral Video System (STS-DMSV)

The SpecTerra Systems, Digital Multi-Spectral Video system (STS-DMSV) is a four CCD[4], compact and lightweight, video imaging system, designed primarily for the acquisition of high-resolution digital multi-spectral[5] imagery of terrain, vegetation, water bodies and coastal environments.

Its spectral resolution enables four selectable bands to be acquired simultaneously in the visible to near-infrared region (0.4 - 1.0 μm). Spatial resolution is in the range of 0.5 to 4.0 metres per pixel, depending upon the height above mean terrain level at which the airplane is flying. For most applications, the recommended pixel size is in the range of 1.5 to 3 metres.

The system uses band-pass filters, typically with bandwidths from 0.1 – 0.8 μm. These may be selected based on individual application specifications.

The STS-DMSV collects GPS[6] information in the image file header. This is navigational GPS information and is not intended for precise registration of imagery. Mostly it is used for instrument triggering data and for approximate locations during image registration.

---

[4] **CCD:** Charged Couple Device, a silicon chip at the heart of every digital camera that takes the place of photographic film.
[5] **Multi-spectral**: The capacity of an optical instrument of subdividing spectral ranges of radiation into bands (intervals of continuous wavelengths), allowing sensors in several bands to form multispectral images.
[6] **GPS**: Ground Positioning system

Fig. 3: The Digital Multi-Spectral Video System

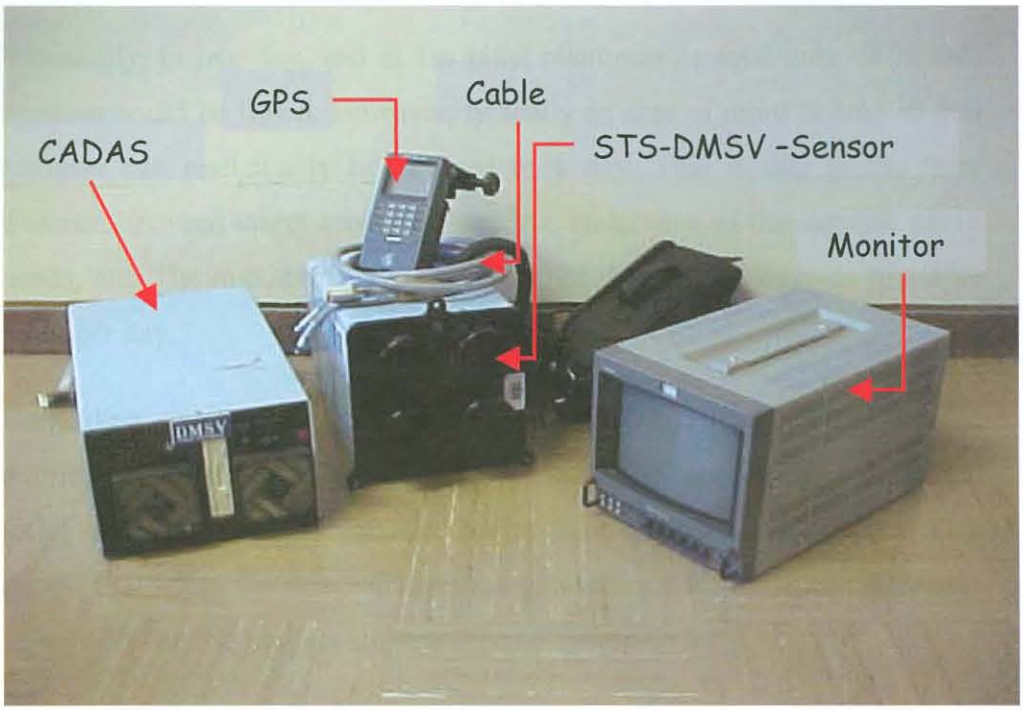

The STS-DMSV has a CCD array of 578 by 740, which represents the size, in pixels, of the image that can be collected.

The basic pre-processing includes standard radiometric and geometric corrections, taking into account systematic distortions due to system effects, such as interlacing[7] and band alignment.

The system can be operated under a wide range of conditions of illumination as the aperture, and therefore the sensitivity of the video cameras, can be adjusted in parallel for the target area. This method of adjustment allows one to retain the inter-band radiometric sensitivity relationships. An operator will adjust the aperture setting for the line or for the whole area by taking a sample frame over the target area and analysing the histograms representing this distribution of the incoming radiation over a 1 to 255 range for the four bands. By changing the aperture and re-

[7] **Interlace:** In video system a picture is "written" on the display device in two halves. Interlace is the process of placing lines of the second half of the picture in-between lines of the first half.

analysing the histograms, he can find the best aperture setting for the target area.

Potentially, in one day, and at 1m pixel resolution, a total area of 20 000 hectares could be flown. However, typically an area of more or less 10 000 hectares can realistically be covered in a day. This is due to the ferry distance between target areas and airports, endurance of the aircraft, client needs, etc. The maximum number of frames that can be taken is just over 1000 per day.

Depending on the topography, the target area is covered by a forward overlap of 60% and a side overlap of 30-35%. The imaging of even limited relief areas will produce smaller pixels than the surrounding ones. This means that when the image frames are geo-referenced, the ones taken over areas with varying heights are stretched to the topography.

The STS-DMSV technical features are listed here:

- Four CCIR[8] format high sensitivity CCD video cameras, recording 578 lines of 740 pixels per line;
- Rigid mounting framework, enabling precise alignment and locking of the positions of the four video cameras;
- Narrow band-pass interference filters that may be interchanged for specific applications;
- Synchronised, digitally controlled irises, enabling reproducible adjustment of settings for varying illumination, atmospheric and albedo conditions, and
- Manually controlled camera integration periods to extend illumination range for imaging.

Filters with bandwidths as narrow as 0.1 μm, within the range 0.4 – 0.8 μm, are available and may be substituted for any or all of the standard set. The narrow band-pass filters are easily interchanged for specific applications;

[8] **CCIR** International Radio Consultative Committee was a global organization responsible for establishing television standards.

however, the four spectral bands typically utilised for vegetation mapping and monitoring are 0.025 µm wide and centred about the principal reflectance spectral features of vegetation:

- Band 1 (blue): pigment absorption band, around 0.45 µm.
- Band 2 (green): relatively higher reflectance band, near 0.55 µm.
- Band 3 (red): chlorophyll absorption band, in the 0.65 – 0. 67 µm waveband interval
- Band 4 (NIR): near-infrared reflectance, 'plateau' band, beyond 0.75 µm.

These band positions relative to the reflectance spectra of a standard green vegetation cover can be seen in the graph below.

Fig. 4: Spectral set up of the STS-DMSV sensor

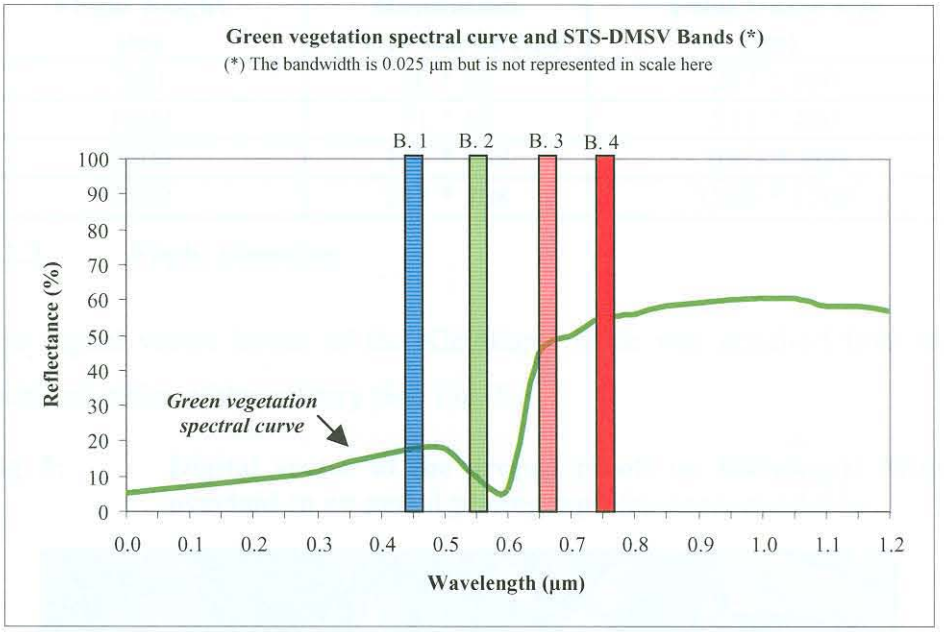

The CADAS (Control And Data Acquisition System) supports the STS-DMSV sensor. This incorporates a ruggedised 486 industrial PC and a single board digital frame grabber that acquires the four spectral channels simultaneously, with 8 bit digital resolution data. Parts of the system are also an on-line hard disk storage device for 300 plus frames of data, a display device and image enhancement and analysis software packages. The digital frame grabber occupies one slot in the frame of the instrument.

A 3-m cable, comprising four coaxial video lines, a coaxial sync line, stepper-motor control line and a 12V power supply from the PC to the sensor head, is supplied with the system. Also provided with the system are:

- Optional reading of navigation and time data from GPS with recording of data in file header records;
- User friendly interactive, menu driven operating software for aircraft and ground based operation.
- Real-time colour display and immediate, post acquisition image processing, enhancement and display capability, enabling review of coverage and data quality control while flying.

Table 2: Spatial resolution and coverage of the STS-DMSV Sensor with 12 mm focal length lens

Flight height (m)	Resolution (Pixel size in cm)	Total frame size (m)
500	36 * 35	257 * 200
1000	71 * 69	533 * 400
2000	142 * 138	1067 * 800
3000	213 * 208	1596 * 1200

4.1.3. Flight planning

The digital vector layout of the Kleinkopjé Mine was acquired from the technical office of the colliery (See Fig. 5.).

Fig. 5: Digital vector of the project pivots on Kleinkopjé Mine, overlaid to an aerial photograph *(no scale available)*

The flight lines and flight height were planned in order to guarantee a 1 m resolution of the raster data, with a 60 % on-line and 30% across-line overlap of the images. Flight direction was planned in order to minimise 'hot spots[9]' (See Fig. 6.).

Fig. 6: Flight plan for the February 1999 aerial survey

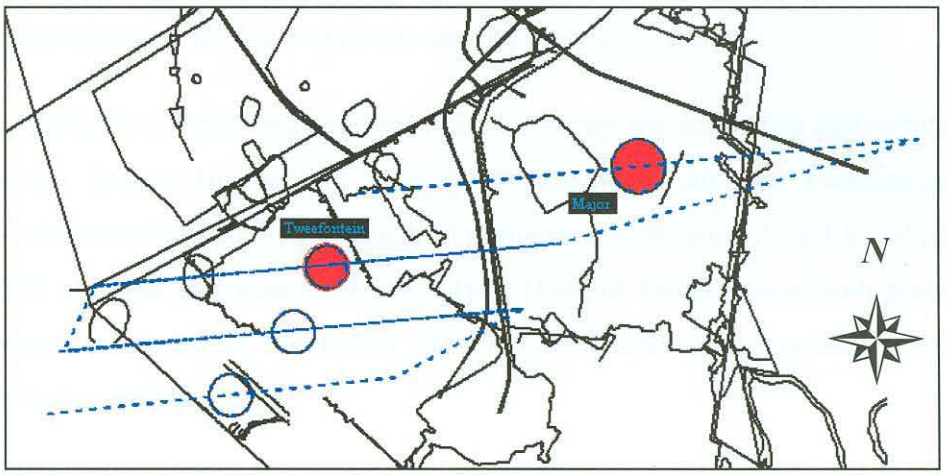

4.1.4. Remote imaging of the pivots

The FLY HIGH Company based in Cato Ridge, Durban, in Kwa-Zulu Natal, operated the JABIRU plane. The platform supplier was contracted by the ARC-ISCW to operate the instrument without the use of an on-board operator. The plane was flown from Cato Ridge to Witbank on the same day of the surveys and ARC-ISCW personnel provided the ground base support.

At Kleinkopjé Mine, pictures of the two pivots were taken over two growing seasons (1998 and 1999). This was motivated by the requirement to monitor the evolution of the crop and map the spatial variability over time for the same crop and for the different fields. The flights were all conducted taking off from the Witbank airport.

During the 1998 season Pivot Major was cultivated with maize while Tweefontein was cropped to dry beans. The first survey was flown on November 11, 1998. This survey provided a full coverage of Pivot

[9] **Hot spots**: In remote sensing, an area where the temperature appears to be much higher than the surroundings, due to the convergence of reflected light on the lenses

Tweefontein but only partial coverage of Major.

A second survey was conducted on February 25, 1999. The more accurate flight planning of this mission was such that the survey was flown at a higher altitude compared to the previous one, allowing the pivots to be included completely in a single frame and providing the acquisition of a full image coverage for the two pivots and the surrounding area.

In 1999, two further surveys were flown during the following agricultural season. During this second season both the Major and the Tweefontein pivots were cultivated with wheat. Planting took place from July 1 to July 2, 1999 at Major and from July 3 to July 5, 1999, at Tweefontein. Both pivots were harvested after November 11, 1999, with harvesting continuing into early December.

In order to catch the crop in two different phases of development, a first flight was carried out on September 14, 1999, during the vegetative stage and the second one on October 7, 1999, at flowering.

The images of the pivots acquired in the course of the four flights are shown in Figures 7 to 10.

Fig. 7: Images acquired for the Major (left) and Tweefontein (right) pivots in December 1998

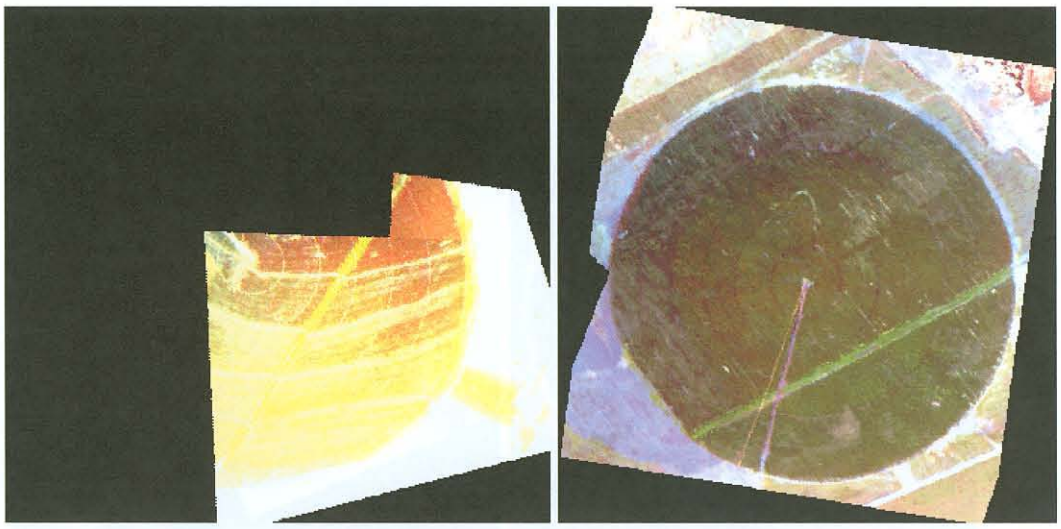

Fig. 8: **Images acquired for the Major (left) and Tweefontein (right) pivots in April 1999**

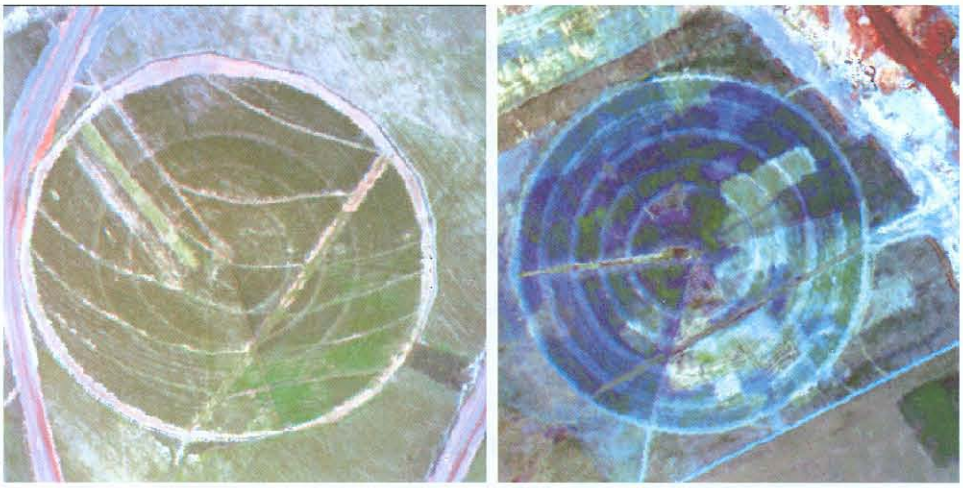

Fig. 9: **Images acquired for the Major (left) and Tweefontein (right) pivots in August 1999**

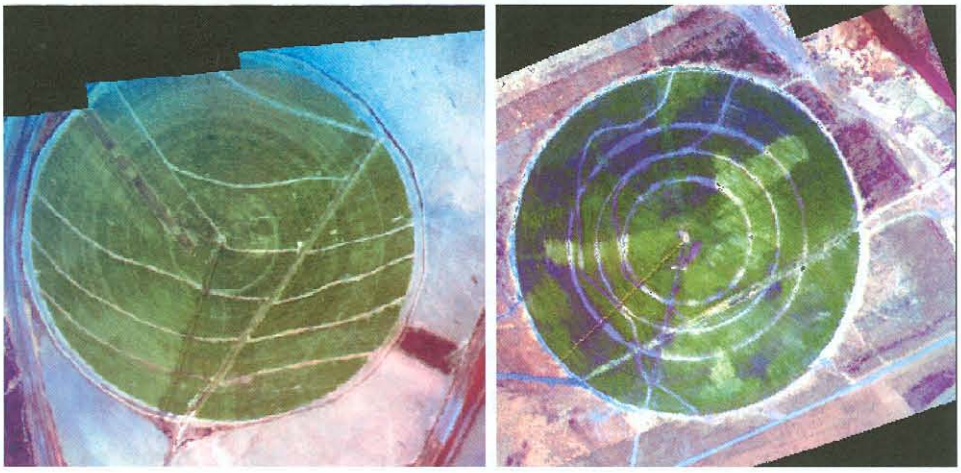

Fig. 10: **Images acquired for the Major (left) and Tweefontein (right) pivots in October 1999**

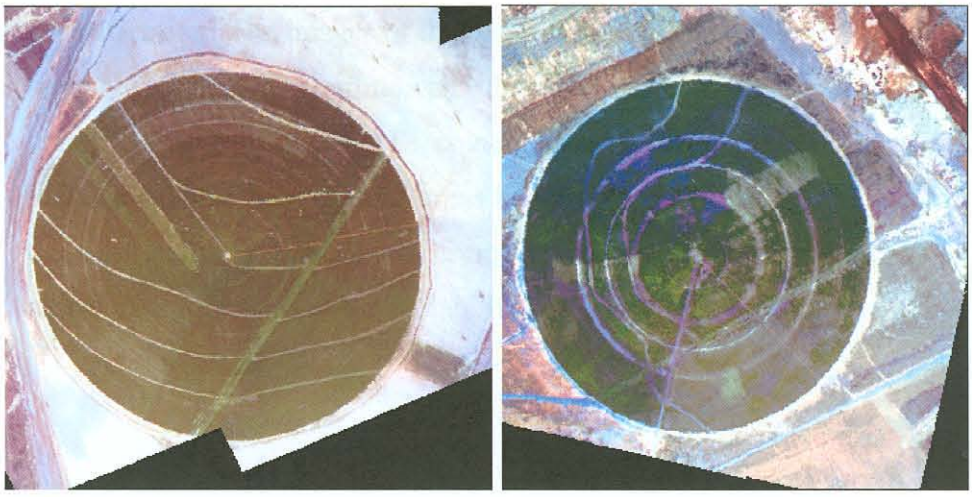

4.2. Data collection

4.2.1. Stratification[10] and sampling plan

A ground truth collection campaign was conducted so as to coincide with the third survey flight in September 1999. The survey had the multiple scope of providing ground truth data for the classification of the acquired images and collect data on the crop condition at the time of flight.

Soil samples were also gathered for analysis of their physical characteristics, as these could have an impact on the spectral features of the bare soil as well as on those of the vegetations itself. Since no previous knowledge was available of the meaning of the spectral features of the images it was decided to proceed with a preliminary unsupervised classification of the images as to identify a number of "classes", spectrally homogeneous within themselves and, at the same time, different from each other. These classes constituted strata for the sampling plan.

This stratification was adopted in order to save on the number of survey points that would have been generated in a traditional grid sampling procedure, while maintaining comparable descriptive accuracy. *(Arabia, G., 1993)* The survey procedure was then structured according to the following plan of action:

a) **Stratification**: The images of the two pivots, collected in February 1999 were classified to outline all those areas that showed marked commonalties in terms of 'colour' and 'texture' (Fig. 11). The identification of homogenous areas based on the external appearance of the canopy implies that the performance and appearance of the crop is an external reflection of the variability of the underlying soil.

[10] **Stratification**: A sampling method in which the population is separated into groups (strata) usually based on some internal similarities, then selecting a random sample within each stratum.

Fig. 11: Stratification of the Major (left) and Tweefontein (right) pivots, where each colour represents a different stratum.

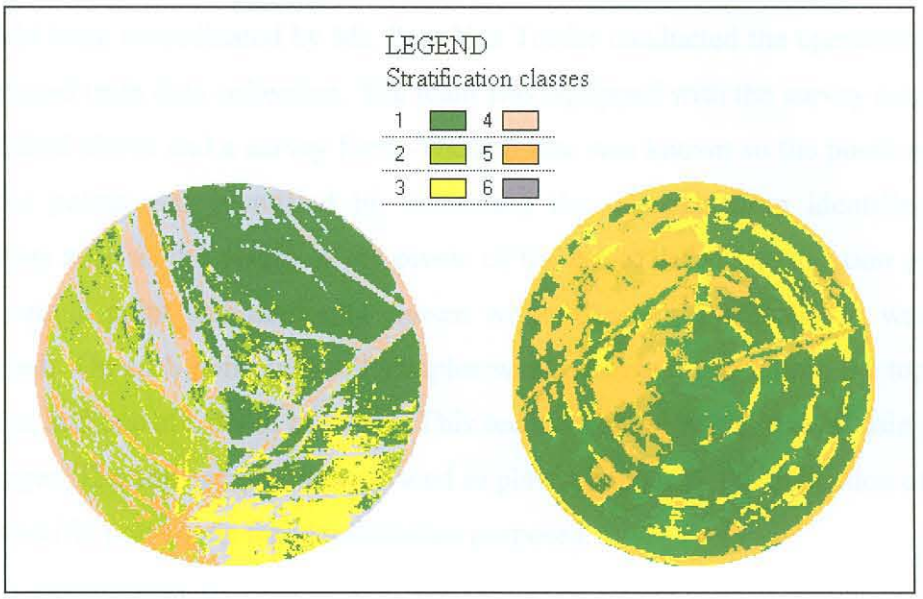

b) **Sample plan:** In order to facilitate the allocation of the sample points, a grid with cells of 20*20 m was drawn over the stratified images, each node of the grid being a candidate sample point. Within each homogeneous area, a set of random points was selected and a survey map was prepared showing the location of the sample points. The grid and the stratification were overlaid to the image of each pivot in order to facilitate the identification of each point that was characterised by an identification number (Fig. 12)

Fig. 12: Sampling plan

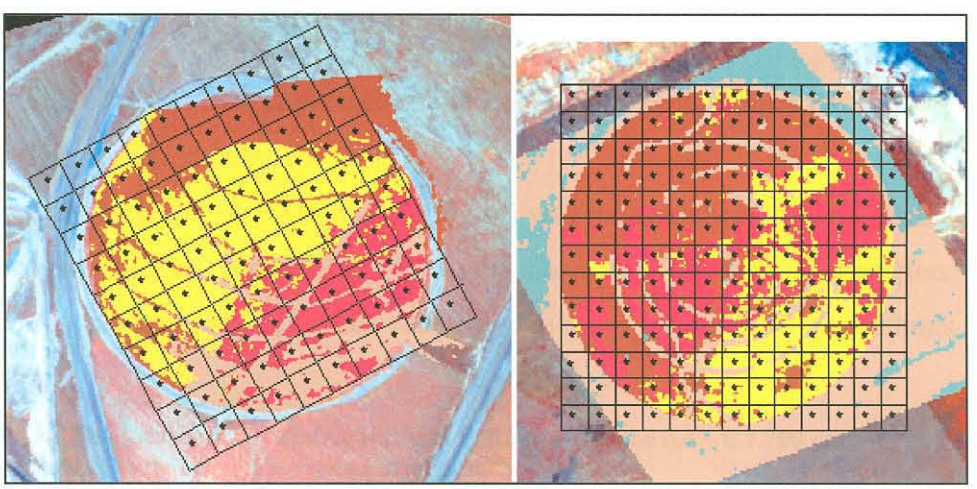

4.2.2. Soil and crop survey

A field team co-ordinated by Mr. Peet Van Torder conducted the operations of ground truth data collection. The team was equipped with the survey map described above and a survey form. The cell size was known so the position of the points was identified by measuring the distance from identified markers such as the centre of the pivots of the target cells. The location of the sample point was randomly chosen within the target cell once it was reached. On each point two soil samples were collected; one within the top 10 cm, and one at a depth of 30 cm. This second sample was extracted using an auger. The soil samples were placed in plastic bags with the indication of the specific point code for identification purposes.

The samples were analysed at the soil physics laboratory of the Department of Plant Production and Soil Sciences, at the University of Pretoria under the supervision of Prof. A. Claassens. The parameters that were measured were the gravimetric water retention capacity at wilting point (–1500 J kg^{-1}) and at field capacity (–10 J kg^{-1}). These values together with the known bulk densities (1.60 and 1.90 Mg m^{-3}) of the soils at Major and at Tweefontein and the reference depths of those spoils allowed the derivation of the available water capacity (AWC) for two soil layers on each pivot. (See Section 6.1.5). These two soil layers were conventionally set, one from 0 to 20 cm and the other from 21 cm to spoil. The following canopy measurements were taken:

- The Ground cover expressed as the fractional interception of PAR[11];
- The Leaf area index (or LAI)[12],

The canopy cover of PAR (0.4 – 0.7 μm) was measured on the grid with a Decagon sufleck ceptometer (Decagon Devices, Pullman, Washington, U.S.A.), making one reference reading above the canopy and 10 readings

[11] **PAR: Photosinthetically Active Radiation**: Radiation in the 0.4 – 0.7 700 μm waveband. The radiation is measured in μmol m^{-2} s^{-1}.
[12] **LAI**: A type of information worked out by calculating the volume of the surface of leaves in relation to the volume of ground that is directly below the plant. The index is measured in m^2 leaves m^{-2} soil

beneath the canopy. The LAI was calculated after measuring leaf area with a LI 3100 belt driven meter (LiCor, Lincoln, Nebraska, U.S.A.) by sampling plans covering 1 m^2 of ground surface.

In the course of this survey, a sample of plant material was also harvested from 1 m^2 of ground surface at each sample site. Fresh mass was measured directly after sampling. Once delivered to the laboratory, plant organs were dried in an oven at 60 °C for 4 to 5 days and weighed again. The above ground dry matter production is expressed in g * 0.25 m^{-2}.

The data were recorded on a survey form and then captured to a spreadsheet. The results of the survey are given in Tables 3 and 4.

The soil and crop data acquired during the ground survey were transformed into maps and subsequently introduced as information layers into a GIS.

Table 3: Soil and canopy measurements for the Major Pivot for wheat in September 1999

Sample	X (Lon)	Y (Lat)	Above ground dry matter production g * m^{-2}	Fractional intercept of PAR	LAI m^2*m^{-2}	AWC 0-20 cm mm	AWC 21 to spoil cm mm	AWC TOT mm
5	24049	-2874515.	108	0.84	1.10			
6	24133	-2874541	158	0.87	1.50			
9	24079	-2874570	83	0.75	0.77	8	65	73
10	23940	-2874574	135	0.91	1.49	11	88	99
11	24164	-2874597	104	0.68	0.79	8	26	34
15	24110	-2874626	137	0.87	1.16	1	51	53
17	23830	-2874632	150	0.92	1.66	12	39	51
20	23914	-2874657	98	0.85	1.04	11	21	32
23	24141	-2874682	88	0.69	1.00	11	51	63
24	24000	-2874684	89	0.61	0.93	10	38	48
27	24224	-2874706	102	0.83	1.36	11	33	44
30	23806	-2874715	96	0.88	1.07	11	23	34
35	23890	-2874742	95	0.86	0.94	11	44	55
37	24253	-2874759	129	0.72	1.11	11	46	57
38	24114	-2874764	193	0.92	2.39	13	47	60
39	23976	-2874769	135	0.79	1.58	19	24	43
48	24143	-2874817	128	0.81	1.24	10	60	71
52	24229	-2874843	140	0.62	1.44	10	27	37
56	23813	-2874856	119	0.90	1.30	10	24	33
59	24034	-2874875	121	0.83	1.43	13	25	38
64	24119	-2874901	97	0.55	0.81	13	39	51
70	23926	-2874932	161	0.86	1.41	12	78	89
73	24292	-2874955	140	0.62	1.19	10	42	52
75	24010	-2874959	95	0.86	0.97	13	74	87
79	24095	-2874987	83	0.58	0.65	9	79	88
83	24181	-2875014	109	0.59	1.45	13	102	116
84	23901	-2875016	80	0.64	0.58	11	42	53
87	24126	-2875043	72	0.46	0.62	11	115	126
91	23933	-2875073	102	0.65	0.74	11	34	45
92	24072	-2875072	81	0.44	0.66	11	81	93

Table 4: Soil and canopy measurements for Tweefontein Pivot for wheat in September 1999

Sample	X	Y	Above ground dry matter Production	Fractional intercept of PAR	LAI	AWC		
						0-20 cm	21 to spoil cm	TOT
	(Lon)	(Lat)	g * m^{-2}		m^2*m^{-2}	mm	mm	mm
10	19840	-2876609	118.7	0.61	0.68	16	28	44
15	20040	-2876569	105.9	0.11	0.64	14	32	46
16	19921	-2876609	113.2	0.39	0.73	15	43	58
20	19759	-2876690	92.1	0.64	0.61	12	25	37
21	19880	-2876649	63.6	0.38	0.46	12	27	39
28	19840	-2876690	106.3	0.69	0.68	19	34	53
32	20080	-2876609	101.1	0.80	0.67	14	51	64
34	20001	-2876649	100.8	0.42	0.77	10	49	59
37	19799	-2876730	71.9	0.34	0.52	13	42	55
38	19921	-2876690	122.8	0.63	0.99	16	15	32
57	19759	-2876810	78.4	0.04	0.52	14	50	64
61	20120	-2876690	101.9	0.57	0.52	12	30	42
65	20040	-2876730	193.1	0.58	0.94	9	43	52
67	19840	-2876810	148	0.78	1,28	13	58	71
68	19961	-2876770	81.8	0.52	0.54	7	14	21
84	20199	-2876730	384.6	0.94	2.29	16	34	50
87	20120	-2876770	183.3	0.77	1.00	16	39	54
88	19799	-2876890	113.4	0.43	0.51	13	39	52
90	19921	-2876850	150.1	0.91	1.36	12	55	67
99	20001	-2876850	129.9	0.68	0.77	21	43	64
100	20120	-2876810	105.2	0.73	0.78	11	37	49
103	19921	-2876890	95.8	0.97	1.37	14	34	48
109	20080	-2876850	57.8	0.63	0.44	15	24	40
110	20199	-2876810	175.1	0.57	1.40	15	51	65
114	19799	-2876970	119.6	0.77	1.04	13	25	38
131	20159	-2876890	107.3	0.39	0.73	13	31	44
135	20080	-2876930	68.4	0.24	0.40	6	36	41
138	20001	-2876970	92.9	0.56	0.74	14	27	40
150	20001	-2877009	94.3	0.37	0.66	14	40	54
151	20120	-2876970	99.1	0.34	0.75	12	51	64
157	20080	-2877009	76.6	0.37	0.43	14	41	55

4.2.3. Harvester data logging

The wheat crop over the two pivots was harvested in spring 1999 and the operation was conducted with a harvester specifically equipped for yield mapping. The equipment consisted of a GPS, a number of sensors to measure grain flow, the moisture content of the seed, the speed of the harvester and several other parameters.

The sensors[13] were situated downstream from the cutting head, and were placed in such a way to measure the grain flow in volume and with a sub-meter resolution.

Determining the sub-metre position was achieved using a Trimble real-time differential GPS receiver that associated each measurement with latitude, longitude and elevation. However, the elevation was only accurate to sub 1.5 metres. The distance covered by the harvester between each measurement was on average 2.6 m and the data is relative to the full width of the harvester table (17.5 m).

The data logger produced two files of 3.960 kB for Major and 2.499 kB for Tweefontein. These files stored the following information: longitude, latitude, grain flow (in kg per logging interval), time, logging interval (either 1, 2 or 3 seconds), distance (m), swath (m), yield (t ha^{-1}), moisture (%), marker data, pass, monitor serial number, field number and name, data type, grain type, GPS status, elevation (m a.s.l.).

The data collected using these sensors allowed the creation of maps showing the value of yield at specific points in the field. It was also possible to create an image of the moisture content of the grain harvested, as well as the variations in elevation across the fields. For Major some 39540 points were measured, whilst for Tweefontein the data logger recorded some 24390 points. (See Chapter 6.1.8).

[13] Model and make of such sensors are not available

5. PROCESSING OF THE REMOTELY SENSED DATA

All the data that were acquired by means of remote sensing such as the STS-DMSV images had to undergo specific and dedicated processing in order to be transformed into information layers and analysed within a Geographic Information and Database System

5.1. Image processing

The STS-DMSV is obviously best operated in cloudless conditions, and, in order to minimise illumination problems and maximise the spectral quality of the data, the best acquisition time ranges from two hours before to two hours after local noon and with an aircraft drift of less than seven degrees from the flight path *(Pinter et Al. 1987).* A number of parameters are taken into consideration to simulate the relative position of the plane with respect to the sun at any given time and account for the particular effects of sun angle on the image frames, especially the so-called 'Hot Spots'. These parameters are: day of year, solar declination angle, time, local standard time, local apparent time, zenith angle, azimuth angle, day length, and sunrise and sunset hours. *(Pinter et Al. 1987)*

However accurate the navigation and optimal the acquisition conditions, the images collected by the STS-DMSV sensor are affected by a number of disturbances and require pre-processing, radiometric correction and calibration. To do this, the images are imported in an 'image processing' software program ERDAS Imagine. This is done interactively for each frame. Usually all frames are imported, but only those falling within the limits of the target area are processed. Within the program, the images are geometrically corrected for projection distortions and georeferenced.

When the whole processing sequence has been accomplished, the resulting images can then be delivered as individual frames or can be mosaiced together to form a seamless overall 'picture' of the surveyed area. These processing phases are discussed in more detail in the following paragraphs.

5.1.1. Image pre-processing

The STS-DMSV system is based on a set of four separate digital video cameras and, accordingly, the data recorded are a combination of four separate video channels each representing a spectral band. These are: band 1, centred on the 0.45 μm wavelength recorded over a range 0.025 μm wide, band 2 centred around 0.55 μm, band 3 on 0.65 μm and finally band 4 (the near-infrared) at 0.75 μm.

In order to reassemble a homogeneous multi-spectral image, these bands require interlacing and alignment as well as the correction of flight influences such as linearity (alignment of the pixels) and pixel movement (pincushion effect[14]) caused by the shape of the lenses. Correction procedures for electronic noise sources, camera view angle and other environmental effects, are also needed in the pre-processing phase. A batch file that corrects each line that was flown drives the pre-processing operation and a specific program for the 'Cosine Lens Distortion' was implemented specifically for the STS-DMSV operations at the ARC-ISCW.

5.1.2. Radiometric corrections

The position of the camera and that of the platform, in terms of height above ground, geographical co-ordinates and direction of flight, influences the STS-DMSV data. This, combined with the sun angle, the time of acquisition, the illumination conditions and the topography of the ground being targeted, have significant effects on the image quality *(Pinter et Al. 1987).* A very immediate demonstration of these effects is the fact that most images have a colour difference in the overlapping area due to the different 'look-angle' at the same area. Radiometric corrections address all the anomalies and the distortions caused by these conditions.

The video of the STS-DMSV has an aperture setting that is adjusted at the beginning of every flight according to the level of illumination available

[14] **Pincushion effect:** Lens aberration (distortion) causing parallel, straight lines at the edge of the image to curve inwards.

from sunlight and the brightness required for the characteristics of a specific target. The adjustment modifies the amount of light that hits the CCD array to make the picture.

If illumination conditions change in the course of the flight (common occurrence) and whenever images of the same target, but from a different acquisition date, need to be compared, the brightness conditions of the images themselves need to be equalised. This is necessary as the differing illumination may mask actual differences of the conditions and status of the target. Several solutions to this problem are possible but the so-called process of 'histogram matching' is the most direct, *(Pinter et Al. 1987).* This procedure is based on the fact that images can be represented as a distribution of pixels over a range of 256 colours, forming a histogram.

'Histogram matching,' means balancing the range of colour levels across the images that have to be compared, to a common variation range. However, in altering the histograms of images, some of the spectral resolution may be lost, and in addition, there can be 'flooding' or, the opposite, 'under-exposure' of the images.

Flooding occurs when there is a distortion towards values in the highest range (255), implying that there could be higher values but these cannot be represented. The phenomenon of 'under exposure' results in the presence of many pixels with values near to or at 0 on the histogram and can take place in parts of the same frame or across the whole series of frame belonging to the same flight. Also this implies a loss of information.

These problems become more complex in the case where frames have actual peaks on the histograms caused by objects that either absorb (peaks near to 0), or reflect a lot of radiation (peaks near to 255).

All these occurrences demand that the histogram matching process be conducted in a recursive manner to achieve the best possible compromise

between 'readability' and 'comparability' of the image frames.

Other radiometric disturbances may occur due to topography of the surface, causing the so-called 'hot spots' on the images, which are areas (usually of round shape) of intense brightness caused by the convergence of reflected light on the lenses. These can become significant if the direction of flight is not planned according to the sun angle, trying to keep, as far as possible, a high angle of incidence between the source of the illumination (the sun), the target and the lenses. These problems are common to all airborne imaging sensors that operate in daytime. However, for digital systems, which produce images with greater contrast than analog systems, these problems are more severe.

Specific formulas and procedures are available to address these problems (*Sabins, Jr., 1978)*. These formulas were transferred into code for the removal of the effects of sun angle and hot spots from the frames. The technical staff in charge of pre-processing carried out this programming work. The whole pre-processing program is structured as a batch procedure that is routinely applied for each and every image acquisition of the STS-DMSV.

5.1.3. Calibration

The images of the STS-DMSV are, as the name suggests, digital. They are composed of a grid of cells (pixels), each of which is characterized by a numeric value. The number characterizing the single pixel, however, is just an indirect indication of the amount of reflected radiation hitting the cell of the CCD array. In order to convert these numbers into radiance[15] values, the image needs to be calibrated. A dedicated calibration would have required the setting up of a ground-truthing procedure based on the use of targets of known reflectance[16]. The nature and requirements of the present project did

[15] **Radiance:** A measure of the amount of radiant energy emitted or received per unit area of a surface over a specified time.
[16] **Reflectance:** Ratio of the radiant energy reflected by a body to the energy incident on it. Spectral reflectance is the reflectance measured within a specific wavelength interval

not necessitate for such activity and so, this transformation was conducted according to pre-defined conversion tables provided by the sensor manufacturer.

5.1.4. Geometric correction

Having completed the pre-processing phase, the radiometric processing and the calibration procedures, the STS-DMSV images are imported to an image processing software package (ERDAS-Imagine©, in the case of this project). Usually all the frames are imported, but only those falling within the boundaries of the target area, as defined by a vector block, are processed.

The single frames are georeferenced to a topographic base. This base is provided by the digital ortho-photo of the target area or by a topographic digital map of adequate scale. The ortho-photos of the target area were acquired from the Kleinkopjé Mine offices; they were scanned and imported into the image processing software together with the raw STS-DMSV images.

The process consists of comparing common features on each image to a set of ortho-photos. Up to 12 ground-control-points on each image are placed on common features in each of the photos. Each ground control point is programmed with a map value that corresponds to the real position on the ground.

The relative size of the STS-DMSV frames compared to the ortho-photos is very small and to place the first frame on the ortho-photo can take up to four hours. Thereafter it takes between 6 and 25 minutes to geographically reference a single frame. (*Sabins, Jr., 1978)*

Georeferencing is completed by the process of mosaicing and map composition, this consists of assembling the single frames to create the full seamless picture of the target area.

5.2. Image enhancement

Image enhancement is the process of making an image more interpretable for a particular application. Enhancement can make important features of digital images and aerial photographs, more comprehensible to the human eye. Enhancement techniques are often used for extracting useful information from images. This information can be contained either within the individual bands or in a combination of bands.

There are many enhancement techniques available. They can range from a simple contrast stretch, where the original values are stretched to fit the range of the display device, to a principal component analysis, where the number of bands is either reduced and new bands are created to account for most of the variance in the data (*Sabins, F. Jr., 1978)*. A combined use of all four bands is usually performed through a 'classification' process. Image processing allows further analyses through the identification and enhancement of geometric features such as specific shapes or patterns, which may identify anomalies in plant health, irrigation or other characteristics (*Sabins, F. Jr., 1978)*.

Images can only be viewed on a computer screen or on a print, using the three primary colours (red, blue and green) and for this reason, two visual reference images are usually produced:

- True Colour - A combination of band 3 (0.65 μm) as red, band 2 (0.55 μm) as green and band 1 (0.45 μm) as blue. These images appear as natural colour.
- False Colour Infrared - A combination of band 4 (0.75 μm) as red, band 3 (0.65 μm) as green and band 2 (0.55 μm) as blue. As vegetation appears very bright in the 'NIR' range (0.75 μm), these images highlight healthy vegetation in the image.

Other enhancements can be achieved by combining data sets of the same area acquired on different dates (but at similar solar angles). Each image can be precisely registered at the time of mosaicing and apply simple image

(pixel for pixel) subtractions to gain difference images that show areas of change and, over time, show vegetation trends and cycles.

For the requirements of this study, a number of 'True' and 'False Colour' compositions were produced. See Fig. 13 and 14.

Fig. 13: False colour composite of Major (left) and Tweefontein (right) Pivots, February 1999.

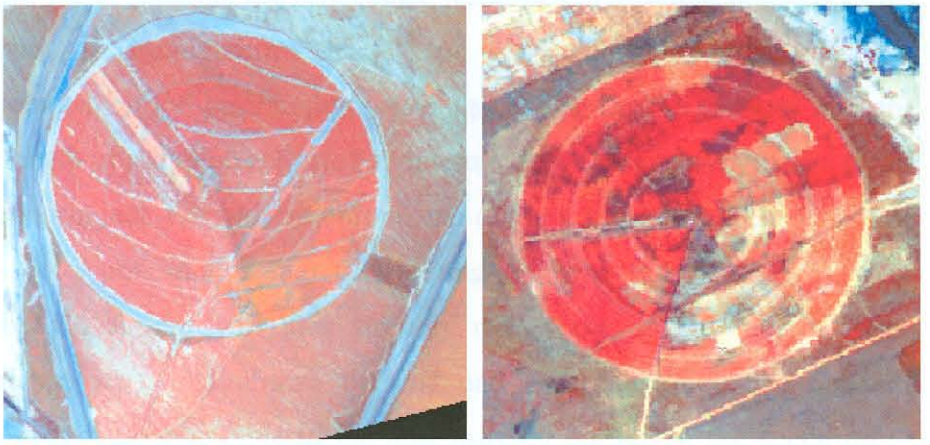

Fig. 14: False colour composite of Major (left) and Tweefontein (right) Pivots, September 1999.

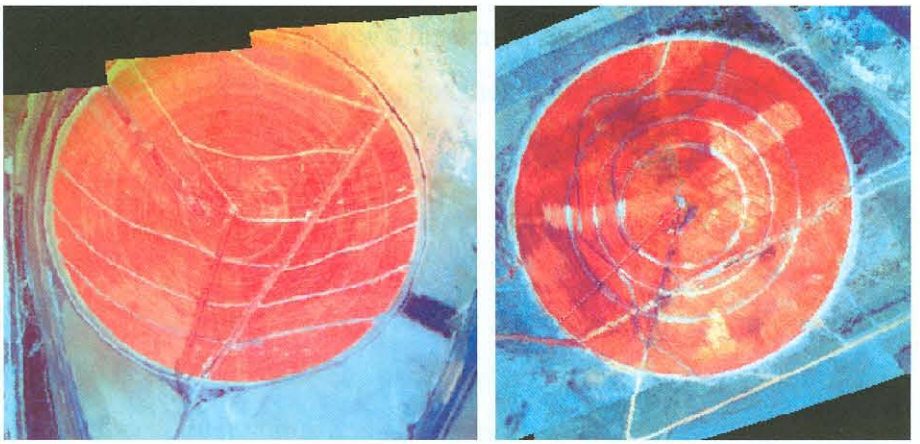

5.2.1. Band values

The selection of the band frequency centres for the STS-DMSV cameras was guided by the general rule provided by the reflectance curve of green vegetation. The scope of this set-up is to use each band as an independent gauging tool in a determined fraction of the electromagnetic spectrum.

From the diagram, in Fig. 4, one can easily see that, for a common feature, the four bands measure the reflectance responses in different portions of the spectrum. In simple terms, each band carries in itself a specific and autonomous bit of information. As a general rule, the amount and the wavelength of radiation reflected is determined by the physical nature of the reflecting object. For vegetation one can observe a dip in the curve around 0.4 – 0.45 μm, this is due to a strong electromagnetic absorbance by chlorophyll. A leaf will thus strongly reflect the 'green radiation' (the colour we see), and absorb the red and blue radiation. The opposite phenomenon is observable in the near-infrared portion of the spectrum (> 0.7 μm), where most radiation is reflected (> 50%) and the rest absorbed as a direct function of the moisture contained in the biomass, *(Guyot, 1990).* Temperature levels in the leaves are measured by much higher frequencies, in the order of 10-12 μm, however these measurements can also be referred to moisture contents *(Guyot, 1990).*

5.2.2. Vegetation indices

The STS-DMSV bands can be variably combined to produce specific vegetation indices that can be used to highlight subtle variations in vegetated surfaces, their status and abundance. A wide array of indices have been tested and studied, ever since Multi-Spectral imaging has been applied to vegetation studies and the most widely used combine the visible red and near-infrared bands, *(Jackson and Heute, 1991).*

The principle behind such vegetation indices is that the levels of visible red and near-infrared radiation reflected by a vegetation canopy, is related to

photosynthetic activity. Photosynthesis is itself a function of chlorophyll contents and moisture availability in the canopy, the greener and wetter the canopy, the healthier and more abundant the vegetation.

As stated in the previous chapter, chlorophyll absorbs red radiation (while reflecting green), so the lower the level of red reflectance the higher the overall chlorophyll contents. At the same time, water reflects the most part of the near-infrared radiation, thus indicating moisture contents in the canopy. So the combination of low reflectance in the visible red and high in the near infrared is indicative of high chlorophyll contents and high moisture contents, consequently emphasizing high photosynthetic activity and thus healthy vegetation. On the same basis, vegetation indices can be related to biomass and to LAI.

Indices can vary significantly in terms of complexity and sophistication. The selection of the most appropriate index, however, is strongly dependent on the type of vegetation cover, its density and also the scope of the analysis. In the present study, the TVI (Transformed Vegetation Index) *(Deering et al. 1975)* was used:

$$TVI = \sqrt{\left(\frac{B4 - B3}{B4 + B3}\right) + 0.5}$$

Where:

B4: Radiance of Band 4 (NIR, 0.75 µm)

B3: Radiance of Band 3 (Visible red, 0.65 µm)

The TVI is derived from the commonly used NDVI (Normalised Differences Vegetation Index) *(Rouse et al. 1974)*:

$$NDVI = \left(\frac{B4 - B3}{B4 + B3}\right)$$

The NDVI has the ability to minimize topographic effects while producing

a linear measurement scale. This measurement scale ranges from –1 to 1 with 0 representing the approximate value of no vegetation; thus negative values represent non-vegetated surfaces. The TVI modifies the NDVI by adding an empirical constant of 0.5 and taking the square root of the results. The constant 0.5 is introduced in order to avoid operating with negative NDVI values. The square root is intended to correct NDVI values that approximate a Poisson distribution[17] and introduce a normal distribution. The TVI vegetation index was applied to the Multi-Spectral images of the Major and Tweefontein pivots collected in the course of the third and fourth flights. These enhancements are shown in Fig. 15 for the February 1999 and September 1999 flights. The index enhancement was applied to the round surface of the pivots only. For image editing purposes, these enhancements were subsequently re-applied over a common background chosen from the February 1999 flight. This is true for all the images shown in the rest of this document.

Fig. 15: Vegetation Index maps of Major (left) and Tweefontein (right) pivots, during the second (top) (February 1999) and third flight (bottom) (September 1999).

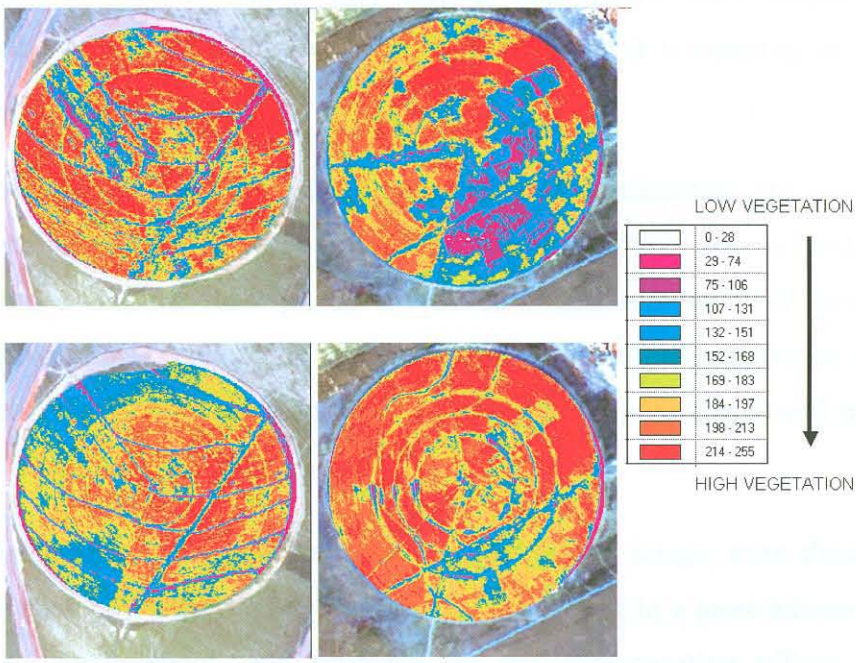

[17] The **Poisson Distribution** is a probability distribution that represents the number of random events occurring over a fixed period of time

The TVI ranges between 0 and 1, and when these values need to be represented in graphical form, the colour resolution permitted by 8 bit computers ranges between 0 and 255. A grey scale could well represent this range, but 255 levels of thematic detail would be difficult to grasp by the human eye and even more difficult to interpret.

Conventionally the '0-255' range is grouped in equal intervals, the number of which is at the discretion of the analyst or is a function of the variability of the index on the image itself. The range can also be divided as a function of the standard deviation from average or even with a specific clustering.

In the figure above (Fig. 15) the range has been divided in 10 equal intervals and the colours assigned to each interval ranges from magenta to red. Magenta represents the lowest levels of the index and consequently the lowest levels of vegetation activity. On the opposite side of the range, red represents the highest levels of vegetation activity.

The change in the condition of the vegetation cover can be clearly seen in these pictures where we are looking at two different stages of the phenological cycle of wheat. The crop is still in the early stages of development in the first image (August 1999) while it is ripening in the September scene.

Some obvious differences in the homogeneity of development are visible over both pivots. For Major, a general decline in the "red" area is evident which is probably the consequence of reduced irrigation in the outer sectors of the pivot. For Tweefontein, there is a marked overall irregularity in the development pattern of the crop that may be due to irregularities in soil type or soil compaction.

These irregularities are also very clear in the August image, even though they are somehow mitigated by the fact that the crop is in a more advanced phase of development, and probably by the compensating effects of irrigation.

5.2.3. Principal components

The Principal Component Analysis (PCA) is a transformation technique of an n-dimensional image (e.g. Multi-Spectral image) that produces a new set of images (components, or bands in our case) that are uncorrelated with one another and ordered with respect to the amount of variation they represent from the original image set. PCA is typically used to uncover the underlying dimensionality of multi-variate data by removing redundancy. In the context of remotely sensed images, the first component typically represents albedo, while the second component most often represents variation in vegetation cover. For example, component 2 has positive loadings on the near-infrared bands and negative loading on the visible bands. As a result, the green vegetation pattern is highlighted in this component *(Erdas Field Guide, 1997, Fung and Le Drew, 1987)*.

As a direct consequence of this, the PCA enhancement was tested in the course of the study as a potential alternative to the Vegetation Index. This can be seen in Fig. 16.

Fig. 16: Principal component maps of Major (left) and Tweefontein (right) pivots for the third flight (September 1999)

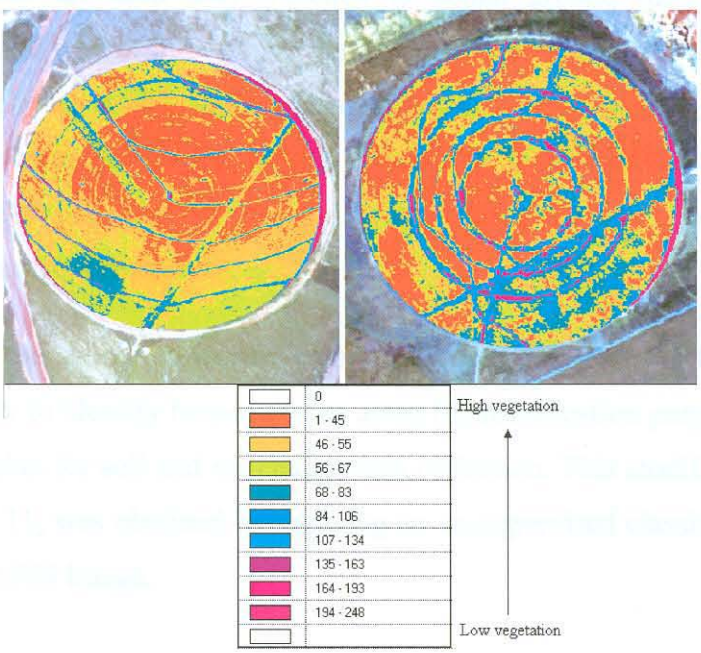

Also the first principal component is represented here in the 0 to 255 range of values, grouped in 10 equal intervals. Because the lower levels of the PC1 (First principal component) account for vegetation in better conditions, the scale is reversed with respect to the TVI. Red, whilst representing vegetation in better condition, is placed at the beginning of the scale and magenta at the bottom. The information provided, however, is totally comparable to the one that can be seen in Figure 15.

5.2.4. Classification

The classification process uses the spectral information represented by the digital data in one or more of the bands, and attempts to identify as a specific 'thematic class' each individual pixel based on this spectral information. Multi-Spectral classification is the process of sorting pixels into a finite number of classes, or categories of data, based on their data values. If a pixel satisfies certain set criteria, it is assigned to the class that corresponds to those criteria. This process is also referred to as image segmentation.

Classifications can either be supervised, where training sites are provided, or unsupervised where spectral classes are grouped first, based solely on their value, and are then later matched to actual ground information. Depending on the type of information that the user wants to extract from the original data, classes may be associated with known features on the ground, or may simply represent areas that look different to the eye of the analyst. An example of a classified image is a land cover map, showing vegetation, barren land, pasture, urban areas, etc.

In this study, the most noteworthy example of 'classification' is the one applied in order to identify homogeneous areas for stratification purposes in the sampling plan for soil and vegetation data collection. This stratification, shown in Fig. 11, was obtained by applying an un-supervised classification to the August 1999 image.

6. THE SPATIAL DATABASE

All the available information considered relevant to the study of the spatial variability of the crop for Pivots Major and Tweefontein has been acquired structured and then stored, so as to be analysed in a GIS environment. This whole process can be described as the pulling together of a 'spatial and temporal database'.

The data was attained from a range of sources such as the airborne images, the ground surveys and the data logger mounted on the harvester. From these, several other information layers were derived. These data can be described as belonging to two broad categories: static and dynamic data. Static data layers refer to those characteristics of the fields that do not change with time. The main static features are:

- The digital elevation model (DEM), made up of points representing the elevation above sea level (a.s.l.) and consequently the shape of the field surfaces. This was as derived from the measurements of the GPS mounted on the harvester data logger.
- The soil depth derived from a grid point augering campaign conducted by the University of Pretoria.
- The AWC map of the soil derived from the analysis on the soil samples collected in the course of the ground survey (see Section 4.2.2.). Three different maps were derived, one for the 0 to 20 cm depth soil layer, one for the 20 cm to spoil layer (or impermeable layer for Major) and one for the total AWC of the soil profile.

Further static data layers are derived from the above. For example:

- The elevation model of the spoil/impermeable layer, obtained by subtracting the depth to spoil map from the surface DEM.

- The depth of vadoze zone[18], obtained by manipulating the spoil DEM so as to represent the thickness of the layer of topsoil that is unlikely to ever be saturated.

The dynamic data represent those information layers, which represent the moment of acquisition and only that, such as the remote sensing images. This is data that can change with time. In detail:

- The Multi-Spectral images of the two pivots and the maps of the vegetation index (TVI) derived from these images.
- The map of the ground cover, of above ground dry matter and of LAI at the time of survey, extrapolated from the sample measurements done during the ground surveys.
- The above ground dry matter production of the crop derived from the analysis of vegetation samples collected in the course of those same ground surveys.
- The yield and moisture contents of the crop as derived from the data logger mounted on the harvester.

The data layers are listed in the following tables (Table 5 – 8).

Table 5: Static data layers for Major Pivot

Data layer topic	Unit	Source	Name of GIS layer
AWC 0-20	mm	Prof. A. Claassens	Maj-AWC-20
AWC 20 to spoil	mm		Maj-AWC-spoil
AWC Total	mm		Maj-AWC-total
Depth to spoil	mm	Auger measurements	Maj-d.t.s.
Depth of vadoze zone	mm	GIS processing	Maj-d.v.z.
Surface DEM	m (a.s.l.)		Maj-Sur-DEM
Spoil DEM	m (a.s.l.)		Maj-Spoil-DEM

[18] **Vadoze zone** The vadoze zone is the depth of soil from the surface down to the water table

Table 6: Dynamic data for Major Pivot

Data layer topic	Unit	Source	Name of GIS layer
Multi-Spectral image		08/99 Flight	Maj-MS-08/99
		10/99 Flight	Maj-MS-10/99
Vegetation Index		Image processing 08/99 flight	Maj-VI-08/99
		Image Processing 10/99 flight	Maj-VI-10/99
Second Principal Component		Image Processing 08/99 flight	Maj-PC1-08/99
		Image Processing 10/99 flight	Maj- PC1-10/99
Wheat yield	$t\ ha^{-1}$	Harvester data logger	Maj-yld
Wheat crop moisture	%		Maj-c.m.
Ground cover	%	Sampling and lab analysis	Maj-g.c.
Top dry matter	$g*m^{-2}$		Maj-t.d.m.
LAI	m^2*m^{-2}		Maj-LAI

Table 7: Static data for Tweefontein Pivot

Data layer topic	Unit	Source	Name of GIS layer
AWC 0-20	mm	Prof. A. Claassens	Twee-AWC-20
AWC 20 to spoil	mm		Twee-AWC-spoil
AWC Total	mm		Twee-AWC-total
Depth to spoil	mm	Auger measurements	Twee-d.t.s.
Depth of vadoze zone	mm	GIS processing	Twee-d.t.v.z.
Surface DEM	m (a.s.l.)		Twee-Sur-DEM
Spoil DEM	m (a.s.l.)		Twee-Spoil-DEM

Table 8: Dynamic data for Tweefontein Pivot

Data layer topic	Unit	Source	Name of GIS layer
Multi-Spectral image		10/99 Flight	Twee-MS-08/99
		08/99 Flight	Twee-MS-10/99
Vegetation Index		Image processing 08/99 flight	Twee-VI-08/99
		Image Processing 10/99 flight	Twee-VI-10/99
First Principal Component		Image processing 08/99 flight	Twee-PC1-08/99
		Image Processing 10/99 flight	Twee- PC1-10/99
Wheat yield	$t\ ha^{-1}$	Harvester data logger	Twee-yld
Wheat crop moisture	%		Twee-c.m.
Ground cover	%	Sampling and lab analysis	Twee-g.c.
Top dry matter	$g*m^{-2}$		Twee-t.d.m.
Leaf Area Index	m^2*m^{-2}		Twee-LAI

6.1. Point data interpolation procedure

The production of most of the maps utilised in the study required the interpolation of point data. These are characterised by a longitude and a latitude co-ordinate for each individual point.

This interpolation is done using the Inverse Weighted Interpolation (IWI) algorithm provided by the GIS Software, ERSI ArcView©[19] *(Watson, D. F. & Philip, G. M., 1985)*. This interpolation determines cell values using a linearly weighted combination of points. The weight is a function of the inverse distance from point to point.

The surface being generated through the interpolation is usually that of a variable that is described by the sample points, but that in reality has a continuous spatial expression over the area of interest (e.g. LAI of the crop).

The IWI lets the user control the significance of the known sample points upon the interpolated values, based upon their distance from them. In other words, the nearer to a measured point, the higher the weight of that point in determining the interpolated value, but the user can, interactively, control this weight as a function of other ancillary variables.

The best results from IWI are obtained when the points representing the surface are sufficiently dense and when they effectively represent the local variation in the surface that is being simulated. If the sampling of input points is sparse or very uneven, the results may not sufficiently represent the desired surface (*Watson and Philip, 1985*). Since the influence of an input point on an interpolated value is distance related, IDW[20] is not ridge preserving (*Philip and Watson, 1982*), this means that the interpolation will create a continuous surface and not be able to represent an abrupt spatial variation (ridge) in the values that are mapped

[19] ERSI ArcView ©: The GIS application product used for the manipulation of the maps.
[20] IDW = Interpolated Distance Weight

6.1.1. Surface DEM

As a typical static map, the surface 'Digital Elevation Model' (DEM) was derived from the data logger linked to a GPS and mounted on the harvester deployed on the pivots. The original data source was a set of points, which were subsequently interpolated. The DEM map is in raster form with a resolution (maximum pixel size) of 2 m. The base and derived documents are illustrated in Figures 17 and 18.

Fig. 17: Point measurements of height a.s.l. from a GPS data-logger mounted on the harvester for Major (left) and Tweefontein (right).

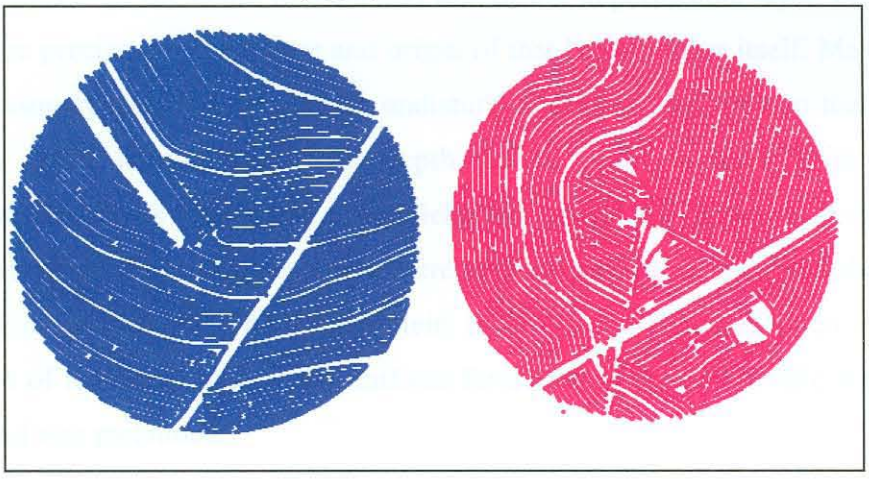

Fig. 18: DEM map of Major (left) and Tweefontein (right).

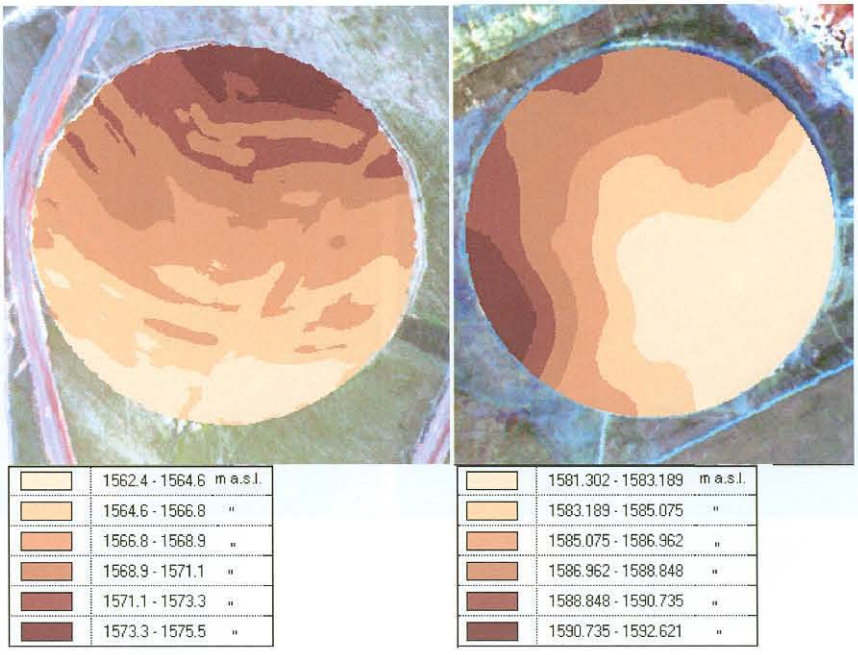

6.1.2. Depth to spoil or impermeable layer maps

Also a static data layer, the depth to spoil or impermeable layer map was derived from an auger sampling campaign conducted over the two pivots in a 40*40 m grid. Here too, the points where interpolated using the IWI procedure. As for the previous example, the map is also here in raster format with a pixel size of 2*2 m. The location of the auger samples and the derived map are shown in Figures 19 and 20.

Major and Tweefontein differ from one another essentially for the characteristic of the depth to spoil and that of the impermeable layer, or, to be more precise, for the nature and origin of that bottom layer itself. Major, as previously stated is set over an undisturbed tract of land. Due to this, it has a fairly homogeneous soil depth and a more uniform level of compaction across the surface of the field. Anomalies are present in certain sections of the field, such as where there is an impermeable layer, but these are of natural origin. The Tweefontein field is a rehabilitated open cast section of the mine, with a non-uniform formation of the soil profile when the land was reclaimed.

Fig. 19: Location of the auger sampling points for Major (left) and Tweefontein (right).

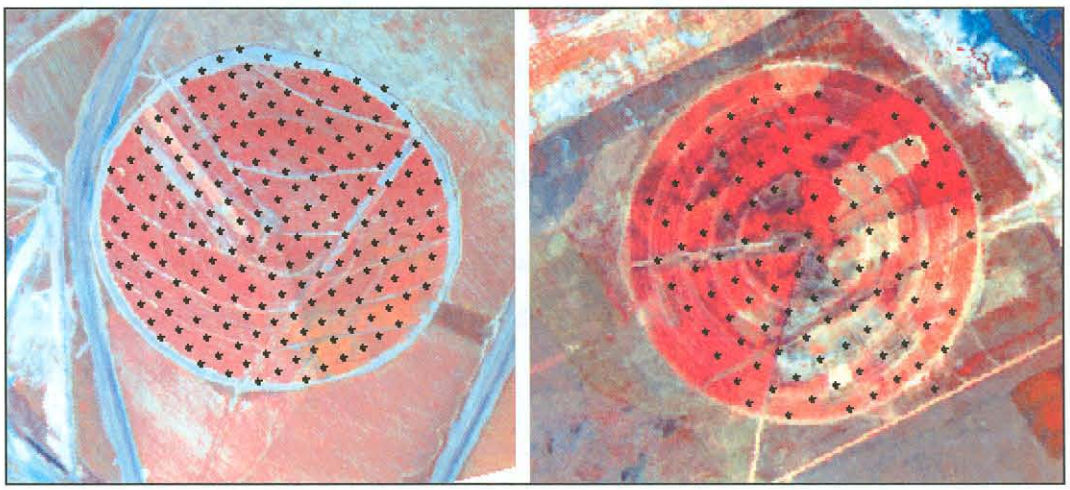

Fig. 20: Depth to the impermeable layer for Major (left) and Tweefontein (right).

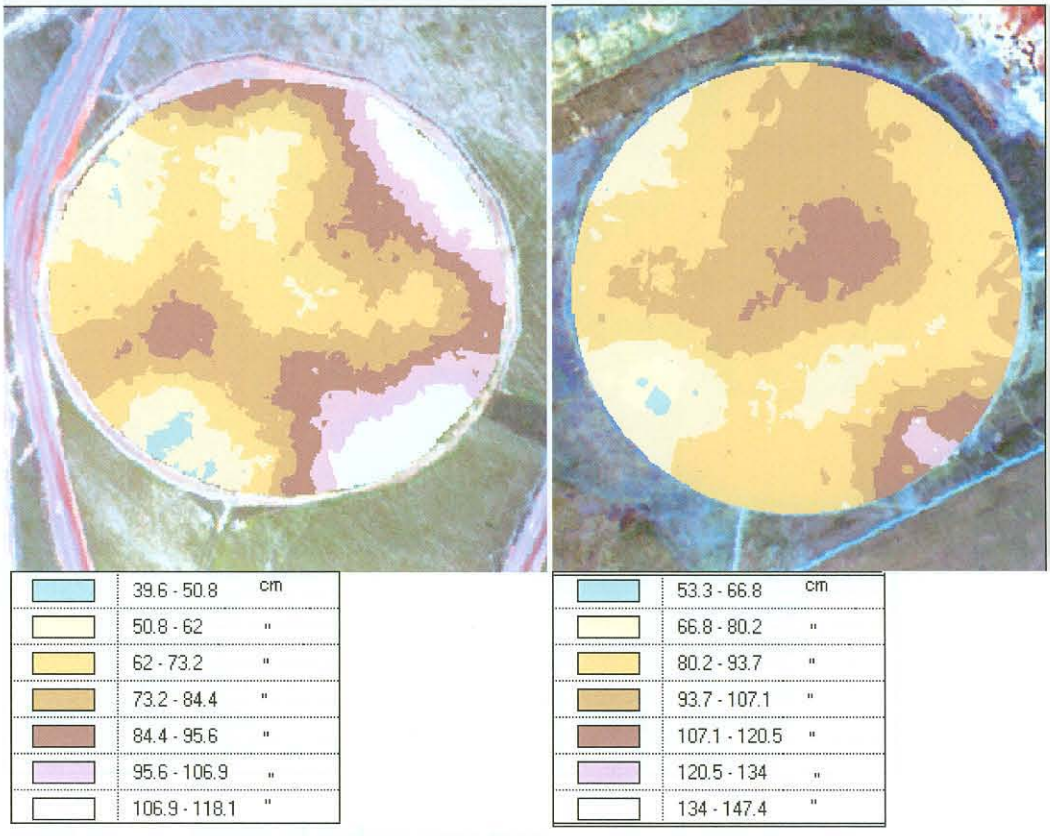

6.1.3. Spoil/impermeable layer DEM

The DEM of the spoil/impermeable layer was created in order to allow the definition of a subsurface drainage pattern. The shape of this layer can determine areas of water accumulation (underground ponding), thus affecting the condition of the vegetation in a way that may not be established by analysing the surface drainage pattern.

The spoil/impermeable layer DEM was derived by subtracting the depth of the soil/impermeable layer itself, as determined with the auger sample, from the surface DEM.

Fig. 21: Spoil/Impermeable layer DEM map of Major (left) and Tweefontein (right).

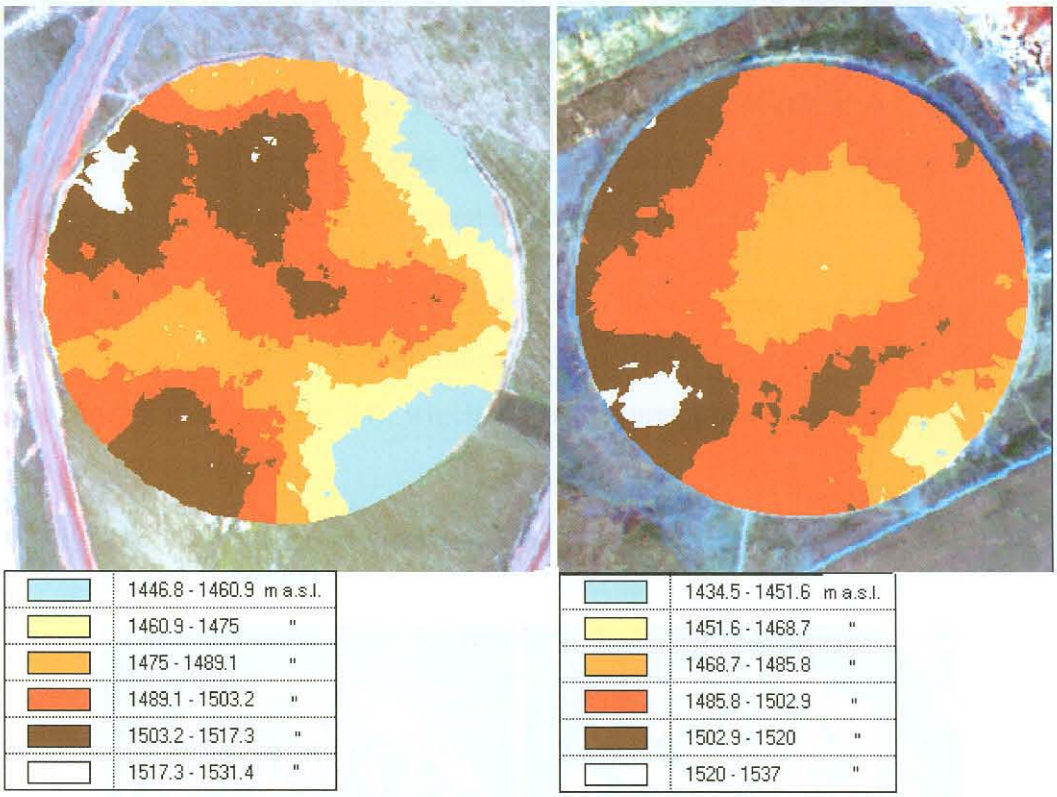

6.1.4. Depth of vadoze zone map

Also part of the 'static' data, the depth represented in this map refers to that portion of the soil layer where, in conditions of normal water supply, there is no water logging caused by underlying micro-topography. This map is derived from the spoil/impermeable layer DEM, by outlining the outer boundaries (the ridge) of the depression areas.

The delineation of the small and medium sized depressions on the spoil or the impermeable layer is performed by simulating the 'fill-up' of each depression until it 'spills over' to a neighbouring one. This simulation is a GIS process where the 'bottom' of the depression is first identified by means of a normal derivate analysis, and then the 'slopes' are identified by progressively 'pulling' the bottom upwards with the condition that the perimeter of the flat projection of the depression increases. The 'spill over' is identified when this surface is subject to a sudden increase, meaning that two or more depressions have come together. The point where this sudden

change takes place is identified as the outer contour of the 'depression', namely the ridge. Connecting all the ridges generates a new surface that makes up the baseline of the portion of the soil profile where it is unlikely to find saturated conditions. This is a more 'meaningful' effective soil depth than the one shown in Figure 20, although soil depth and water holding capacity may not be that important under irrigation.

The following pictures illustrate the various 'depressions' on the spoil layer (Fig. 22.), the derived micro drainage lines (Fig. 23.) and the depth of the vadoze zone map (Fig. 24), which just as the previous ones is in raster form with pixel size of 2m.

Fig. 22: Micro depressions of Major (left) and Tweefontein (right).

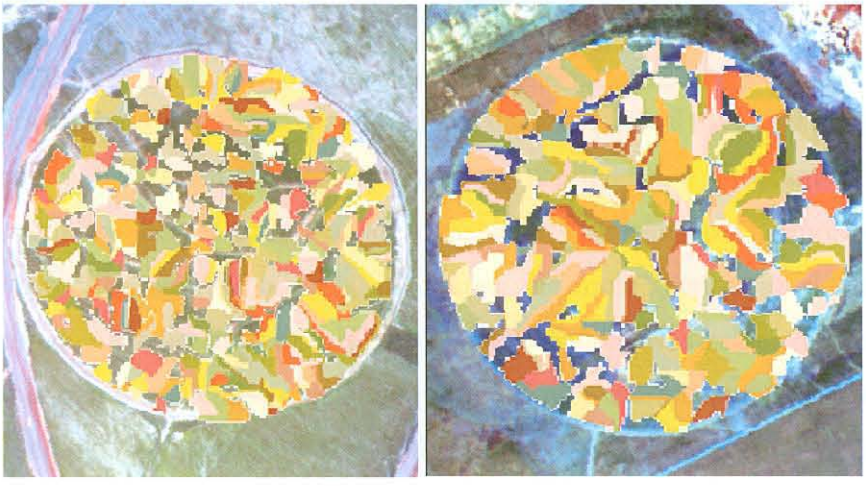

Fig. 23: The micro drainage lines for Major (left) and Tweefontein (right).

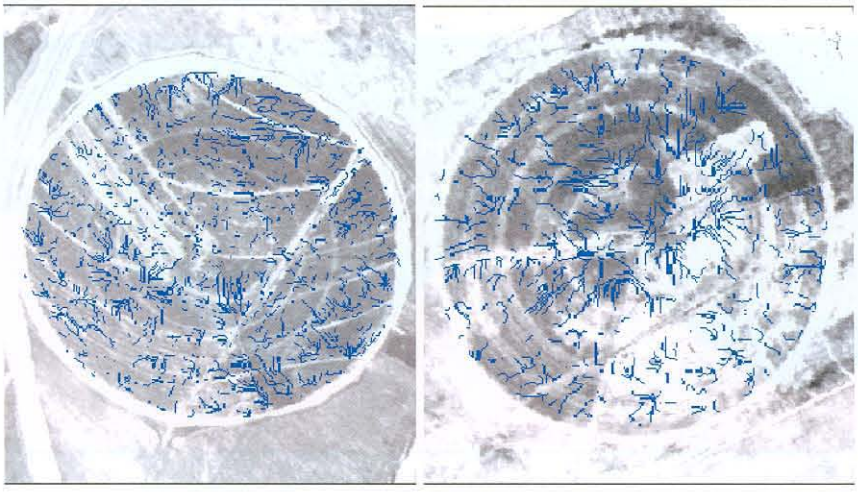

Fig. 24: The depth of the vadoze zone map for Major (left) and Tweefontein (right).

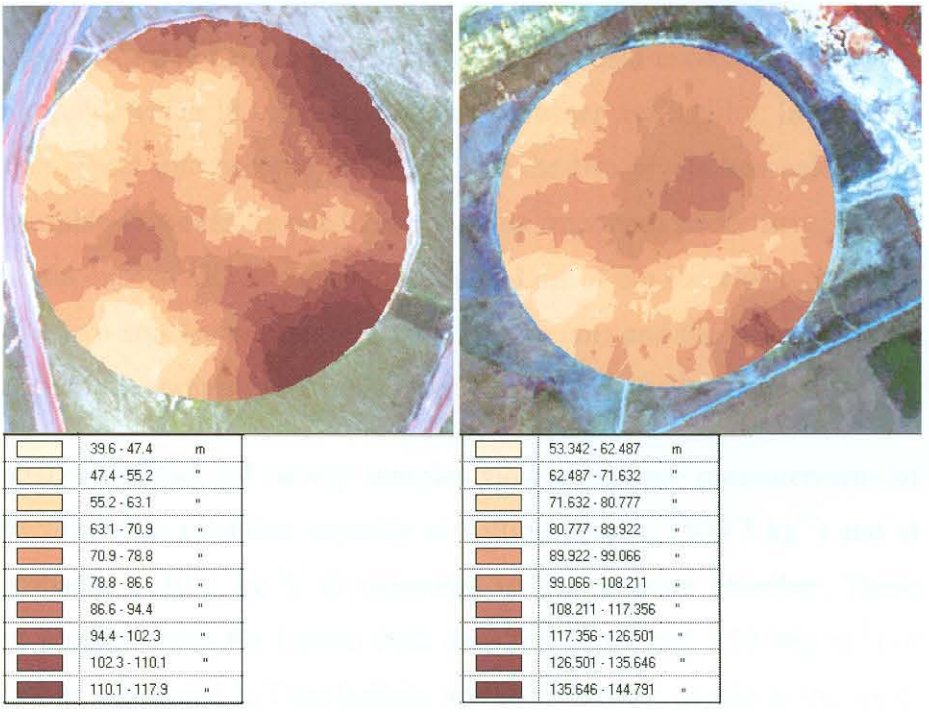

As this analysis is conducted with raster data, the actual size and shape of the micro and medium depressions may change as a function of the minimum number of cells that are considered to make up a 'depression'. The lower the number of cells, of course, the more 'depressions' can be identified. As a function of this, the drainage pattern was calculated over a variable number of cells contributing to the flow accumulation. These were, in order: 20, 50, 100, 200 and 500, thus generating alternative drainage pattern maps to be used in the analysis described above.

Fig. 25: Representation of the soil profile and the vadoze zone

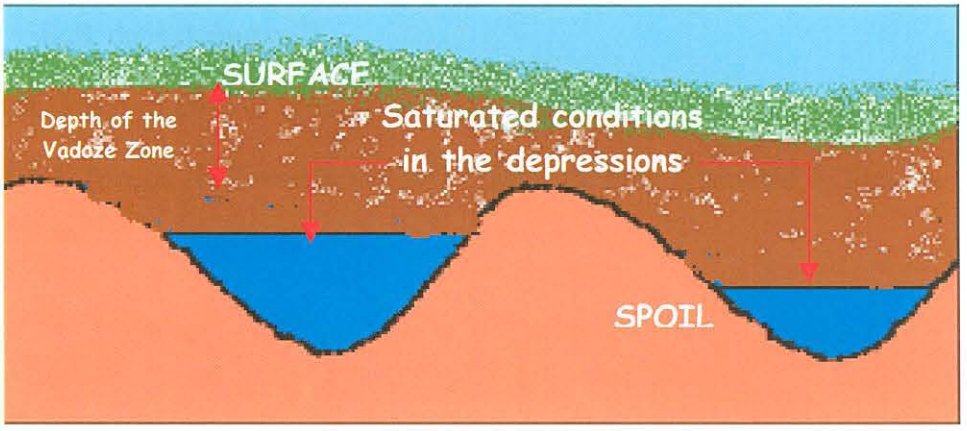

6.1.5. Available water capacity maps

The appearance and condition of the crop on the field is conditioned by its water supply, which in turn is a function of water availability. In order to take this aspect into account, the AWC for the two pivots was calculated. This variable however, is not likely to be as important under irrigation as one would expect with dry land conditions. Last of the static data, this was done for two soil layers: the root zone (0 –20 cm) and the layer from the root zone to the spoil/impermeable layer.

The analysis of the soil survey samples yielded the two measurements of gravimetric water retention capacity at wilting point (–1500 J kg^{-1}) and at field capacity (–10 J kg^{-1}), as measured in the pressure chamber. These values, together with the known bulk densities (1.60 and 1.90 Mg m^{-3}) of the soils at Major and at Tweefontein, and the reference depths to the spoil, allowed the derivation of the AWC for the two soil layers and for the total profile on each pivot. The following equation was used for the calculation of the AWC:

$$AWC = , FC - PWP * BD * Z$$

Where:

FC = Field capacity (g g^{-1})

PWP = Permanent wilting point (g g^{-1})

BD = Bulk density (mg m^{-3})

Z = thickness of the soil layer(s) (mm)

The AWC maps for Tweefontein and Mayor are here illustrated in Figures 26, 27 and 28.

Fig. 26: **Available water capacity map in the surface 20 cm layer for Major (left) and Tweefontein (right).**

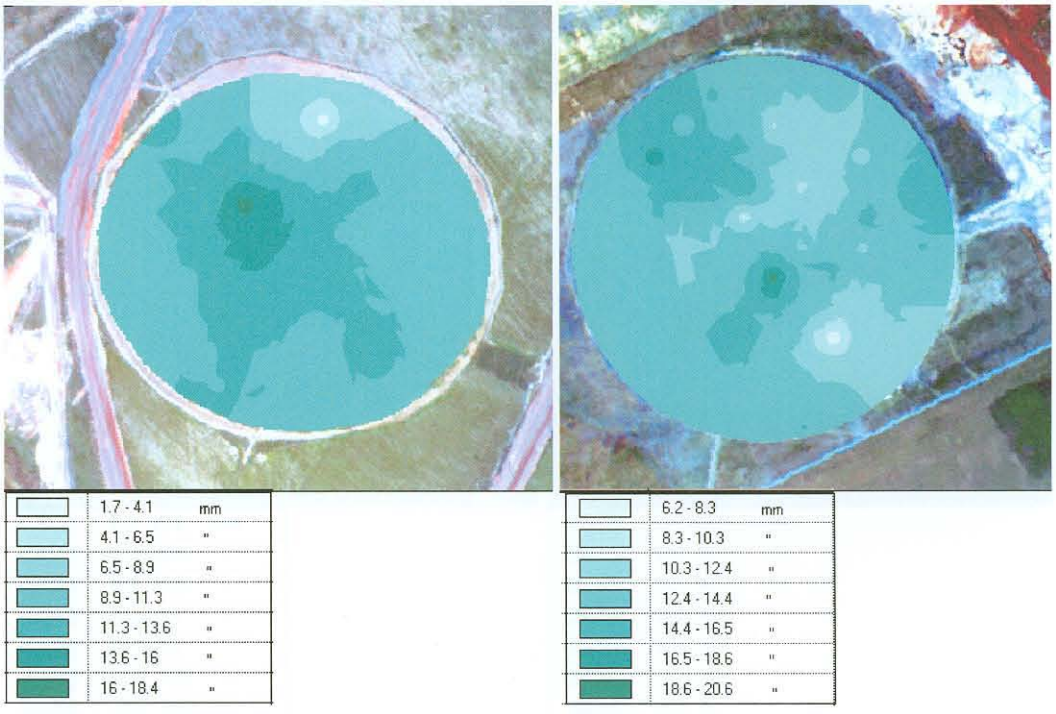

Fig. 27: **Available water capacity map in the 20 cm to spoil/impermeable layer for Major (left) and Tweefontein (right).**

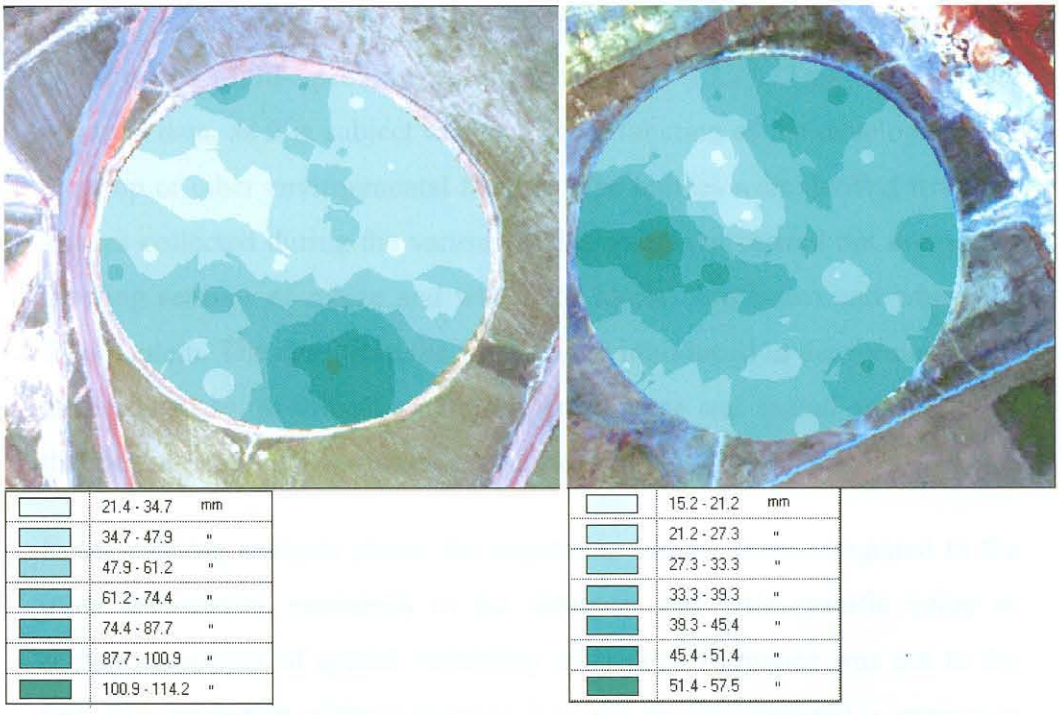

Fig. 28: Total Available Water Capacity map for Major (left) and Tweefontein (right).

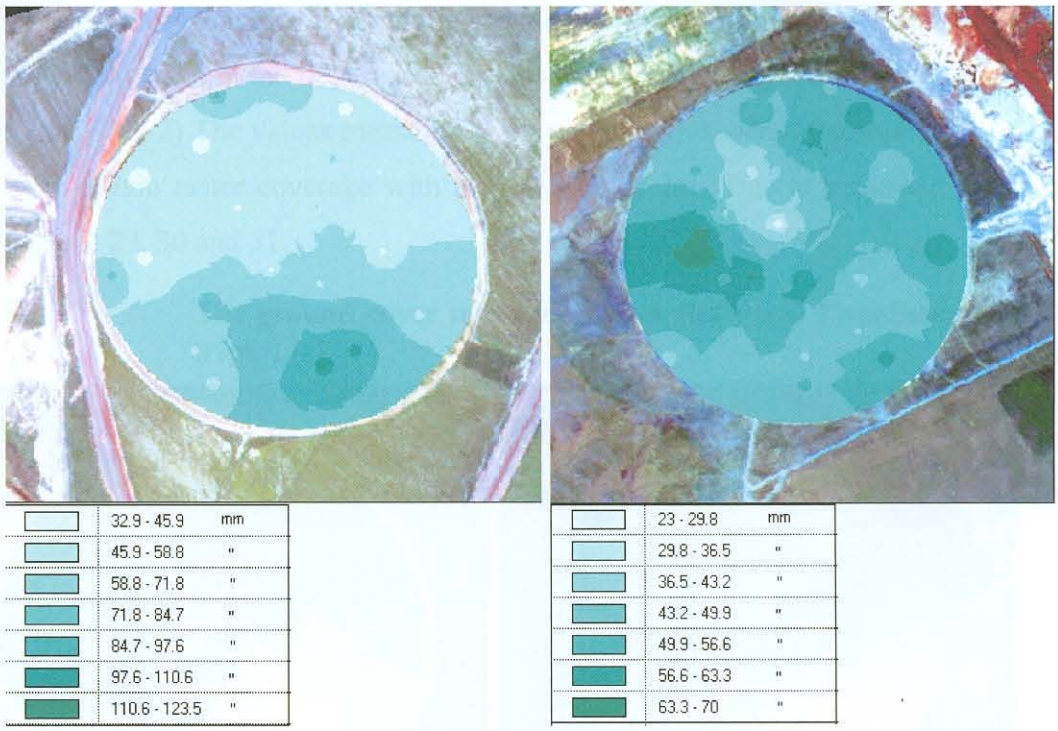

6.1.6. Vegetation index maps

The vegetation index maps are the result of a specific combination of the bands of the Multi-Spectral images (See Section 5.2.2.). This is, of course, dynamic data, as it is subject to change as a function of the development of the crop or other environmental factors. The indices were derived from the images collected during the various flights that were carried out during the growing seasons of maize and wheat for Major, and beans and wheat for Tweefontein. The data from the flights were introduced in the form of maps in the database, as indicator of crop performance and spatial variability of that performance. These images are shown in Figure 15.

In the ensuing analysis phase, the vegetation indices were compared to the other information contained in the database and their specific value as remote indicators of spatial variability of crop performance was put to the test. The resolution of these maps is 2 m and the unit mapped is expressed in a generic scale ranging between 0 and 100.

6.1.7. Ground cover, top dry matter and leaf area index maps

The maps of ground cover, above ground dry matter production and LAI were derived from the field measurements conducted during the survey (See Section 4.2.2) The values measured at the single points were interpolated so as to obtain raster coverage with a pixel size of 2m. This is presented in Figures 29, 30 and 31.

Fig. 29: The ground cover maps for Major (left) and Tweefontein (right).

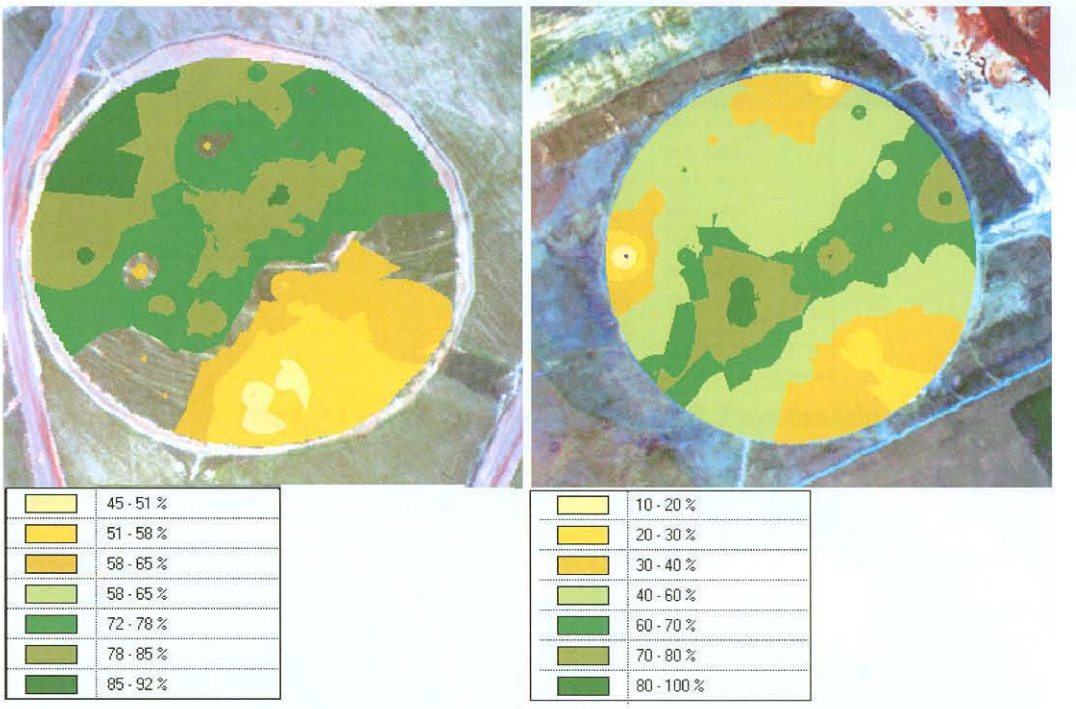

Fig. 30: **The above ground dry matter production maps for Major (left) and Tweefontein (right).**

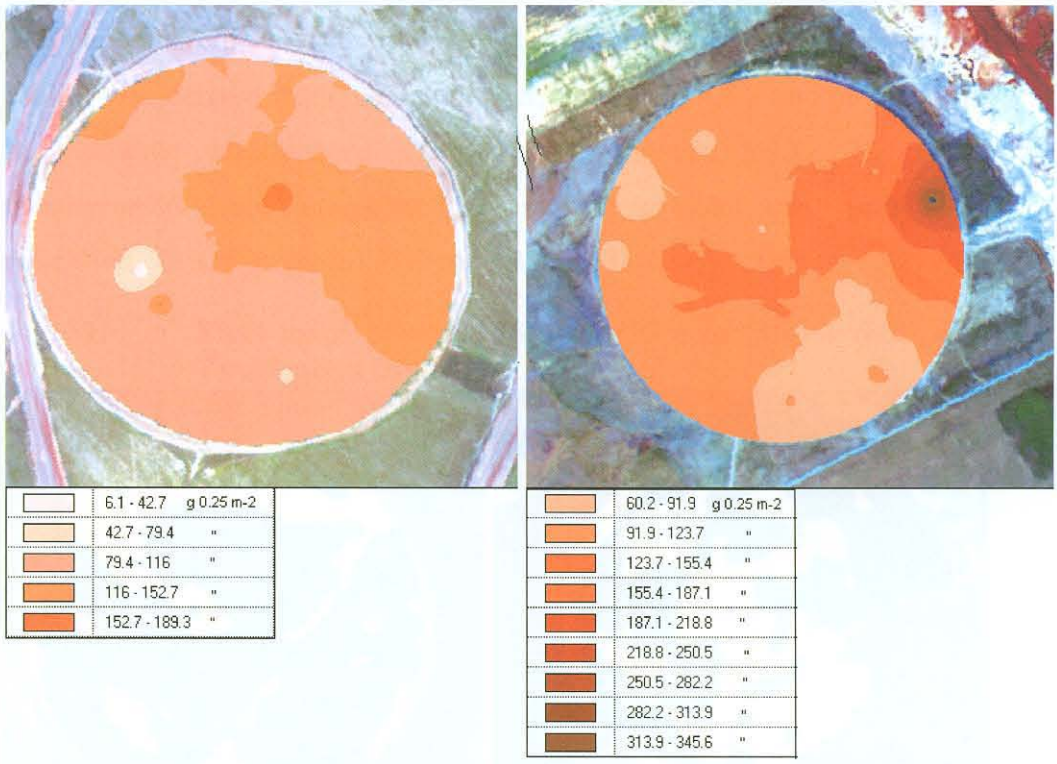

Fig. 31: **The LAI maps for Major (left) and Tweefontein (right).**

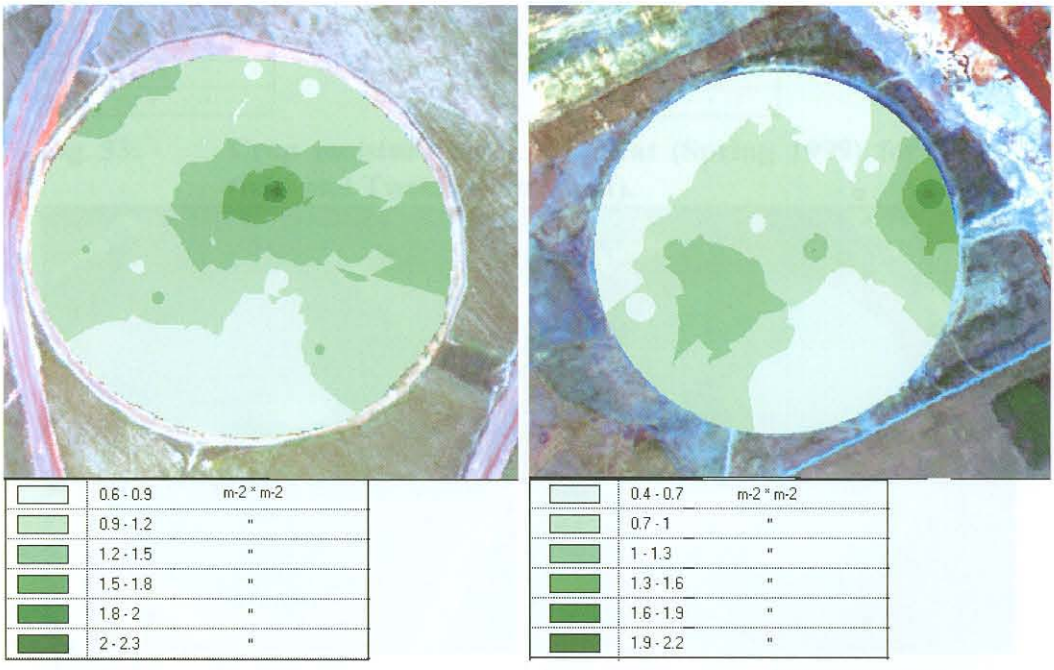

6.1.8. Yield and crop moisture at harvest map

The yield and crop moisture maps of the wheat harvest, as for the surface DEM, were derived from the data logger, linked to a GPS and mounted on the harvester deployed on the pivots (see section 4.2.3). The point measurements were interpolated to produce a raster map with 2 m resolution. This is presented in Figures 32 and 33.

Fig. 32: Yield maps of wheat (Spring 1999) for Major (left) and Tweefontein (right).

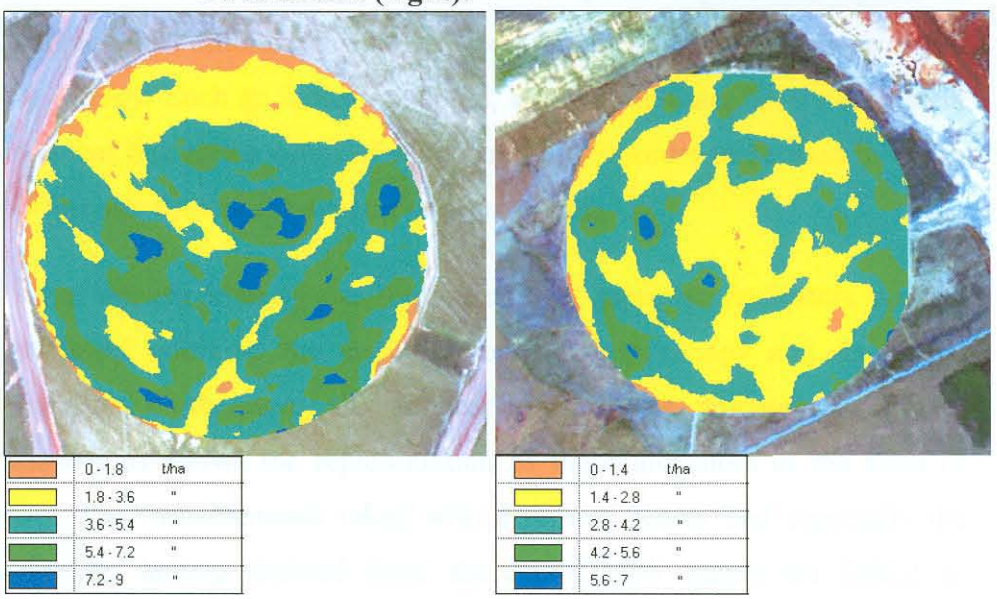

Fig. 33: Crop moisture maps of wheat (Spring 1999) for Major (left) and Tweefontein (right).

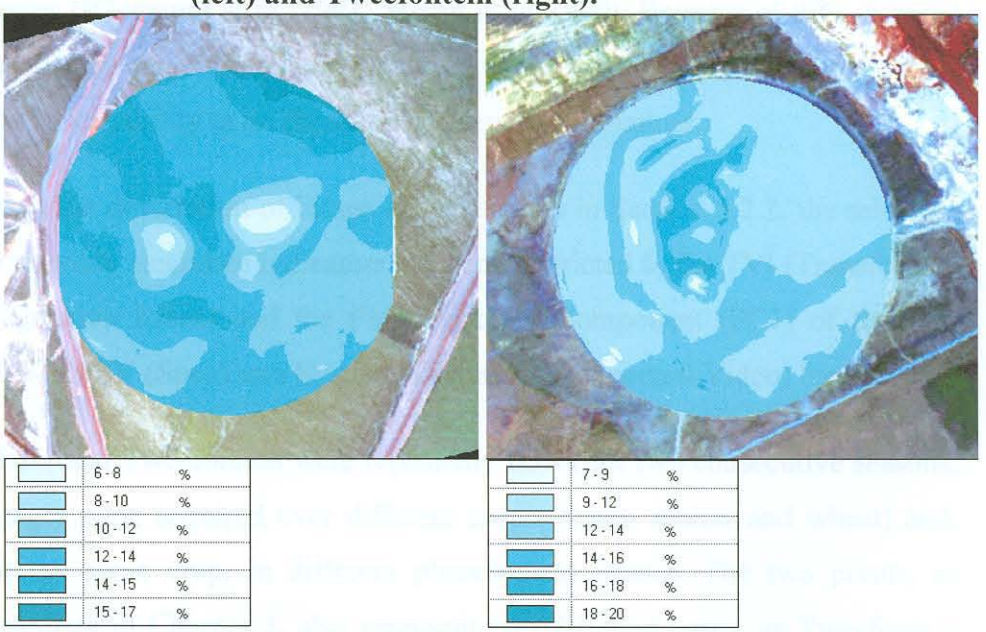

7. DATA ANALYSIS

Before engaging in the actual data analysis, it is necessary to devise ways to evaluate performance and variability over the surface of the pivots and the first step in this quest is to identify a spatial measure for these variables.

This spatial measure has to be generalised, repeatable and scientifically consistent and an effective indicator of spatial variability should, theoretically, be a numerical value, with a spatial expression, capable of identifying and outlining anomalies in development and performance over a crop canopy. Such an indicator should, at the same time, have a consistent functional link to the cause of such variability in order to be used in future applications without the support of ground truth.

Remote sensing imagery has the potential of supplying indicators that are capable of outlining the condition of the crop canopy and its spatial variability. Furthermore, the application of image processing and GIS technologies allows the representation of these indicators in the form of maps. The measurements taken with a remote sensor and especially the vegetation indices derived from the STS-DMSV bands are linked to physical variables such as photosynthetic activity and water contents in the leaves *(Wiengand et al. 1991, Steven et al 1990).* Because of this, in some cases, they can contribute to resolving the causes and circumstances of such spatial variability in an objective and repeatable manner.

From the description of image enhancements in Section 5.2.2, the selection of possible candidate indicators has been restricted to the TVI (Transformed Vegetation Index) and the First Principal Component (PC1) of the four STS-DMSV (SpecTerra Systems-Digital Multi-Spectral Video) bands.

Major and Tweefontein were repeatedly flown for two consecutive seasons, images were acquired over different crops (beans, maize, and wheat) and, for the same crop, in different phenological phases. The two pivots, as described in Chapter 3, also represent two different cases, as Tweefontein

was set up over a rehabilitated open cast section, while Major is over virgin land. Both performance and spatial homogeneity is expected to differ between the two due to the different nature of the substratum and the different levels of compaction resulting from the rehabilitation works at Tweefontein.

Since the pivots irrigate the crops, these can be considered as, more or less, indifferent to the major climatic contingency of water availability. The characteristics of the irrigation water though, rich in gypsum, could cause accumulation of this salt in the soil and thus influence anomalies over the crop canopy.

The correct labelling of such an occurrence is extremely difficult, as it may be masked or confused with other factors such as soil compaction or fertility. Another occurring problem, especially on the rehabilitated site (Tweefontein), is the possibility of water logging due to differing soil compaction over the field.

It is thus assumed that most of the spatial variability and anomalies in the crop development and productive outcome is due to the soil physical properties (e.g. drainage) but also soil characteristics or management practices (cultivation, fertilising, etc.).

Pests and weeds could also be considered cause for additional irregularities in the canopy of the crop. But, even though airborne remote sensing is a particularly suitable tool for detecting and managing these hazards, in the case of this project the frequency of over-flight was insufficient for the monitoring or even outlining of such events. The occurrence of pest infestations especially, is a rather sudden event, usually characterized by a rapid development. The early warning and identification of such hazards may require weekly and even more frequent monitoring in order to be effectively controlled.

The analysis was addressed at highlighting possible differences in the crop

canopy over different periods within the same season and across the two pivots. Further scope of the analysis is to try to explain the causes of possible performance difference and variability between the 'virgin' Major and the rehabilitated Tweefontein.

7.1. Analysis procedures

In general, at the beginning of an analysis it is assumed that the cause–effect relation between events is unknown. In the specific case of this study however, the differing genesis of Major and Tweefontein and their soil characteristics provide strong enough clues for the spatial variability of the crop canopy. Scope of the analysis, in this case, is to prove the spatial connection between soil characteristics and vegetation performance using remote sensing. Also among the objectives of the study is to identify, among a number of variables, the one or ones, that are most significant in determining the spatial variability.

The method of analysis chosen to identify the variable or variables that can best explain spatial variability is a 'Pearson-r' correlation between the various maps described in the previous chapters. A correlation is a measure of the relation between two or more variables. 'Pearson-r' correlation determines the extent to which values of the variables are related to each other. The value of the correlation (i.e. correlation coefficient) does not depend on the specific measurement units used, thus making it particularly suited to the comparison of maps, with the same pixel number, but representing very different characteristics.

The correlation analyses between maps are carried out on a one to one basis and a straight line, sloped upward or downward can graphically represent this correlation. This line is called the regression line or least squares line, because it is determined such that the sum of the squared distances of all the data points from the line is the lowest possible.

Correlation coefficients can range from –1.00 to + 1.00. The value of –1.00

represents a perfect negative correlation, whilst a value of +1.00 represents a perfect positive correlation.

Three main analysis procedures were followed to verify the effectiveness of remotely sensed data as indicators of variability, and in order to identify causes of this variability:

- Overall correlation analysis: This first process has the scope of validating remotely sensed indicators for the explanation of canopy variability. It consists of running a statistical correlation analysis between the values of the indicators and the variables measured over the crop canopy (dynamic and static) on a one to one basis.

- Focal correlation analysis: The scope of this second analysis is to identify 'where', over the surface of the pivots, the indicators work best in explaining the physical variables statistically. This process was carried out in an attempt to represent the statistical correspondence between indicator and spatial variables, in the form of maps. It can be described as a 'local or focal analysis' and is also a regression, but performed on a much-reduced spatial scale. The correlation is conducted along a moving window that spans across the various pairs of maps being compared. The correlation coefficient obtained within each window is assigned to the window itself so that, at the end, the variability of the correlation coefficient itself can be mapped. The size of the windows of analysis is arbitrary and several were tested.

- Variability analysis: A third analysis had the aim of highlighting the differences in variability between the two pivots and within the same pivot, over two seasons and with different crops. This was done by extracting all the relevant information from the maps in the form of summary statistics and distribution graphs, and by comparing the various values.

7.1.1. Overall correlation analysis

The procedure was centred on the exploration of the statistical correlation between the TVI and the PC1, with all the other data layers describing the crop, the soil, and the hydraulic and structural characteristics of the fields (static data layers). The TVI and the PC1 were derived from the images of the flights carried out during the wheat season, in September and October 1999. These two dates roughly corresponded to the vegetative development and flowering stages of the crop on both pivots. The TVI and PC1 are used as independent variables, and so too are the values of yield and crop moisture contents at harvest. This second layer is probably of scarce value to the determination of crop performance, but it is considered because, being available spatially, it may say something on the moisture condition of the soil at harvest time. These four variables are also compared with each other so as to explore how interrelated they are.

The program script for the correlation procedure is made up by a protocol named 'Covariance'[21]. This procedure calculates a covariance matrix and a correlation matrix between the active grid themes (the maps being compared), sending output to a file.

Within the GIS ArcView© definitions, a map is defined as a 'grid' and the procedure requires the 'grid' themes to be active in a view[22]. It also requires that the grid themes that are to be compared be spatially the same in terms of geographical co-ordinates, projection, containing rectangle (extents) and resolution. Grid themes are the format in which the raster thematic data layers are stored in ArcView©, each pixel or 2*2 m cell of a map is characterised by a unique spatial location. All the pixels of a map can be structured as a list where the numeric value of the map has a unique position that can be characterised by a code or order number. Two maps can then be compared as two corresponding sequences of values in which these same

[21] **Covariance**: This program was obtained through an internet users/developers network working on the GIS, ArcView©
[22] A view is the user interface of the program ArcView Spatial Analyst.

values are considered as two characteristics of the same pixel.

In order to run the procedure, the script of the program was connected to a button in the user interface and the analysis was conducted within the program 'Spatial Analyst©' that is a subprogram of Arc View©.

The result of the program was a simple correlation coefficient between maps, and the results of the analyses that were performed are illustrated in Tables 9 and 10.

The black boxes in the table indicate correlations of the data layers with themselves (and thus equal to 1) and analyses already conducted and reported in the upper part of the table. The correlations between the TVI and the PC1 were also skipped as irrelevant to the scope of the study. Such is also considered the correlation between crop moisture contents at harvest, the TVI and PC1. The grey shaded boxes with the numbers in bold, represent the best correlations both positive and negative (inverse correlation), obtained in this analysis.

Table 9: Major Pivot: Correlation coefficients (*r*) between the various data layers

Data Layers	TVI		1st Principal Component		Ground Cover	Above ground Dry Matter	LAI	Yield	Crop Moisture Contents	AWC			Depth To Spoil	Depth Vadoze Zone
	8/99	10/99	8/99	10/99						0-20	20 to spoil	Tot		
Maj-VI-08/99					-0.07	0.13	0.12	0.40		0.17	-0.07	-0.02	-0.03	-0.08
Maj-VI-10/99					0.11	0.14	0.20	0.31		0.09	-0.15	-0.14	-0.07	-0.07
Maj-PC1-08/99					0.20	-0.06	-0.07	-0.41		-0.20	-0.14	0.17	-0.08	-0.08
Maj- PC1-10/99					-0.03	-0.12	-0.17	-0.24		-0.13	0.04	0.05	0.03	0.03
Maj-g.c.						0.32	0.55	-0.33	0.30	-0.05	-0.75	-0.81	-0.44	-0.40
Maj-t.d.m.							0.82	0.16	-0.18	-0.14	-0.43	-0.39	0.05	-0.02
Maj-LAI								0.07	-0.21	0.24	-0.55	-0.57	-0.02	-0.03
Maj-yld									-0.69	0.36	0.21	0.28	0.16	0.06
Maj-c.m.										-0.25	-0.19	-0.23	-0.23	-0.23

Table 10: Tweefontein Pivot: Correlation coefficients (*r*) between the various data layers

Data Layers	TVI	1st Principal Component	Ground Cover	Above ground Dry matter	LAI	Yield	Crop Moisture Contents	AWC			Depth To Spoil	Depth Vadoze Zone
								0-20	20 to spoil	Tot		
Twee-VI-08/99			0.15	0.20	0.19	0.29		0.11	0.10	0.12	-0.03	-0.03
Twee-VI-10/99			0.17	0.18	0.18	0.28		0.15	0.04	0.08	-0.07	-0.07
Twee-PC1-08/99			-0.19	-0.20	-0.20	-0.32		-0.12	-0.05	-0.08	-0.02	-0.02
Twee- PC1-10/99			-0.22	-0.17	-0.18	-0.27		0.15	0.04	-0.20	0.09	0.09
Twee-g.c.				0.59	0.80	0.18	-0.05	0.28	0.00	0.07	-0.12	-0.12
Twee-t.d.m.					0.84	0.30	-0.27	0.17	0.17	0.22	0.07	0.07
Twee-LAI						0.35	-0.07	0.26	0.18	0.25	-0.00	-0.00
Twee-yld							-0.23	0.04	0.30	0.32	-0.09	-0.09
Twee-c.m.								0.12	-0.27	-0.25	0.07	0.07

The correlation analysis yielded very poor results for both Major and Tweefontein. Most of the correlation coefficients (***r***) were below 0.36.

Better results had been expected for the correlation between the TVI and variables such as above ground dry matter production or yield, or between soil depth and above ground dry matter or yield. This expectation was based on the theory of vegetation indices, and on the expected link between soil depths, water availability and yield. For this second case, a possible explanation for the poor results could be attributed to the fact that wheat, with a limited root depth, is less sensitive to the structure of the subsoil, especially under conditions of irrigation. In other words, when irrigated, wheat is indifferent to the soil physical properties.

However, another explanation for these results, can be found in the interpolation procedure, and therefore in the creation of poorly representative maps. The soil depth, assuming the accuracy of measurement at the augering points, once interpolated and transformed into maps, possibly compared poorly with the data derived from the images, or with those interpolated from the ground surveys and the harvester data logger.

The interpolation process generates a raster map (GRID), which is made up of many more pixel values than the measurements. If the interpolation process generates maps that are scarcely representative of reality, the correlation of these maps will be compromised by the presence of an overwhelming number of 'wrong' values, masking the true correspondence of two phenomena. One could possibly look at the simple correlation between the measured values, but these derive from differing sampling campaigns and since they vary greatly in sample size, cannot be compared.

Some correlations, relative to the LAI, ground cover, and the above ground dry matter maps were an exception. For Major, the *r* between LAI and ground cover was 0.55, and between the LAI and above ground dry matter was 0.82. For Tweefontein, the *r* was 0.80 between LAI and ground cover and 0.84 between LAI and above ground dry matter. An *r* of 0.59 was also

reported between above ground dry matter and ground cover. An explanation for these good correlation coefficients between LAI, ground cover and top dry matter probably lies in the fact that the maps that are being compared were generated from data collected on the same points. Consequently they had the same exact spatial origin and followed very similar interpolation procedures. On these points the data were already highly correlated and carried on this association throughout the interpolation process.

The Major pivot also recorded a significant negative correlation of –0.69 between the yield map and the crop moisture contents at harvest. These two values also have a common point origin and were subject to the same interpolation procedure, just as in the case of the ground survey measurements.

For pivot Major, good *r* values were reported between AWC, ground cover and LAI. These results are actually the most interesting as they derive from the comparison of totally independent data sources, with different source points and therefore also a different interpolation course. The *r* value between the AWC of the 20 cm to spoil layer and ground cover was –0.75, and the *r* between the total AWC and ground cover was –0.81. LAI reported an *r* of –0.55 with AWC (20 cm to spoil), and an *r* of –0.57 with the total AWC.

A positive and not a negative correlation between AWC and biomass proxies such as ground cover and LAI would have been expected. However, we are aware that the south most portion of Major actually has a plinthic layer around 110 cm depth. This layer can cause water logging on a large portion of the pivot.

The fact that 'Depth to spoil' and 'Depth to the vadoze zone layer' did not appear to affect the performance of the crop is most probably connected with the fact that it is an irrigated system and for the same reasons as for the AWC.

The crop did show a certain degree of variability both in the Vegetation Index and the Yield maps on both pivots. Other possible causes (fertility, texture, chemistry, management, etc.) should be explored, with this implying that the possible causes for spatial variability should also be transformed into maps and processed according to the procedure described above. Water logging, probably a major cause of variability, however, was not estimated as no spatialised water budget was calculated over the surface of the pivots.

7.1.2. Focal correlation analysis

The analysis of the "focal" correlation used the same statistical procedure as the previous overall analysis but with the additional objective of highlighting the local correlation between data layers and representing this statistical correspondence in the form of a map.

The difference between the two procedures lies in the fact that the correlation between the various data layers, instead of being investigated over the whole surface of the pivot, taking into account all the cells of the grid, was performed locally on a much-reduced focal area. This was done using a 'moving window' where the size of this 'window' is variable, as a function of the target resolution of the output map.

A user interface was implemented within ArcView© Spatial Analyst for this procedure, providing the option of running the analysis over any two selected maps (in GRID format) and for variable size windows, starting from a minimum of 3*3 pixels. Each window size is 'valid', as it represents a 'valid' correlation for the specific area analysed, however, a smaller window produces a 'salt and pepper' effect that makes it scarcely 'readable'.

Several options of sizes were consequently tested and the 20*20 pixel window was finally chosen for output, as it achieves the best visual effect over the pivots. This is illustrated in Figures 34 and 35.

The various comparison maps are illustrated in Appendix 2.

Some interesting local high correlation values did occur in the comparison between the yield values and the soil depth (to spoil/impermeable layer) map, thus suggesting a link between crop performance and the condition of the substratum, at least in specific areas of the field. This event was much more evident for the Tweefontein pivot which was actually the one on a rehabilitated site and thus prone to differential subsidence of spoil, while Major is not prone at all.

In addition to the graphical comparison, a set of statistics was extracted from the various maps. These statistics summarise the correlation values in ranges from –1 to + 1 in bins of 0.1 and, for each pair of maps being compared, the percentage of points within each correlation bin is reported (See Tables 11 and 12).

The results of the correlation experienced in the first analysis were confirmed in this second one. For Major, the correlations were significant for LAI and above ground dry matter, as well as for ground cover and depth of the vadoze zone, ground cover and LAI, and ground cover and above ground dry matter. For Tweefontein, the results were positive for LAI and ground cover as well as for above ground dry matter and ground cover.

The fact that positive correlation coefficients occurred locally suggests the presence of factors such as, for example, the presence of small depressions or local differences in soil texture.

Fig, 34: **Correlation map between above ground matter production and LAI for Pivot Major with a moving window of 20*20 pixels**

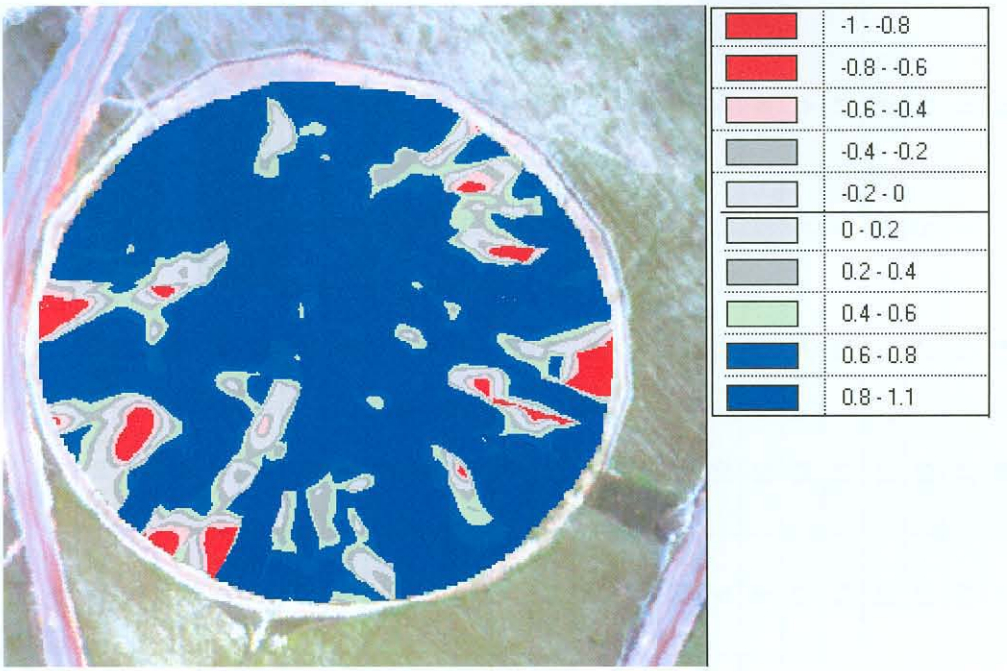

Fig. 35: **Correlation map between above ground dry matter production and LAI for Pivot Tweefontein with a moving window of 20*20 pixels**

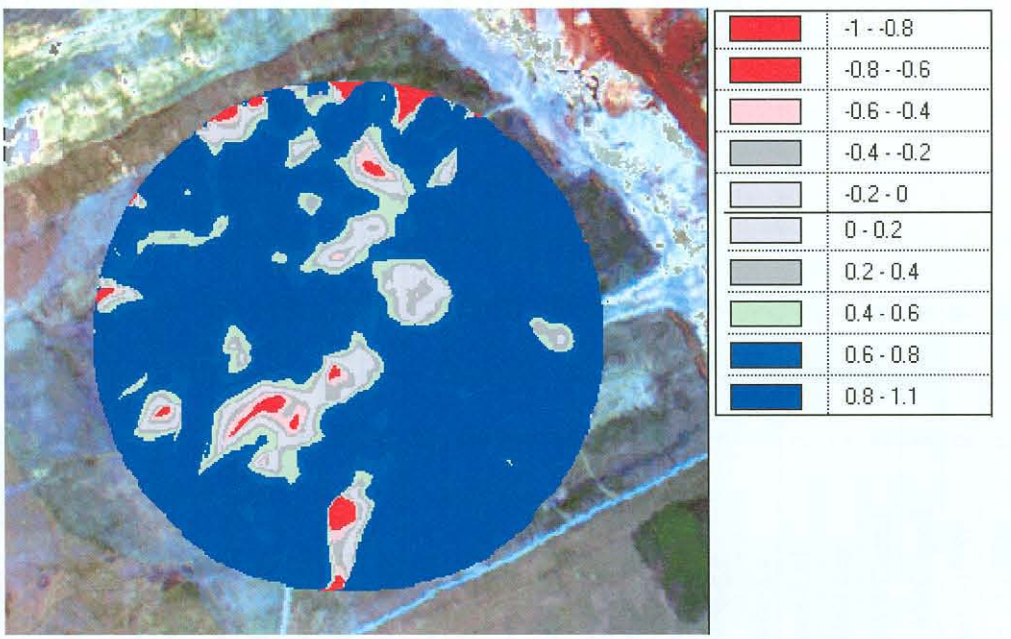

Table 11: Summary statistics of focal correlations for wheat, 1999 for Major and Tweefontein

GIS layers compared		r RANGE (%)											
		-1 to –0.8	-0.8 to –0.6	-0.6 to -0.4	-0.4 to -0.2	-0.2 to 0	0 to 0.2	0.2 to 0.4	0.4 to 0.6	0.6 to 0.8	0.8 to 1	0.6 to 1	-1 to -0.6
Maj-t.d.m.	Maj-LAI	2	1	1	2	3	3	4	6	11	66	77	3
Maj-g.c.	Maj-d.v.z.	1	9	13	14	13	14	13	12	9	2	11	11
Maj-g.c.	Maj-LAI	4	3	3	2	3	3	5	8	15	56	70	6
Maj-g.c.	Maj-t.d.m.	6	3	3	4	4	4	5	8	13	51	64	8
Maj-AWC-total	Maj-LAI	4	9	11	12	12	13	13	13	10	4	14	13
Maj-AWC-total	Maj-t.d.m.	18	15	10	8	8	8	8	8	8	10	19	32
Maj-AWC-total	Maj-g.c.	15	16	13	9	7	7	8	7	7	10	18	31
Maj -AWC-spoil	Maj-LAI	17	11	8	8	7	8	7	8	9	16	26	29
Maj -AWC-spoil	Maj-t.d.m.	20	12	9	8	8	8	7	7	7	13	20	32
Maj -AWC-spoil	Maj-g.c.	16	12	9	7	6	7	7	8	10	19	29	28
Maj-yld	Maj-g.c.	6	11	12	11	10	11	11	11	11	5	16	18
Maj-yld	Maj-AWC-20	2	9	10	10	11	12	11	13	15	8	23	11
Maj-VI-10/99	Maj-yld	0	0	1	5	15	25	28	19	5	1	6	0
Maj-VI-08/99	Maj-yld	0	0	2	6	12	20	26	21	12	1	13	0
Twee-LAI	Twee-g.c.	3	2	2	2	3	4	6	10	17	51	5	68
Twee-t.d.m.	Twee-g.c.	3	3	3	3	4	5	8	12	17	41	6	59
Twee-yld	Twee-LAI	2	6	9	10	12	14	13	14	14	5	9	19
Twee-yld	Twee-t.d.m.	2	8	10	11	11	13	13	13	13	5	11	18
Twee-yld	Twee-AWC-total	3	8	10	11	11	13	13	13	12	6	11	19
Twee-yld	Twee-AWC-spoil	3	8	9	11	12	12	12	13	13	6	11	18
Twee-yld	Twee-VI-10/99	0	0	2	4	8	16	23	31	15	1	0	16
Twee-yld	Twee-VI-08/99	0	0	2	5	9	18	23	28	14	1	0	15

7.1.3. Variability analysis

The analysis of variability within and between the pivots, and over two seasons, was performed through the comparison of the main statistics of the performance indicators, TVI and PC1, as well as that of the yield maps. The statistics were drawn from the maps of the TVI and the PC1 for the flights of the 1998 and 1999 seasons and from the yield map relative to the 1999 season

From the various maps, the main statistics were extracted for each growing season, and from the two flights. These are: minimum (Min), maximum (Max), Mean, Median, Mode and Standard Deviation (SD). These values have been compared to derive a percentage variation within the season (flight 1 and flight 2), across seasons and between the two pivots (Tweefontein over Major).

The TVI variation over Pivot Tweefontein, (See Table 12) for the summer crop (beans) and within the season, shows a marked decrease of minimum values, a moderate increase in maximum and median and a significant increase in the values of the standard deviation, considered as a measure of variability. This variation takes place from the vegetative development phase to the pod-filling phase.

The interpretation of this can be that, with the progression of the season, there are portions of the field where the crop failed, consequently lowering the minimum as well as increasing the variability, as measured by the SD.

This level of crop failures and the increase in variability under an irrigation regimen may signify that, all other things being equal (fertilizer, pesticides, etc), for Pivot Tweefontein, the problems rest with the soil, its profile, its fertility or its physical characteristics.

These same variations were not experienced for wheat (the winter crop), and this may be interpreted as a higher adaptability of the crop to the particular conditions of Tweefontein.

For the Pivot Major, a comparison was not possible within the summer season because only data for the flowering stage was available. For the winter season the values of minimum, maximum and mean of the vegetation index, show a marked

decay from vegetative development to grain filling. The standard deviation, as a measure of within field variability, also decreases.

This could all be due to the particular subsoil set-up of Major where, the presence of a fairly shallow impermeable layer in the bottom (South) portion of the pivot affects the growth of maize in the later stages, thus affecting the overall statistics of crop performance.

Table 12: Analysis of the Vegetation Index variability: Statistics

Pivot		Tweefontein (rehabilitated) -				Major (virgin)			
Season		SUMMER		WINTER		SUMMER		WINTER	
Crop		Beans	Beans	Wheat	Wheat	NO DATA	Maize	Wheat	Wheat
Phenological Phase		Veg. Dev.[23]	Pod filling	Veg. Dev.	Maturity		Flowering	Veg. Dev.	Maturity
Average per survey	Min	14	4	27	28		5	15	5
	Max	247	255	249	250		255	255	213
	Mean	167	170	194	199		186	175	161
	Median	169	179	200	208		196	181	167
	Mode	167	186	209	218		209	195	175
	SD	23	40	29	26		39	32	24
Variation within the season (Flight 1 over flight 2)	Min	-71 %		+4 %		NO DATA		-67 %	
	Max	+3 %		+0.4 %				-16 %	
	Mean	+2 %		+3 %				-8 %	
	Median	+6 %		+4 %				-8 %	
	Mode	+11 %		+4 %				-10 %	
	SD	+77 %		-11 %				-26 %	
Seasonal Average	Min	9		27		5		10	
	Max	251		249		255		234	
	Mean	169		196		186		168	
	Median	174		204		196		174	
	Mode	176		213		209		185	
	SD	32		27		39		28	
Variation across seasons (Winter over summer)	Min	+206 %				+100 %			
	Max	-0.6 %				-8 %			
	Mean	+16 %				-9 %			
	Median	+17 %				-11 %			
	Mode	+21 %				-11 %			
	SD	-14 %				-29 %			

The overall comparison of the two pivots within the same season (see Tables 13), although referring to two very different crops, such as beans and maize, shows that Tweefontein has higher minimum values in summer and in winter, lower maximum and mean values in summer and higher in winter. Both in summer and winter Pivot Major shows a lower variability as indicated by the standard

[23] Veg. Dev: vegetative development

deviation. This is possibly a consistent demonstration of the higher uniformity over the virgin site, as compared to the rehabilitated one.

Table 13: Analysis of the Vegetation Index variability: Variations across the pivots

SEASON		SUMMER	WINTER
Variations in Major over Tweefontein	Min	+44 %	+64 %
	Max	-2 %	+6 %
	Mean	-10 %	+14 %
	Median	-13 %	+15 %
	Mode	-18 %	+13 %
	SD	-23 %	-2 %

The analysis of the PC1 (Table 14) provides results and variations that are inverted and highly enhanced, with respect to the TVI. The variation within season for summer crops, on Tweefontein and Major, shows the expected behaviour of an overall increase in values from vegetative development to grain filling. The opposite happens for the winter crop (wheat).

As for the variation from season to season and within the same pivot, (Table 15) Tweefontein shows an increase of all main statistics and variability from summer to winter crops, while Major has an almost completely opposite behaviour.

What this data show is that Major has an overall better performing canopy for summer and winter crops. The variability of the canopy is higher for summer crops (again due to the influence of impermeable layers on deep root systems) but lower for winter crops when there is more control of the water balance due to irrigation and absence of rainfall.

A consideration deriving from this analysis is that PC1 could be used alternatively to TVI in virtue of its enhancement of the variations.

Table 14: Analysis of the First Principal component: Statistics

Pivot		Tweefontein (rehabilitated) -					Major (virgin)		
Season		SUMMER		WINTER			SUMMER	WINTER	
Crop		Beans	Beans	Wheat	Wheat		Maize	Wheat	Wheat
Phenological Phase		Veg. Dev.	Pod Filling	Veg. Dev.	Maturity		Flowering	Veg. Dev.	Maturity
Average per survey	Min	16	36	3	15	NO DATA	50	2	28
	Max	255	255	253	251		255	255	248
	Mean	51	106	61	52		100	64	57
	Median	46	100	53	42		91	57	50
	Mode	43	91	47	30		77	42	41
	SD	22	34	34	30		33	34	25
Variation within the season (Flight 1 over flight 2)	Min	+125 %		+400 %			NO DATA	+1300 %	
	Max	0 %		-0.8%				-3 %	
	Mean	+108 %		-13 %				-11 %	
	Median	+117 %		-21 %				-12 %	
	Mode	+112 %		-36 %				-2 %	
	SD	+60 %		-13 %				-24 %	
Seasonal Average	Min	26		9			50	15	
	Max	255		252			255	251	
	Mean	78		56			100	60	
	Median	73		47			91	53	
	Mode	67		38			77	41	
	SD	28		32			33	29	
Variation within the season (Flight 1 over flight 2)	Min	+125 %					+400 %		
	Max	0 %					-0.8%		
	Mean	+108 %					-13 %		
	Median	+118 %					-21 %		
	Mode	+112 %					-36 %		
	SD	+60 %					-13 %		

Table 15: Analysis of the PC1: Variations across the pivots

SEASON		SUMMER	WINTER
Variations in Major over Tweefontein	Min	92 %	66 %
	Max	0 %	-0.2 %
	Mean	27 %	7 %
	Median	25 %	13 %
	Mode	15 %	8 %
	SD	19 %	-7 %

The comparison between the yield maps (See Table 16), shows that there is a common maximum value between the two pivots (11 t ha^{-1}) but a higher mean yield on Major (24 %).

The variability, as measured by the standard deviation, is also higher for Major.

These results confirm what resulted from the analysis of the TVI and PC1, and that is that wheat, though producing less over Pivot Tweefontein, has a higher homogeneity. This again could be due to the plinthic layer in the lower portion of Major that affected the outcome of the crop in the later stages of development causing water logging.

Table 16: Analysis of Yield: Statistics

Pivot		Tweefontein (rehabilitated)	Major (virgin)
Season		WINTER	WINTER
Crop		Wheat (t/ha)	Wheat (t/ha)
Average over the Pivot	Min	0	0.0
	Max	11	11.0
	Mean	1.5	1.8
	Median	1	1.0
	Mode	0	0.0
	SD	1.4	2.0
Variations in Major over Tweefontein	Min	0%	
	Max	0%	
	Mean	+24%	
	Median	0%	
	Mode	0%	
	SD	+ 41%	

7.1.4. Analysis of the indicator's distributions

In addition to the variability analysis and the statistical comparison of indicators, a set of diagrams were produced to highlight differences in behaviour between the rehabilitated site (Tweefontein) and the virgin pivot (Major) as well as the difference of behaviour of the summer and winter crops over the same pivot. These diagrams are relative to the distribution of the pixel values over the pivots (See Figures 36 to 43). The first diagram (Fig. 36) compares the level and distribution of the pixel values for maize (second flight, flowering phase, February 2, 1999) and wheat (fourth flight, also flowering phase, October 1999) over Pivot Major. Both the distributions show a shift towards the high values of the TVI as they tend towards the maximum values of the indicator in the phenological cycle, as well as the maximum for green biomass for both crops.

Maize has higher values due to the higher level of biomass with respect to wheat. The crop, however, is also less homogeneous as can be deduced by the wider spread of the curve, this means a higher variability of physiological condition

across the field. The curve for wheat peaks at a lower level of TVI but is also less spread out. An interpretation of this is that wheat seems to be better adapted (more homogeneous) to the cultivation conditions.

Fig. 36: Major pivot: Distribution of TVI for maize and wheat.

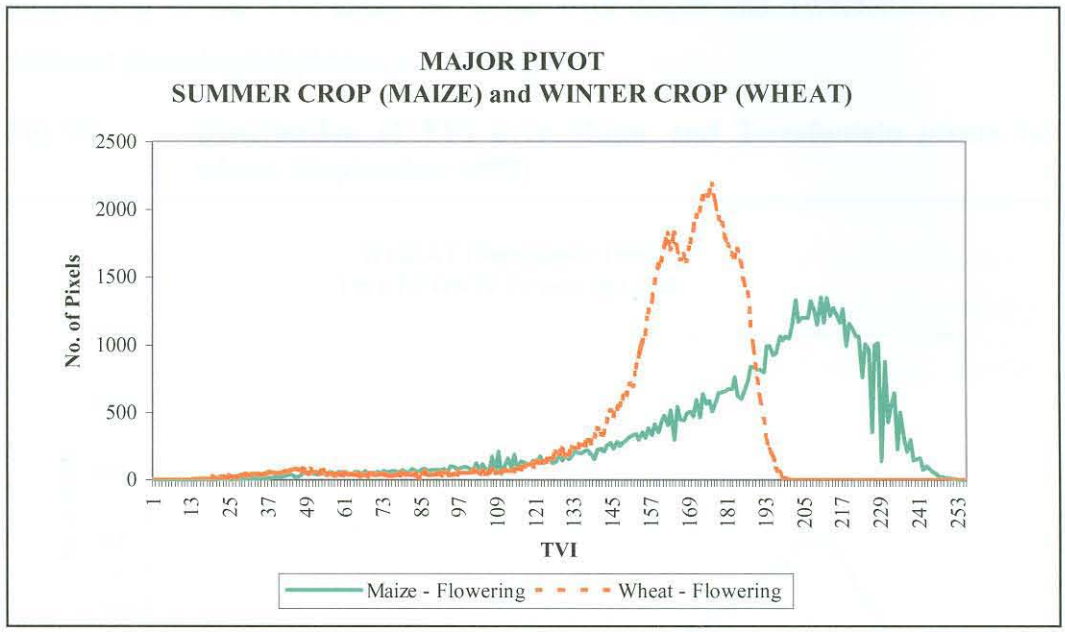

The same analysis has been conducted for the Tweefontein pivot (Fig. 37). The comparison here is between beans and wheat at the same time of survey.

Fig. 37: Tweefontein pivot: Distribution of TVI for beans and wheat.

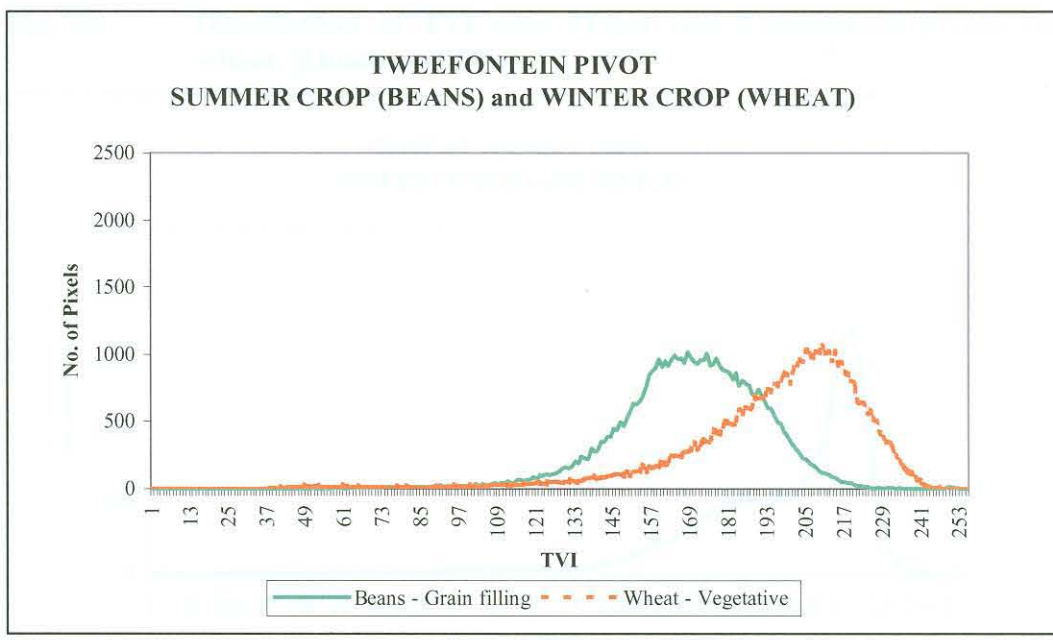

Wheat shows a higher overall maximum of the indicator (TVI), while the high spread of the index for both crops is roughly comparable. The reason for such a distribution could, in this case, be attributed to the characteristics of the pivots. What is shown in the two following diagrams (Figures 38 and 39) is the distribution of the TVI index for wheat over Major and Tweefontein, in two different phenological phases, a month apart.

Fig. 38: Distribution of TVI over Major and Tweefontein pivots for wheat. (September 1999)

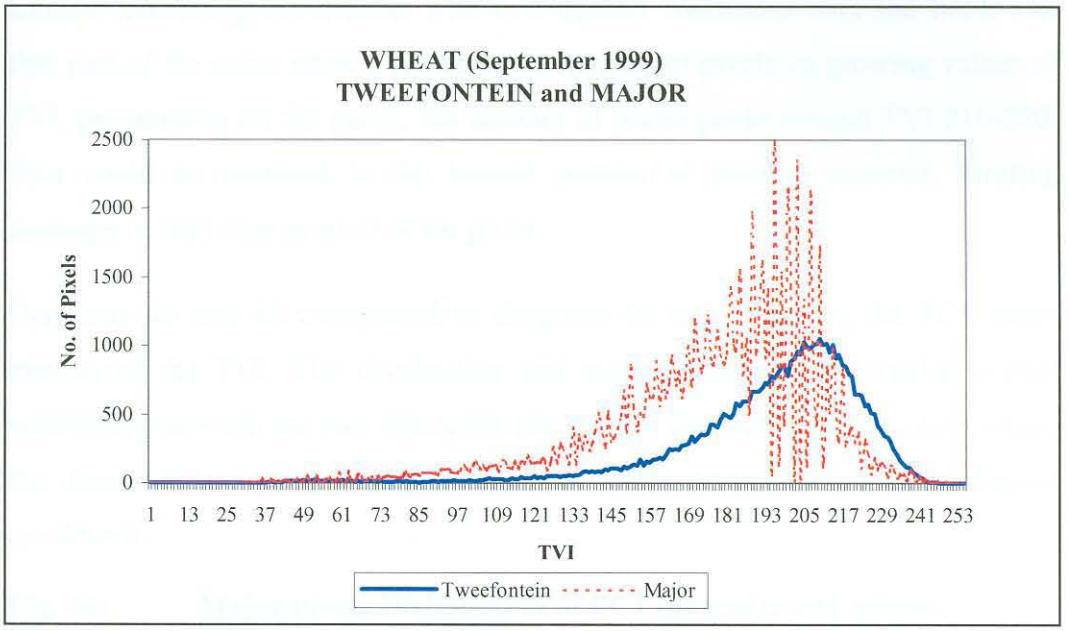

Fig. 39: Distribution of TVI over Major and Tweefontein pivots for wheat. (October 1999)

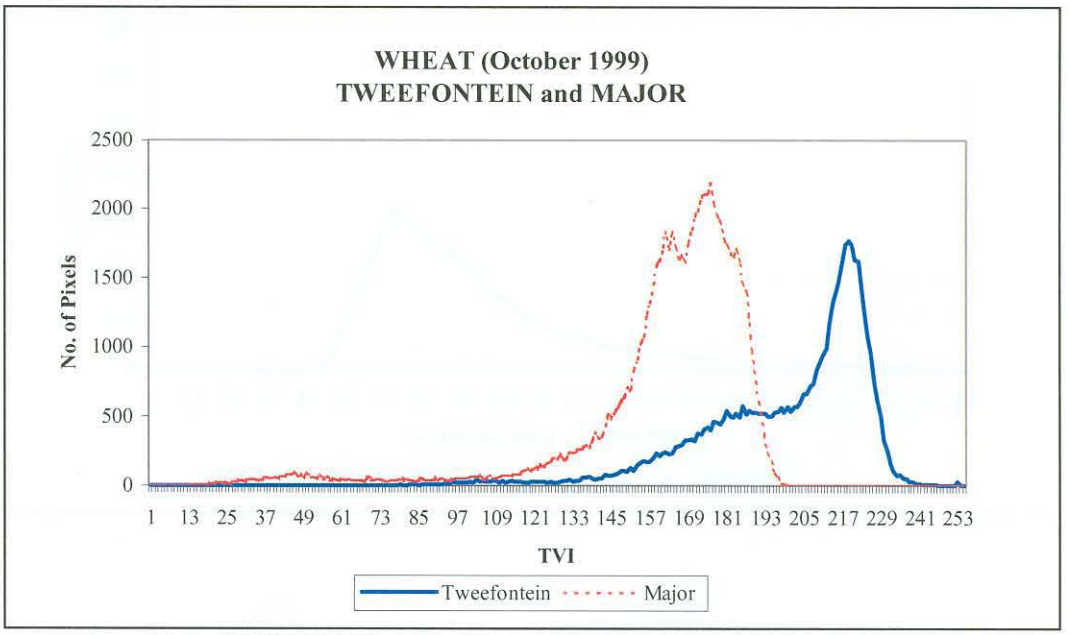

As was clear from Figure 37, Tweefontein seems to have higher values of the TVI index while the spread is roughly comparable. The variability of the index, however, was much higher over Major in the September survey and then it stabilized in October. There are not enough elements of analysis to explain such an event, it could however be attributed to a very recent irrigation event which resulted in peaks of high IR absorption to the wet crop.

The shape of the curve for Major in the October flight (See Fig. 39) shows another interesting occurrence, with two distinct conditions over the field. The first part of the curve show a rather stable number of pixels on growing values of TVI, progressing on the curve, the number of pixels peaks around TVI 210-220. This could be ascribed to the known portion of plinthic material, limiting drainage in the lower portion of the pivot.

Diagrams 40 and 41 correspond to diagrams 36 and 37, using the PC1 index instead of the TVI. The distribution and overall trends show similar overall behaviours between the two indicators but with an inverted scale of values where the lower PC1 indicates higher biomass levels and/or better physiological conditions.

Fig. 40: Major pivot: Distribution of PC1 for maize and wheat.

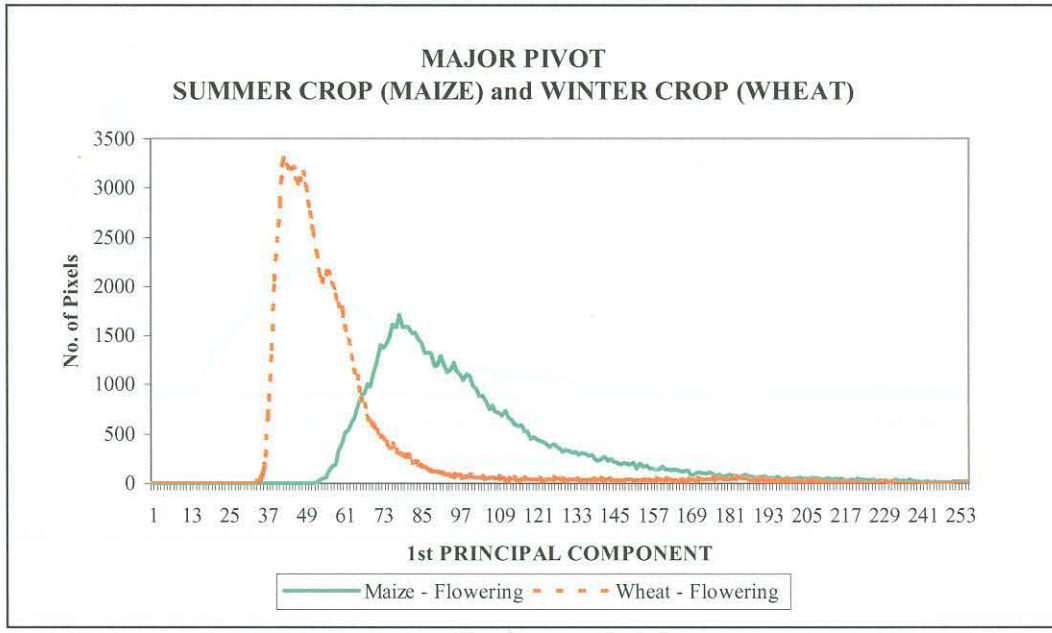

Fig. 41: Tweefontein pivot: Distribution of PC1 for the beans and wheat

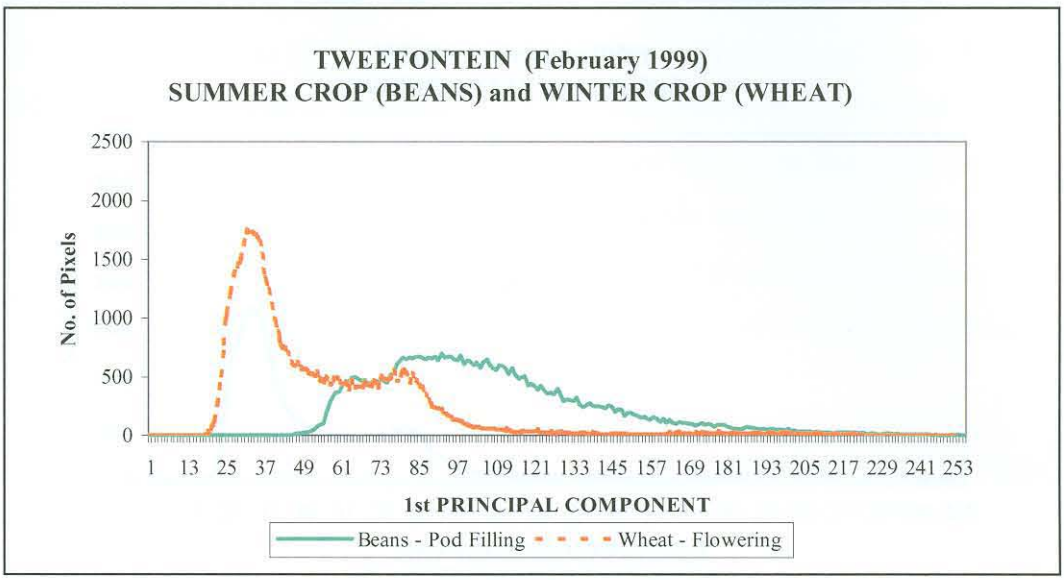

The same trend is apparent in Fig. 42 and 43, which are comparable to Fig. 38 and 39. A slight difference appears for the high variability of wheat over Tweefontein in September; the PC1 reflects it as an overall lower value.

Fig. 42: Distribution of PC1 over Major and Tweefontein pivots for wheat. (September 1999)

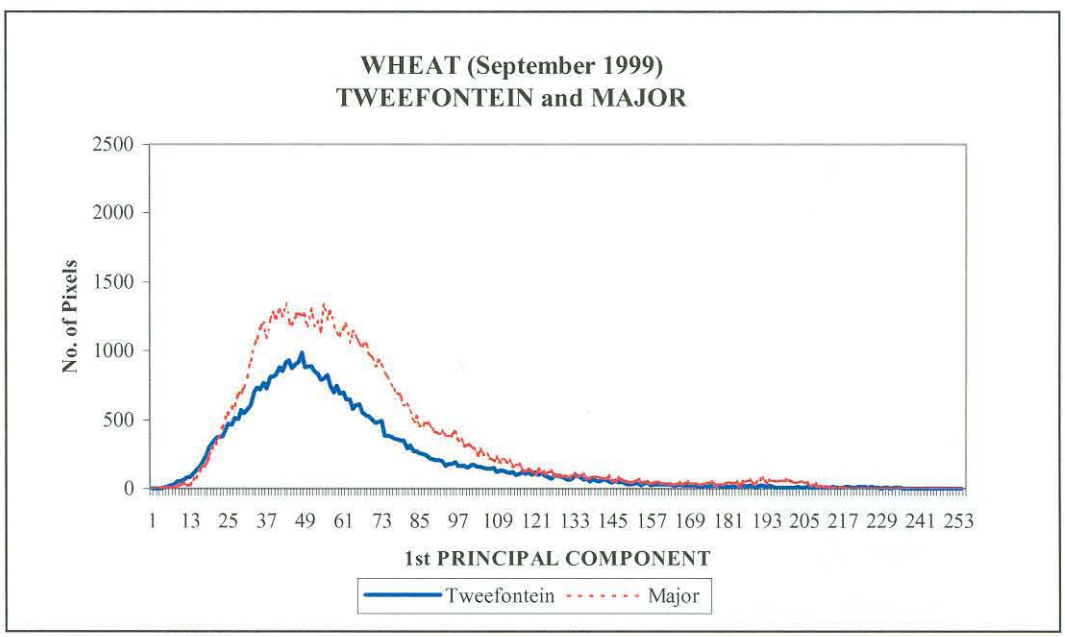

Fig. 43: Distribution of PC1 over Major and Tweefontein pivots for wheat. (October 1999)

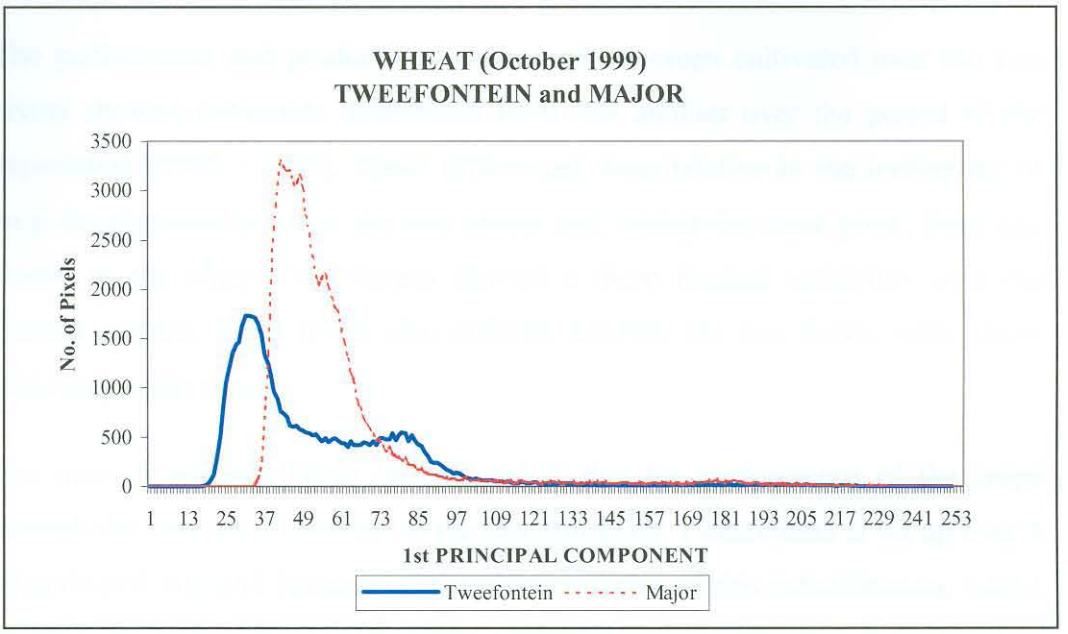

8. DISCUSSION AND CONCLUSIONS

The performance and productive outcome of the crops cultivated over the two pivots showed noticeable differences from one another over the period of the experiment (1998 - 1999). These differences were relative to the uniformity of crop development between the two pivots and, within the same pivot, from one season to the other. Tweefontein showed a more marked variability over the planted surface. Yield levels also differed between the two fields, with Major achieving better results.

The main hypothesis being investigated is that the performance of the crops through the seasons differs due to the fact that Pivot Tweefontein is set up over a rehabilitated site and because of the characteristics of this rehabilitation, whilst Major is set on virgin land. The various hypotheses that were explored in the data analysis can be summarised as follows:

- Better performance and less variability should be experienced on the pivot on virgin land (Major) as compared to the one on rehabilitated land (Tweefontein). The causes of this are problems with sub-soil/soil preparation practices in the rehabilitation process. The location of areas with different levels of soil compaction may affect the drainage and should be identified by the soil profile to spoil/impermeable layer and reflected on the surface by the variability in the crop canopy.

- Better performance and less variability should be experienced for winter crops (wheat) with respect to summer crops (maize and beans), especially on rehabilitated profiles under irrigated conditions where there is control over the water balance. The possible conclusion is that rehabilitated pivots can be irrigated successfully in winter while they can take only supplemental irrigation in summer, otherwise there could be water logging. Alternatively, in summer, crops that can take 'wet feet' should be used, or else crops should be produced under dry land conditions, in some areas.

- Rehabilitation should be appropriate and a slight slope given to the surface to allow drainage. Alternatively a drainage system should be built.

For Pivot Tweefontein, the variability of the crop canopy can be attributed to the non-uniform preparation of the soil when the land was reclaimed from open cast mining. For Pivot Major, on the other hand, the internal variability may also be due to the soil substratum. In this case it is not ascribed to any human activity, but rather to the presence of a shallow impermeable layer in certain areas.

The limited duration of the experiment made it impossible to return to the site and verify the assumptions. This means that the comparison of the two pivots does not authorise any definitive conclusion or recommendation of 'best practices' for either soil preparation or cultivation.

However, the foremost achievement of this study was the design and implementation of a system for the analysis of spatial variability over cultivated fields, and such a system has the potential of evolving into an innovative crop management tool.

The whole technological approach relies on the use of remote sensing and GIS and this requires a certain level of evolution and revision in the way the data is acquired, stored and even analysed. The use of imagery as a source of information guarantees timeliness of data availability and a synoptical and thus complete view of the fields. This guides and sets the standard for all the other data gathering actions. On the analysis side, the amount of data made available by remote sensing and processed by a GIS is such that traditional and interactive analysis and interpretation is somewhat limiting. The system requires a high level of automation of the analysis procedure and this drives toward the rationalisation of such procedures. The basis of the whole philosophy is that the data that are run through the system are the most objective and synoptic as technically possible and the evaluation of the data itself is conducted through strictly analytical and statistically consistent procedures.

LIST OF FIGURES

Fig. 1: Flow chart of the methodological approach 18
Fig. 2: The Jabiru micro-light aircraft 20
Fig. 3: The Digital Multi-Spectral Video System 21
Fig. 4: Spectral set up of the STS-DMSV sensor 23
Fig. 5: Digital vector of the project pivots on Kleinkopjé Mine, overlaid to an aerial photograph *(no scale available)* 24
Fig. 6: Flight plan for the February 1999 aerial survey 25
Fig. 7: Images acquired for the Major (left) and Tweefontein (right) pivots in December 1998 26
Fig. 8: Images acquired for the Major (left) and Tweefontein (right) pivots in April 1999 27
Fig. 9: Images acquired for the Major (left) and Tweefontein (right) pivots in August 1999 27
Fig. 10: Images acquired for the Major (left) and Tweefontein (right) pivots in October 1999 27
Fig. 11: Stratification of the Major (left) and Tweefontein (right) pivots, where the each colour represents a different stratum. 29
Fig. 12: Sampling plan 29
Fig. 13: False colour composite of Major (left) and Tweefontein (right) ivots, February 1999. 41
Fig. 14: False colour composite of Major (left) and Tweefontein (right) pivots, September 1999. 41
Fig. 15: Vegetation Index maps of Major (left) and Tweefontein (right) pivots, during the second (top) (February 1999) and third flight (bottom) (September 1999). 44
Fig. 16: Principal component maps of Major (left) and Tweefontein (right) pivots for the third flight (September 1999) 46
Fig. 17: Point measurements of height a.s.l. from a GPS data-logger mounted on the harvester for Major (left) and Tweefontein (right). 52
Fig. 18: DEM map of Major (left) and Tweefontein (right). 52

Fig. 19: Location of the auger sampling points for Major (left) and Tweefontein (right).....53
Fig. 20: Depth to the impermeable layer for Major (left) and Tweefontein (right).....54
Fig. 21: Spoil/Impermeable layer DEM map of Major (left) and Tweefontein (right).....55
Fig. 22: Micro depressions of Major (left) and Tweefontein (right).....56
Fig. 23: The micro drainage lines for Major (left) and Tweefontein (right).....56
Fig. 24: The depth of the vadoze zone map for Major (left) and Tweefontein (right).....57
Fig. 25: Representation of the soil profile and the vadoze zone.....57
Fig. 26: Available water capacity map in the surface 20 cm layer for Major (left) and Tweefontein (right).....59
Fig. 27: Available water capacity map in the 20 cm to spoil/impermeable layer for Major (left) and Tweefontein (right).....59
Fig. 28: Total Available Water Capacity map for Major (left) and Tweefontein (right).....60
Fig. 29: The ground cover maps for Major (left) and Tweefontein (right).....61
Fig. 30: The Top dry matter production maps for Major (left) and Tweefontein (right).....62
Fig. 31: The LAI maps for Major (left) and Tweefontein (right).....62
Fig. 32: Yield maps of wheat (Spring 1999) for Major (left) and Tweefontein (right).....63
Fig. 33: Crop moisture maps of wheat (Spring 1999) for Major (left) and Tweefontein (right).....63
Fig, 34: Correlation map between top matter production and LAI for Pivot Major with a moving window of 20*20 pixels.....75
Fig. 35: Correlation map between top top dry matter production and LAI for Pivot Tweefontein with a moving window of 20*20 pixels.....75
Fig. 36: Major pivot: Distribution of TVI for maize and wheat.....82
Fig. 37: Tweefontein pivot: Distribution of TVI for beans and wheat.....82

Fig. 38: Distribution of TVI over Major and Tweefontein pivots for wheat. (September 1999) 83
Fig. 39: Distribution of TVI over Major and Tweefontein pivots for wheat. (October 1999) 83
Fig. 40: Major pivot: Distribution of PC1 for maize and wheat. 84
Fig. 41: Tweefontein pivot: Distribution of PC1 for the beans and wheat 85
Fig. 42: Distribution of PC1 over Major and Tweefontein pivots for wheat. (September 1999) 85
Fig. 43: Distribution of PC1 over Major and Tweefontein pivots for wheat. (October 1999) 86

LIST OF TABLES

Table 1: Characteristics of the Jabiru Engine 19
Table 2: Spatial resolution and coverage of the STS-DMSV Sensor with 12 mm focal length lens 24
Table 3: Soil and canopy measurements for the Major Pivot for wheat in September 1999 32
Table 4: Soil and canopy measurements for Tweefontein Pivot 33
Table 5: Static data layers for Major Pivot 49
Table 6: Dynamic data for Major Pivot 50
Table 7: Static data for Tweefontein Pivot 50
Table 8: Dynamic data for Tweefontein Pivot 50
Table 9: Major Pivot: Correlation coefficients (r) between the various data layers 70
Table 10: Tweefontein Pivot: Correlation coefficients (r) between the various data layers 70
Table 11: Summery statistics of focal correlations for wheat, 1999 for Major and Tweefontein 76
Table 12: Analysis of the Vegetation Index variability: Statistics 78
Table 13: Analysis of the Vegetation Index variability: Variations across the pivots 79
Table 14: Analysis of the First Principal component: Statistics 80
Table 15: Analysis of the PC1: Variations across the pivots 80
Table 16: Analysis of Yield: Statistics 81

APPENDIX 1: STATIC AND DYNAMIC MAPS75

Pivot Major

Static Maps	Unit	Page
Available Water Capacity map of the first 20 cm of soil	mm	95
Available Water Capacity map from 20 to the spoil/ impermeable layer	mm	96
Total Available Water Capacity map	mm	97
Depth to spoil map	mm	98
Depth of vadoze zone map	mm	99
Surface DEM map	m (a.s.l.)	100
Spoil DEM map	m (a.s.l.)	101
Dynamic Maps		
Multi-Spectral image 08/99 Flight		102
Multi-Spectral image 10/99 Flight		103
Transformed Vegetation Index (TVI) map 08/99 flight		104
Transformed Vegetation Index (TVI) map 10/99 flight		105
First Principal Component (PC1) map 08/99 flight		106
First Principal Component (PC1) map 10/99 flight		107
Wheat yield map 11/99	$t\ ha^{-1}$	108
Wheat crop moisture map, yield 11/99	%	109
Ground cover map 08/99	%	110
Top dry matter map 08/99	$g*m^{-2}$	111
LAI map 08/99	m^2*m^{-2}	112

Pivot Tweefontein

Static Maps	Unit	Page
Available Water Capacity map of the first 20 cm of soil	mm	113
Available Water Capacity map from 20 to the spoil/ impermeable layer	mm	114
Total Available Water Capacity map	mm	115
Depth to spoil map	mm	116
Depth of vadoze zone map	mm	117
Surface DEM map	m (a.s.l.)	118
Spoil DEM map	m (a.s.l.)	119
Dynamic Maps		
Multi-Spectral image 08/99 Flight		120
Multi-Spectral image 10/99 Flight		121
Transformed Vegetation Index (TVI) map 08/99 flight		122
Transformed Vegetation Index (TVI) map 10/99 flight		123
First Principal Component (PC1) map 08/99 flight		124
First Principal Component (PC1) map 10/99 flight		125
Wheat yield map 11/99	$t\ ha^{-1}$	126
Wheat crop moisture map, yield 11/99	%	127
Ground cover map 08/99	%	128
Top dry matter map 08/99	$g*m^{-2}$	129
LAI map 08/99	m^2*m^{-2}	130

Pivot Major: AWC 0 - 20 cm

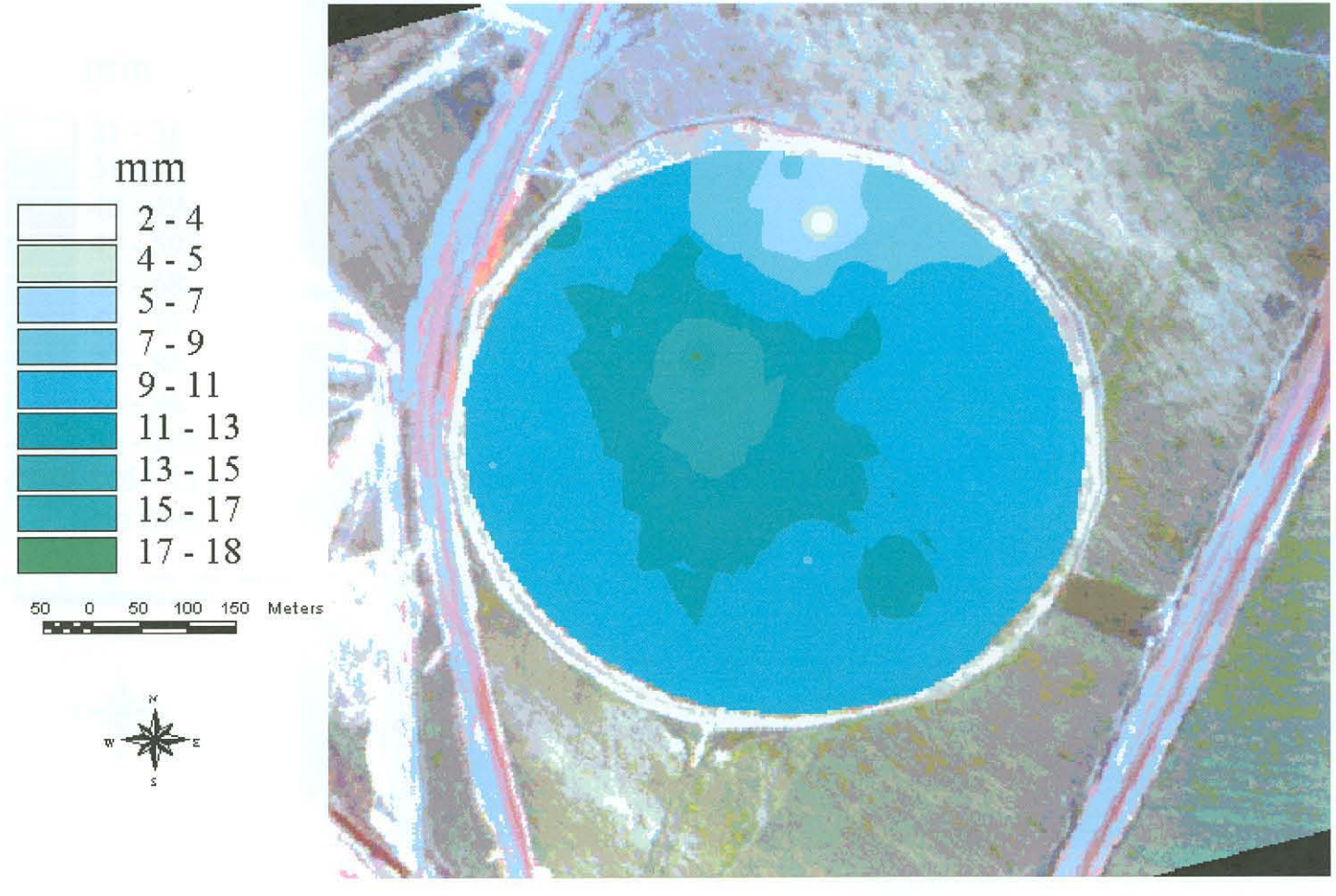

Pivot Major: AWC 20cm - Spoil/impermeable layer

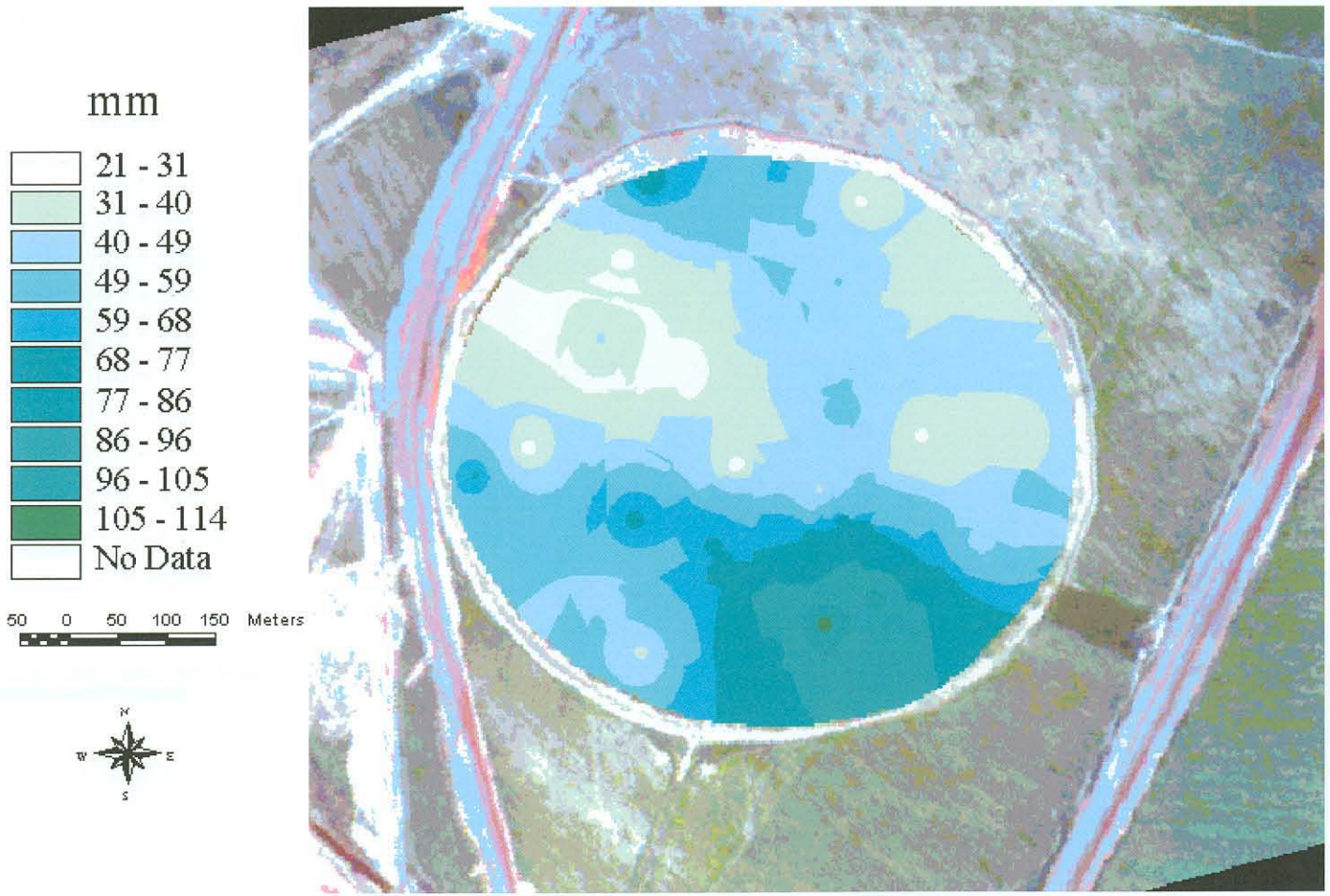

Pivot Major: AWC total

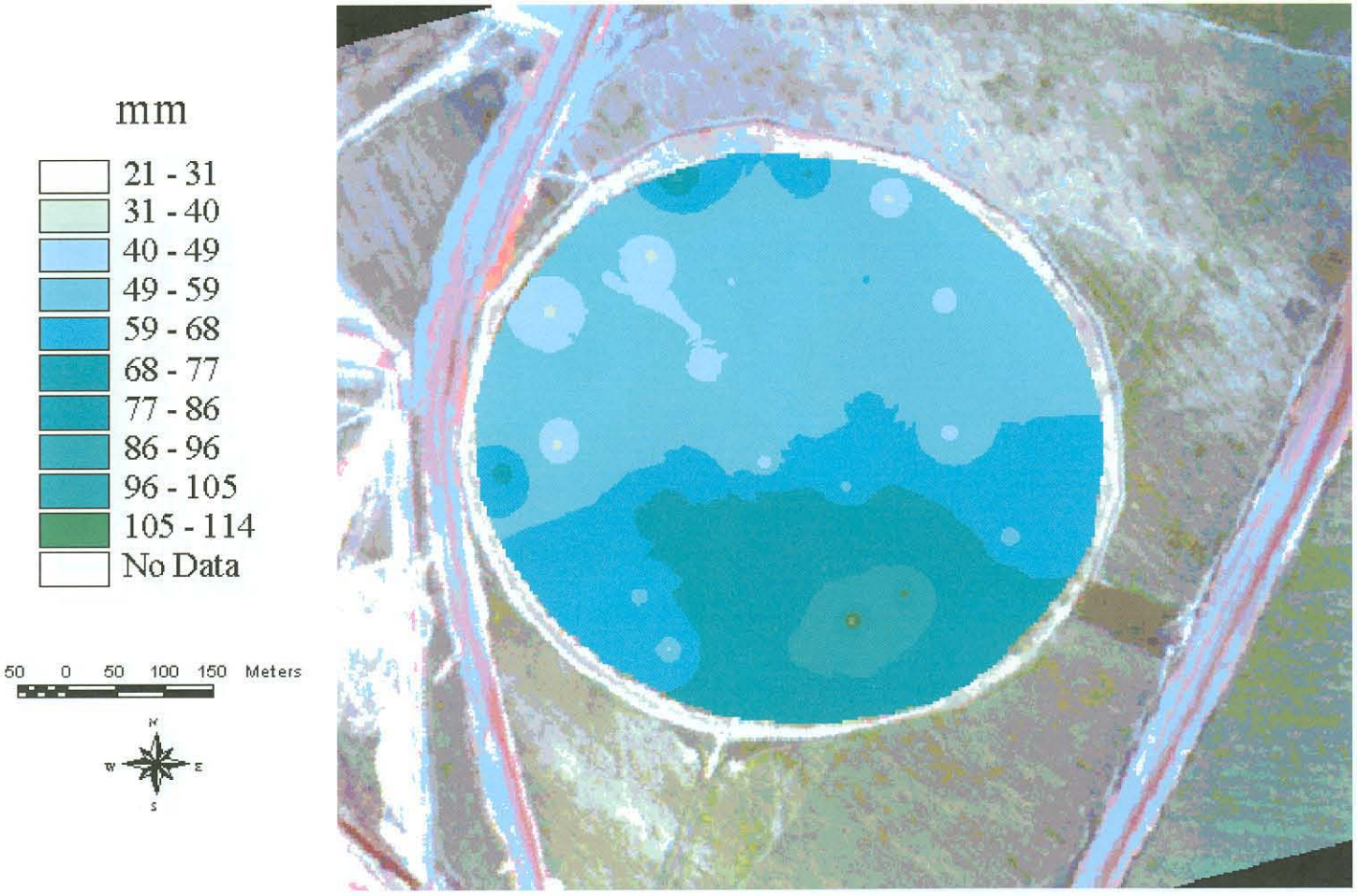

Pivot Major: Depth to Spoil/Impermeable Layer

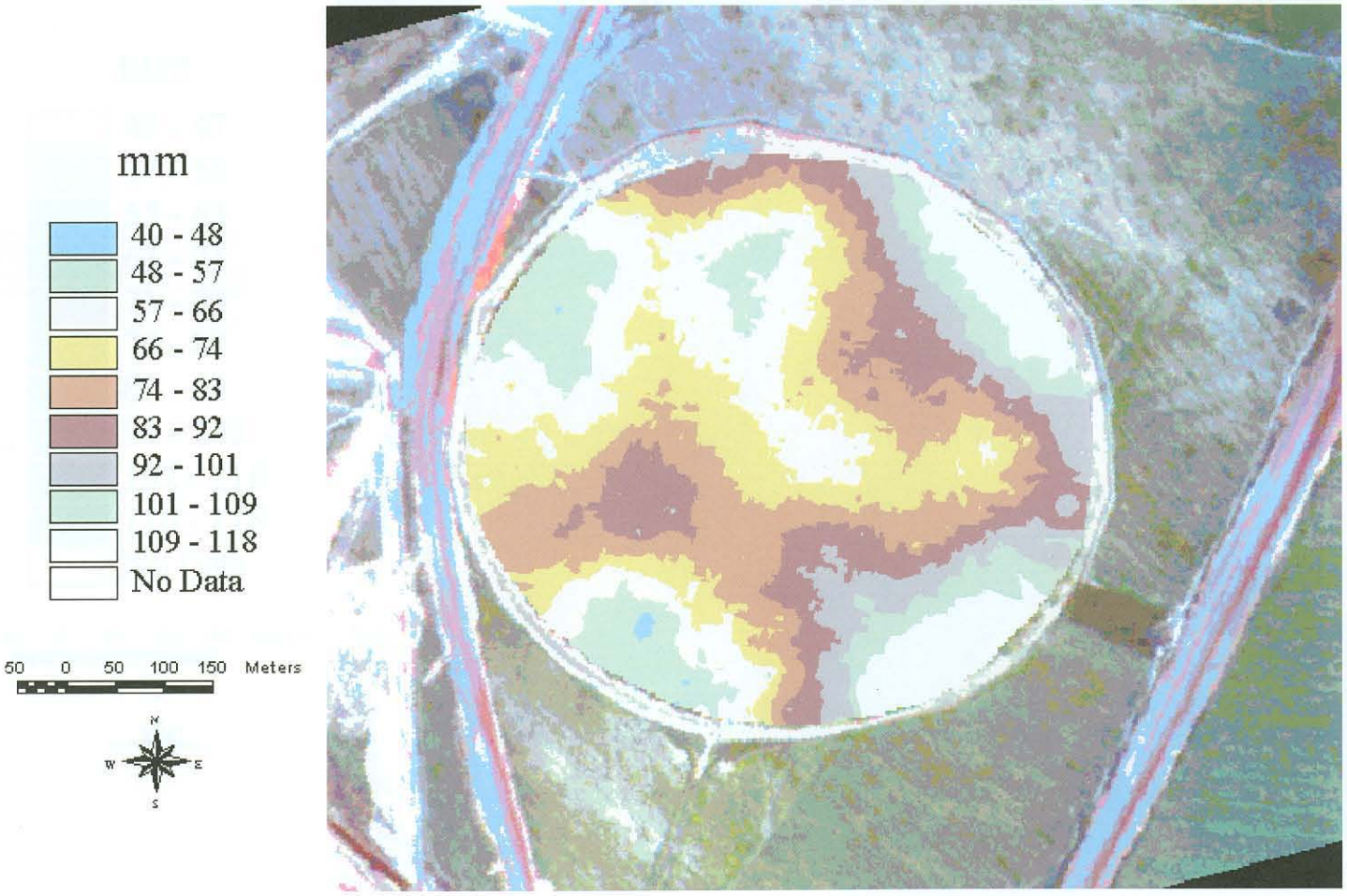

Pivot Major: Depth to Vadoze Zone

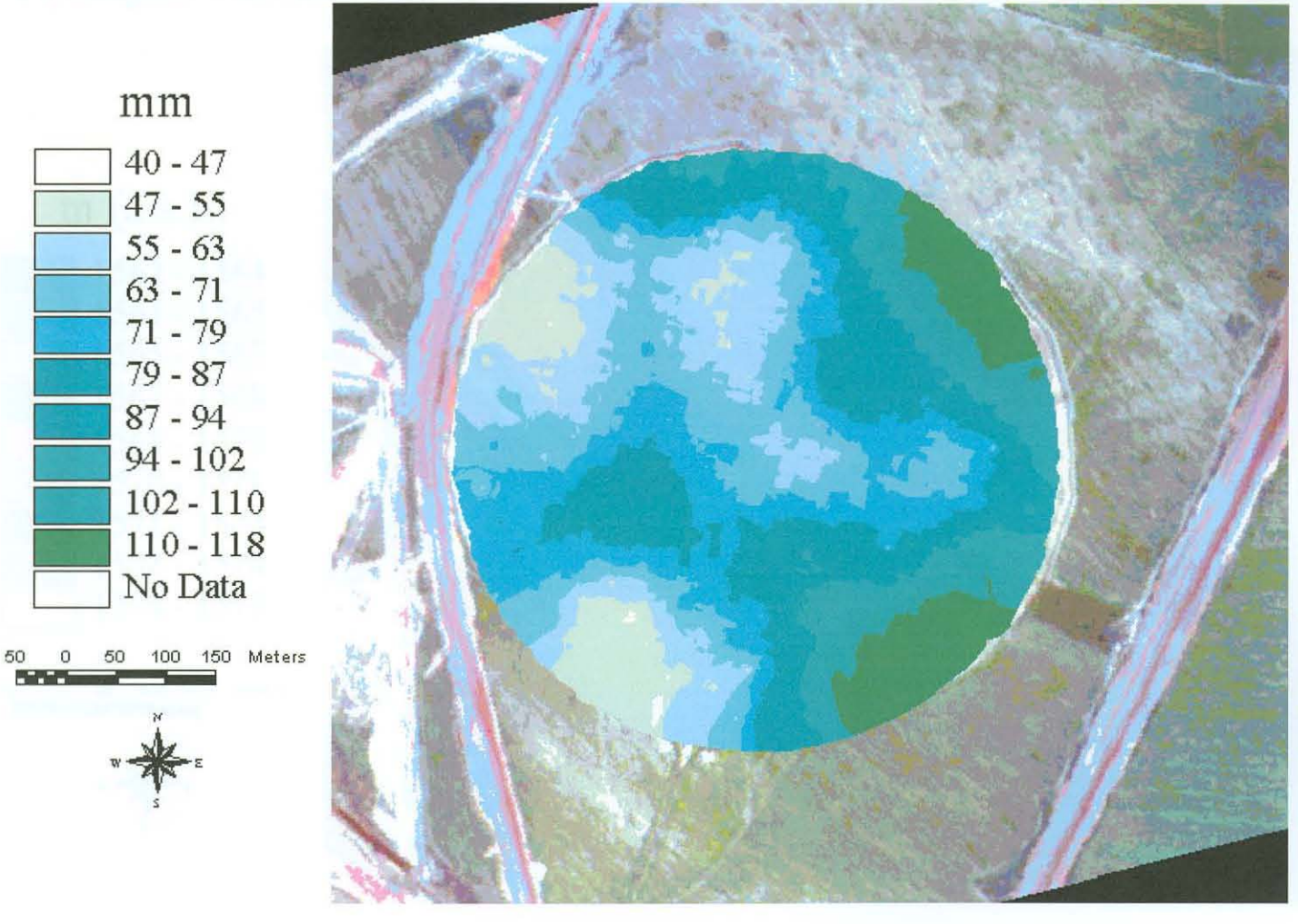

Pivot Major: Surface DEM

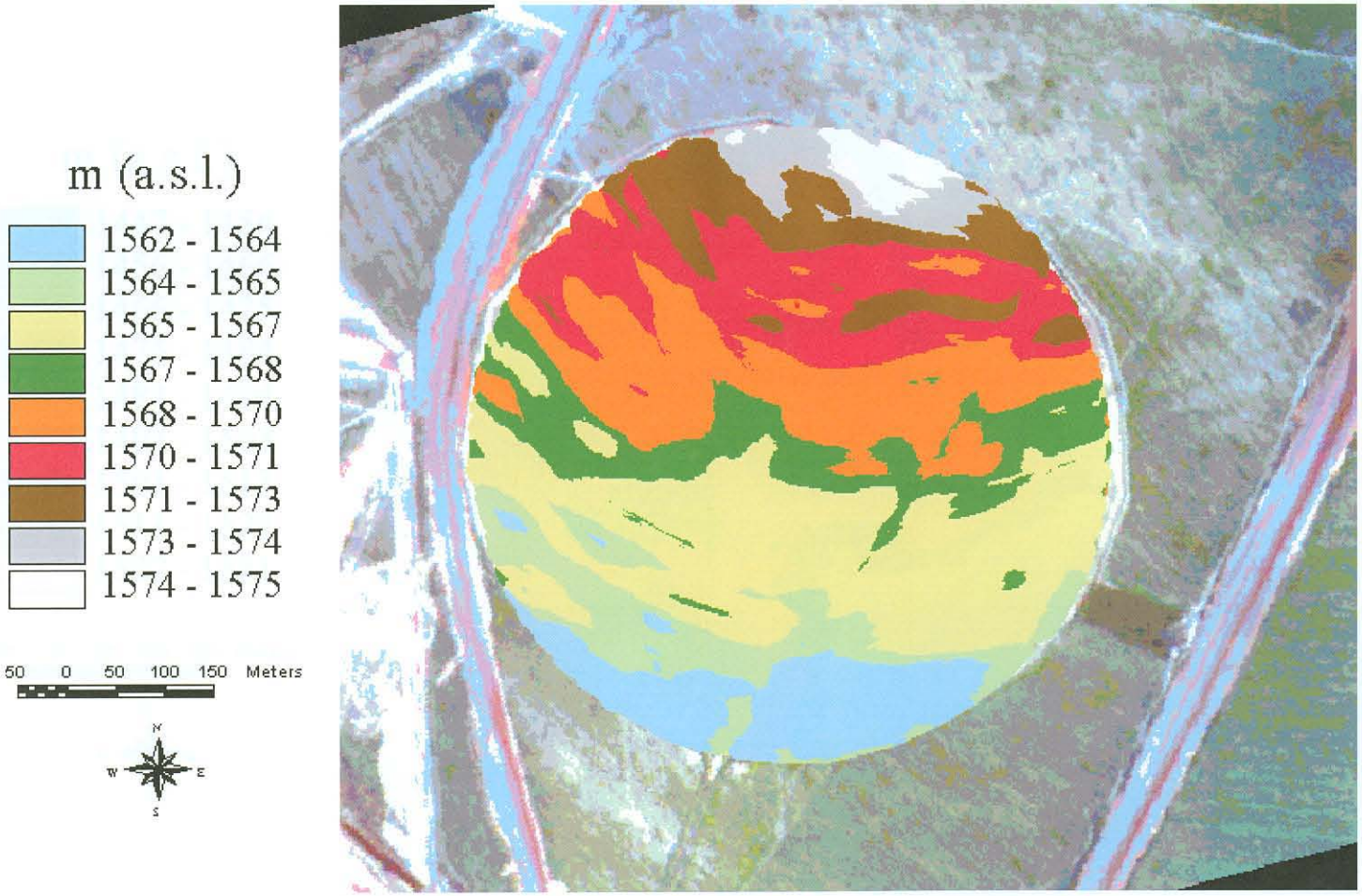

Pivot Major: Spoil DEM

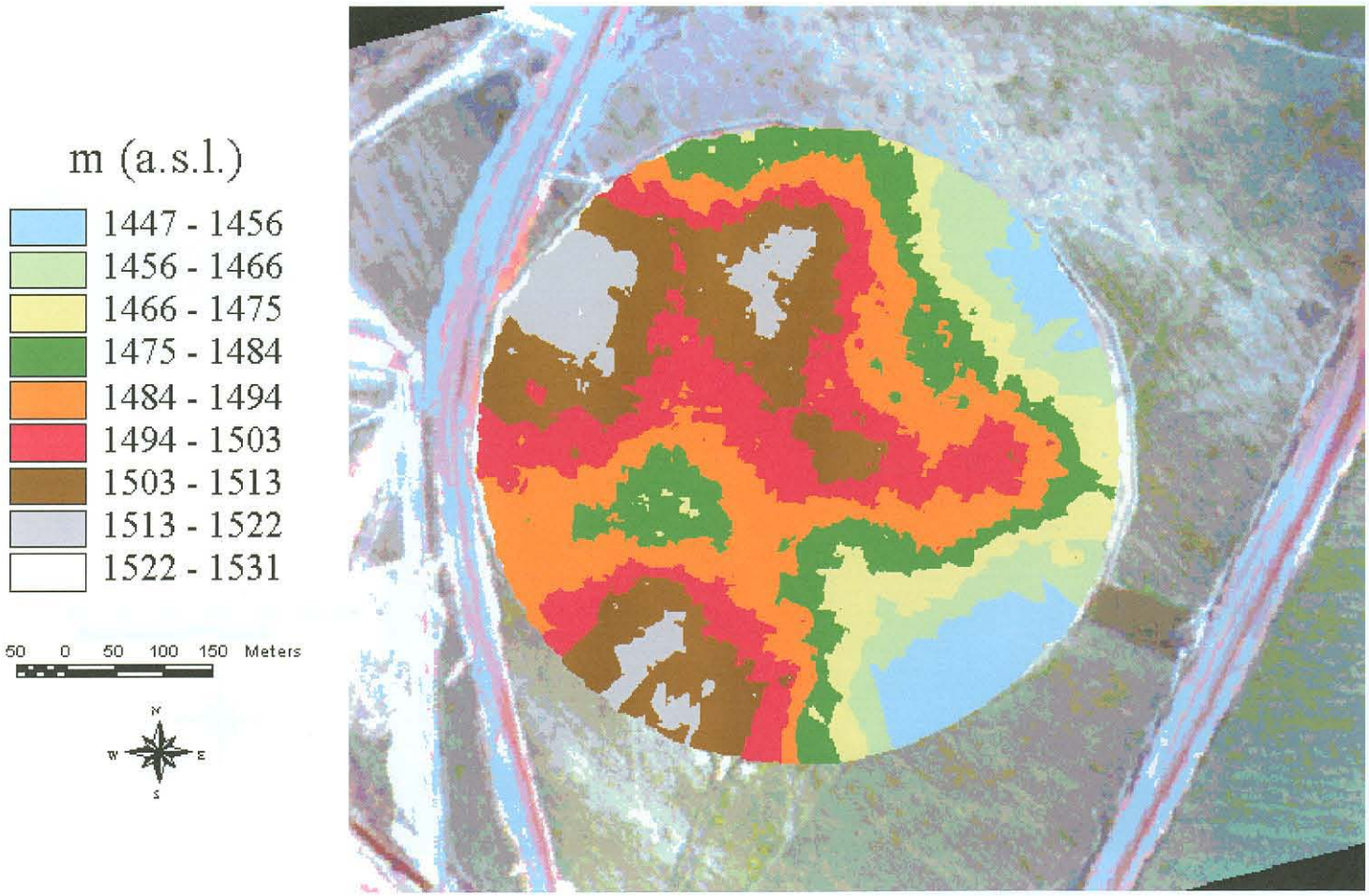

Pivot Major: 08/99 Flight

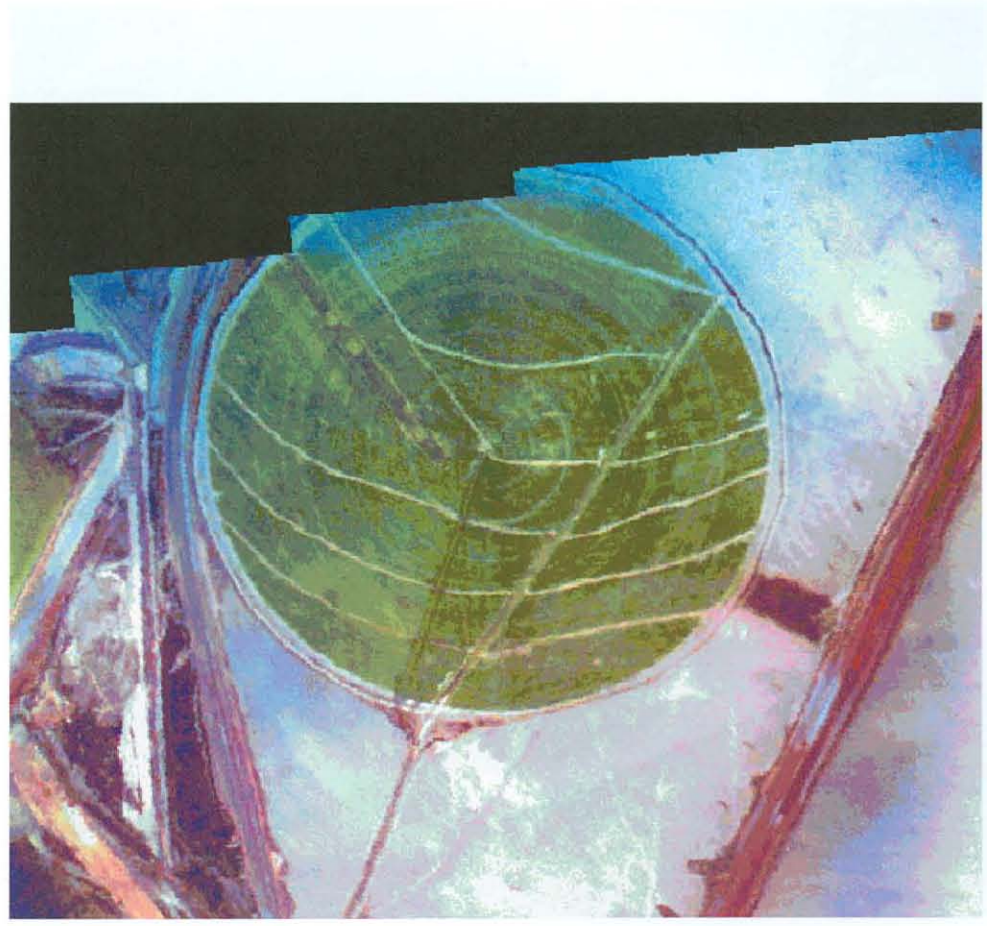

50 0 50 100 150 Meters

Pivot Major: 10/99 Flight

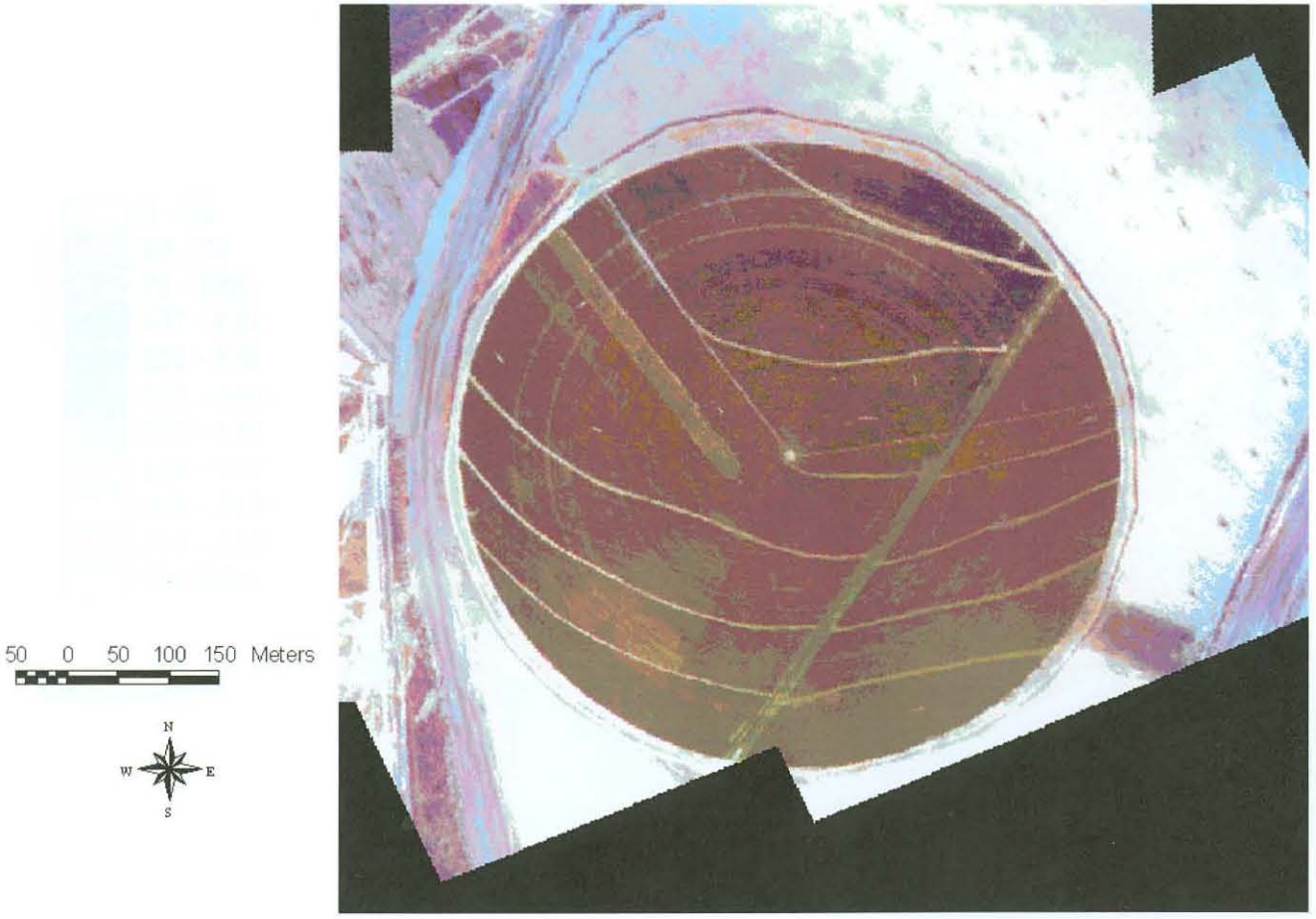

Pivot Tweefontein: TVI 08/99 Flight

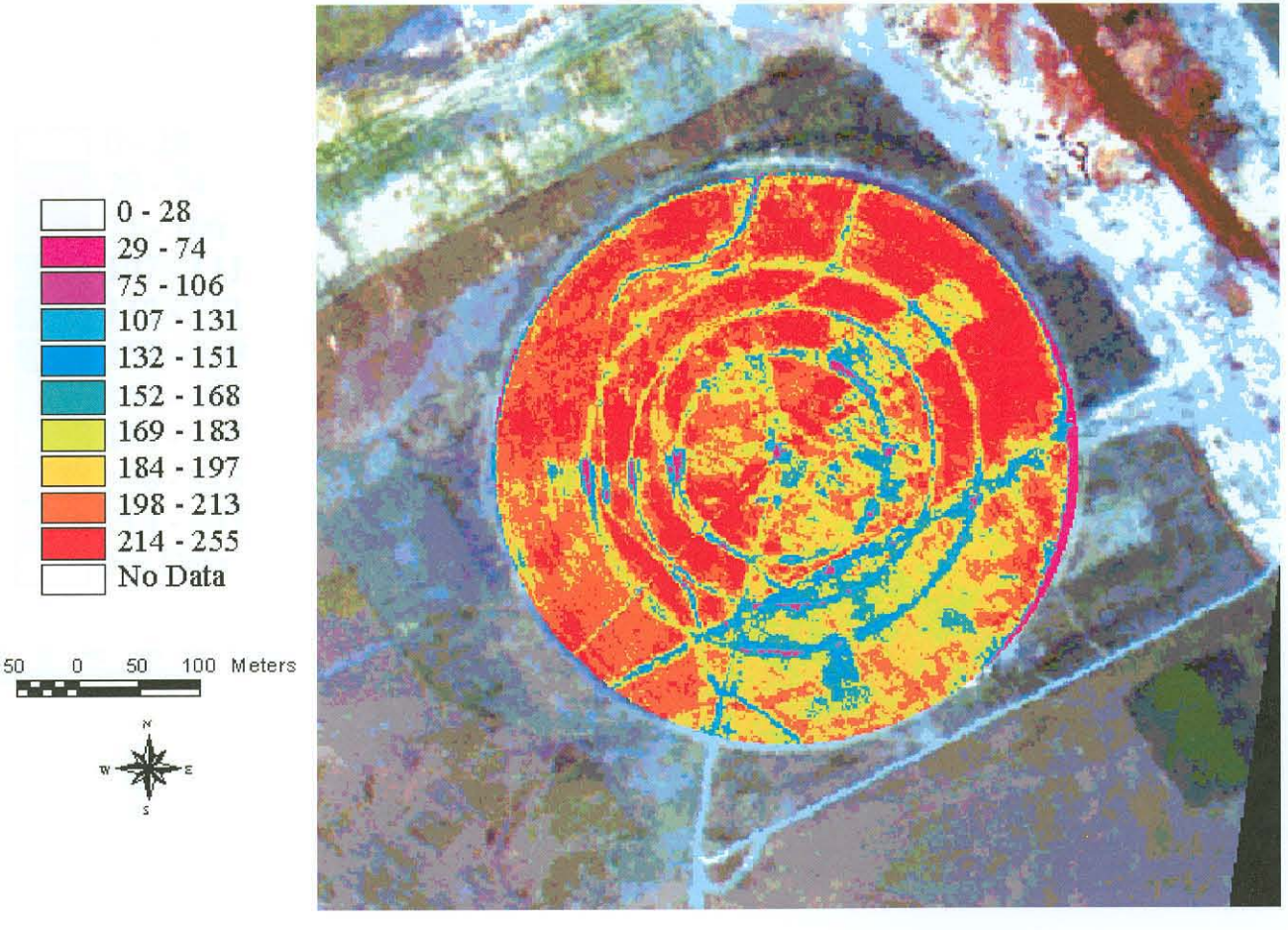

Pivot Major: TVI 10/99 Flight

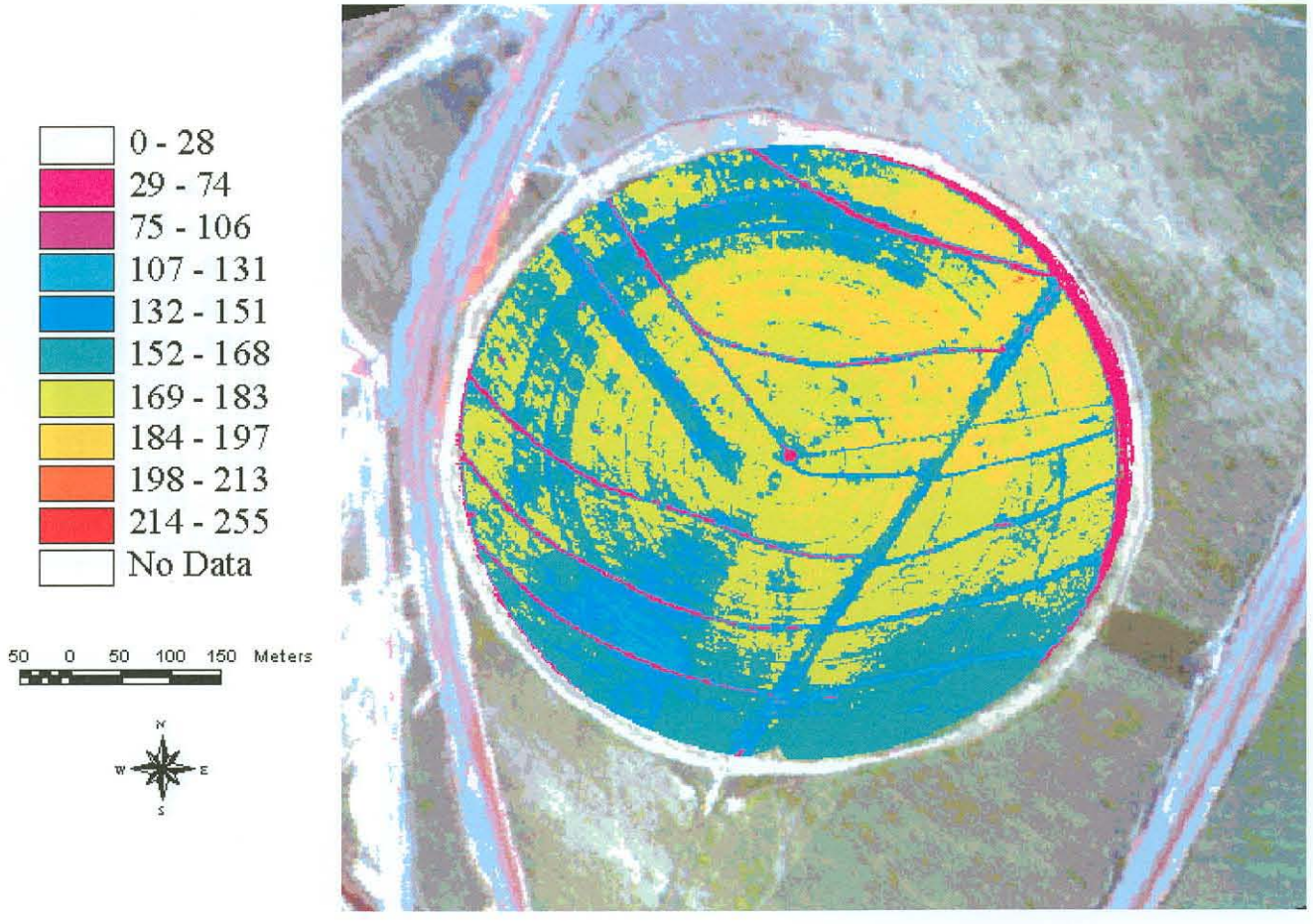

Pivot Major: PC1 08/99 Flight

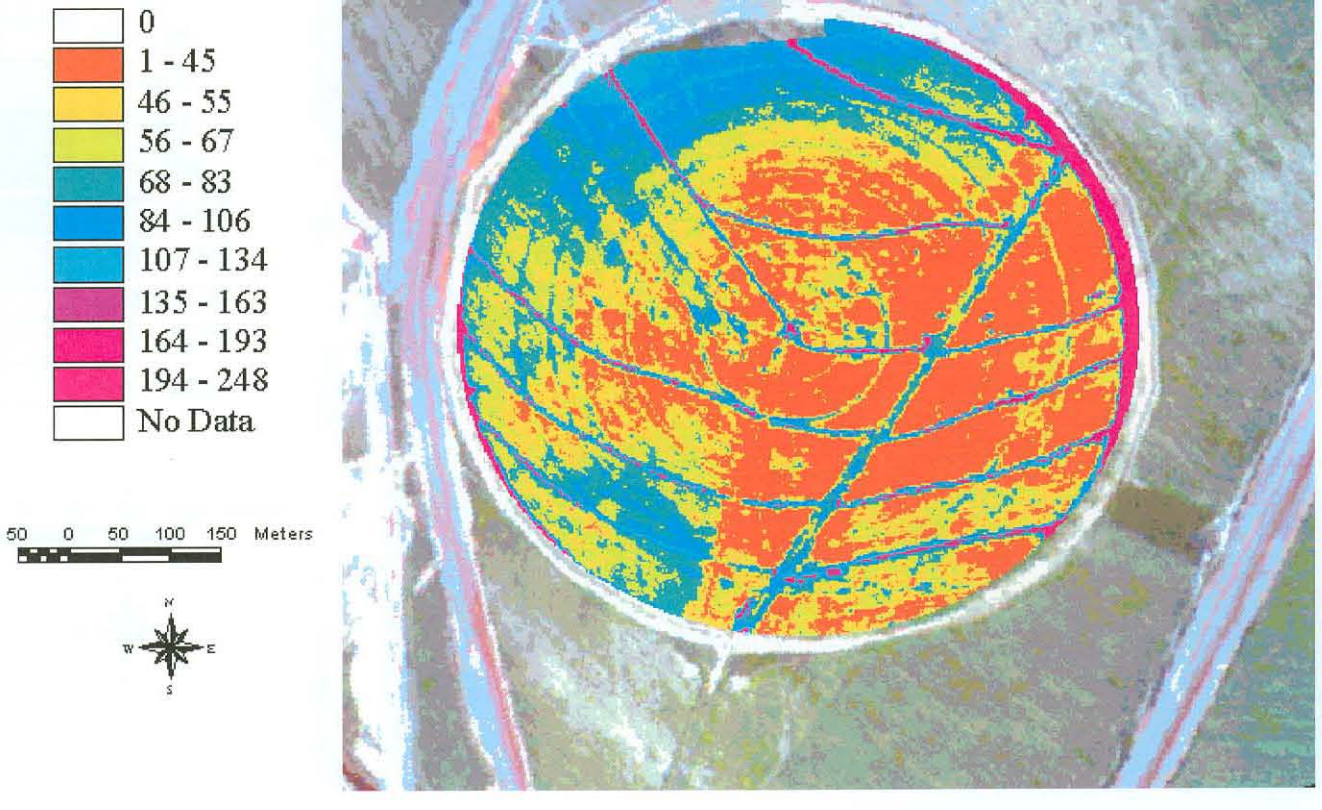

Pivot Major: PC1 10/99 Flight

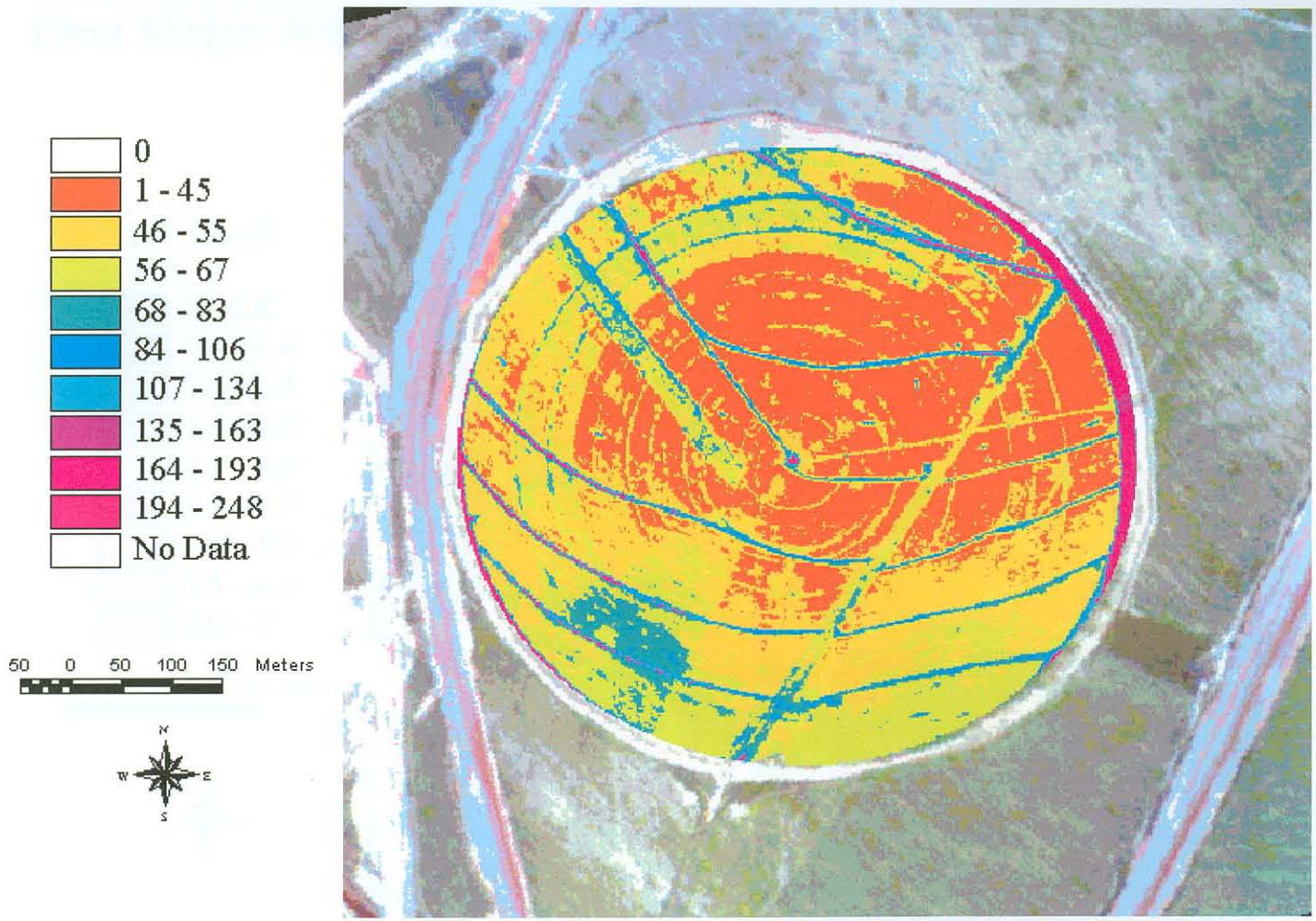

Pivot Major: Wheat yield, harvest 11/99

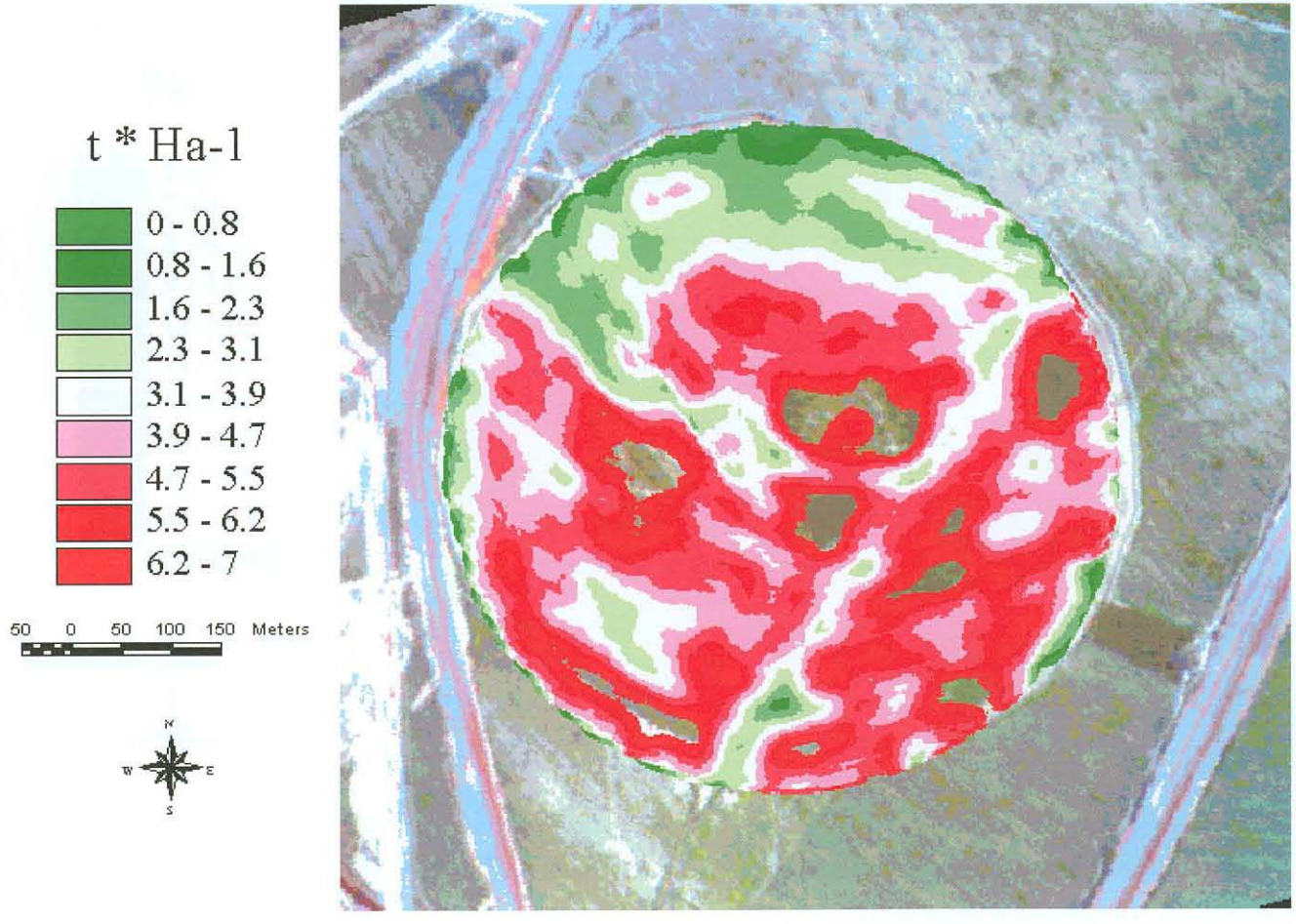

Pivot Major: Wheat moisture % at harvest

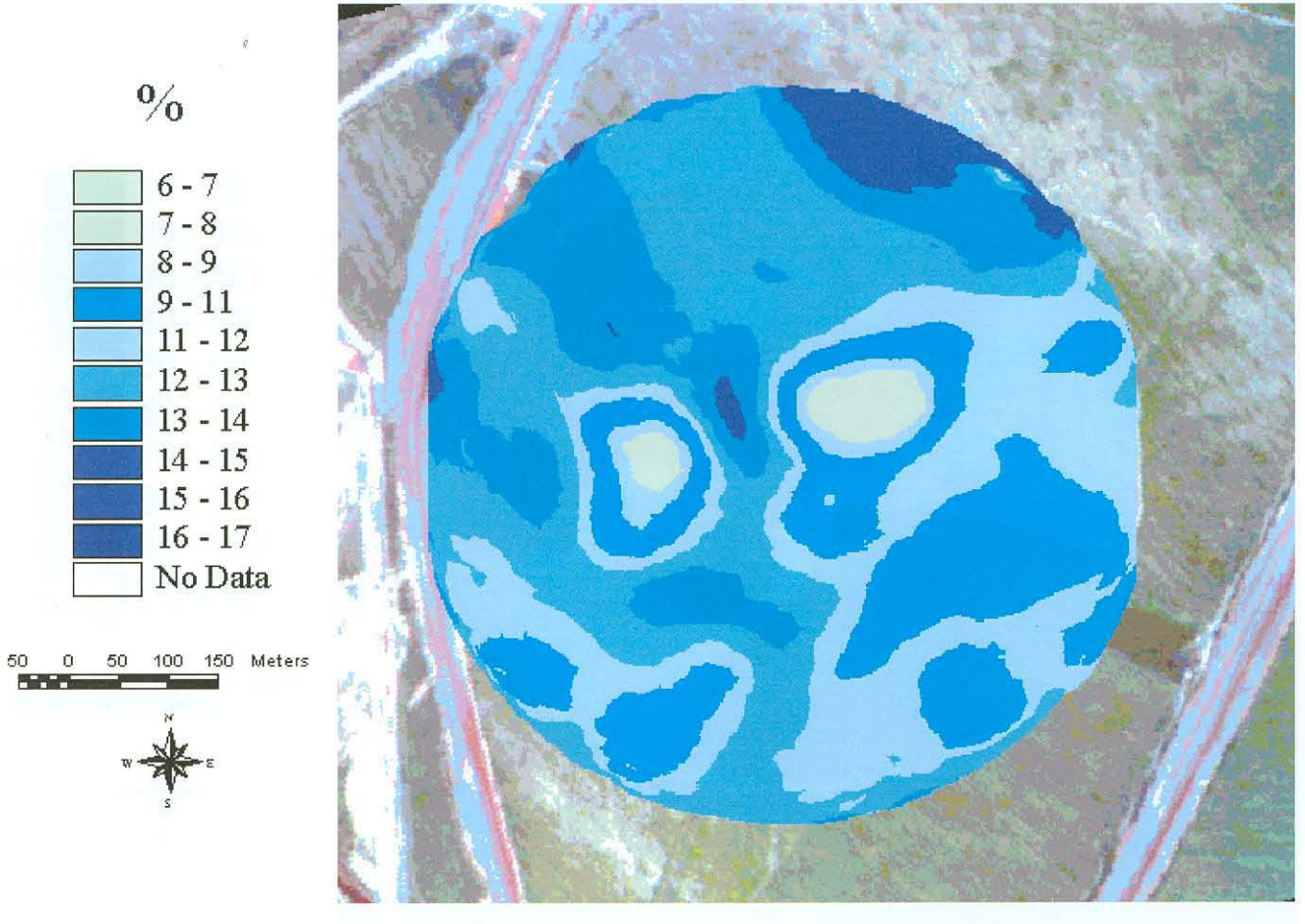

Pivot Major: Ground Cover 08/99

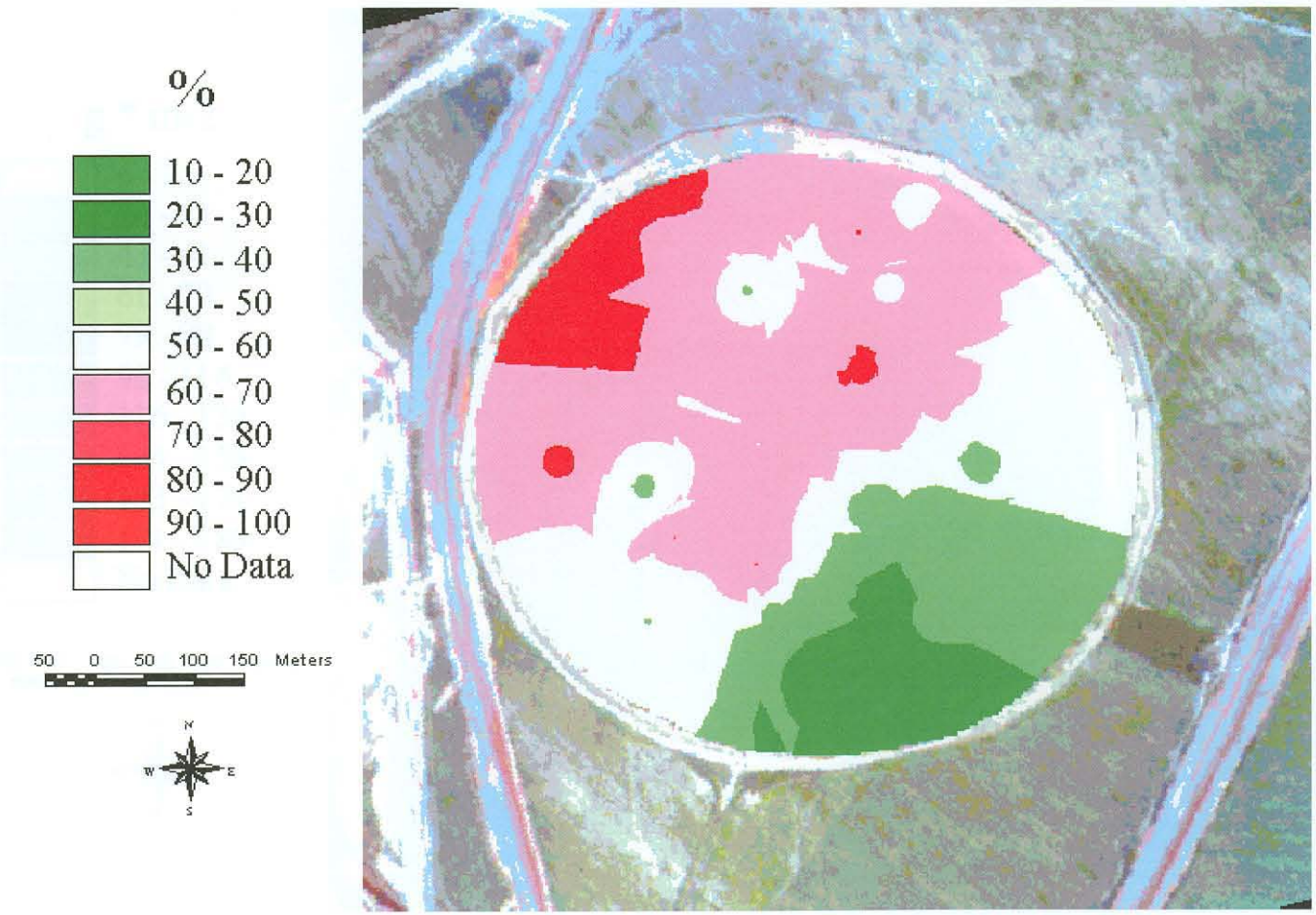

Pivot Major: Top dry matter 08/99

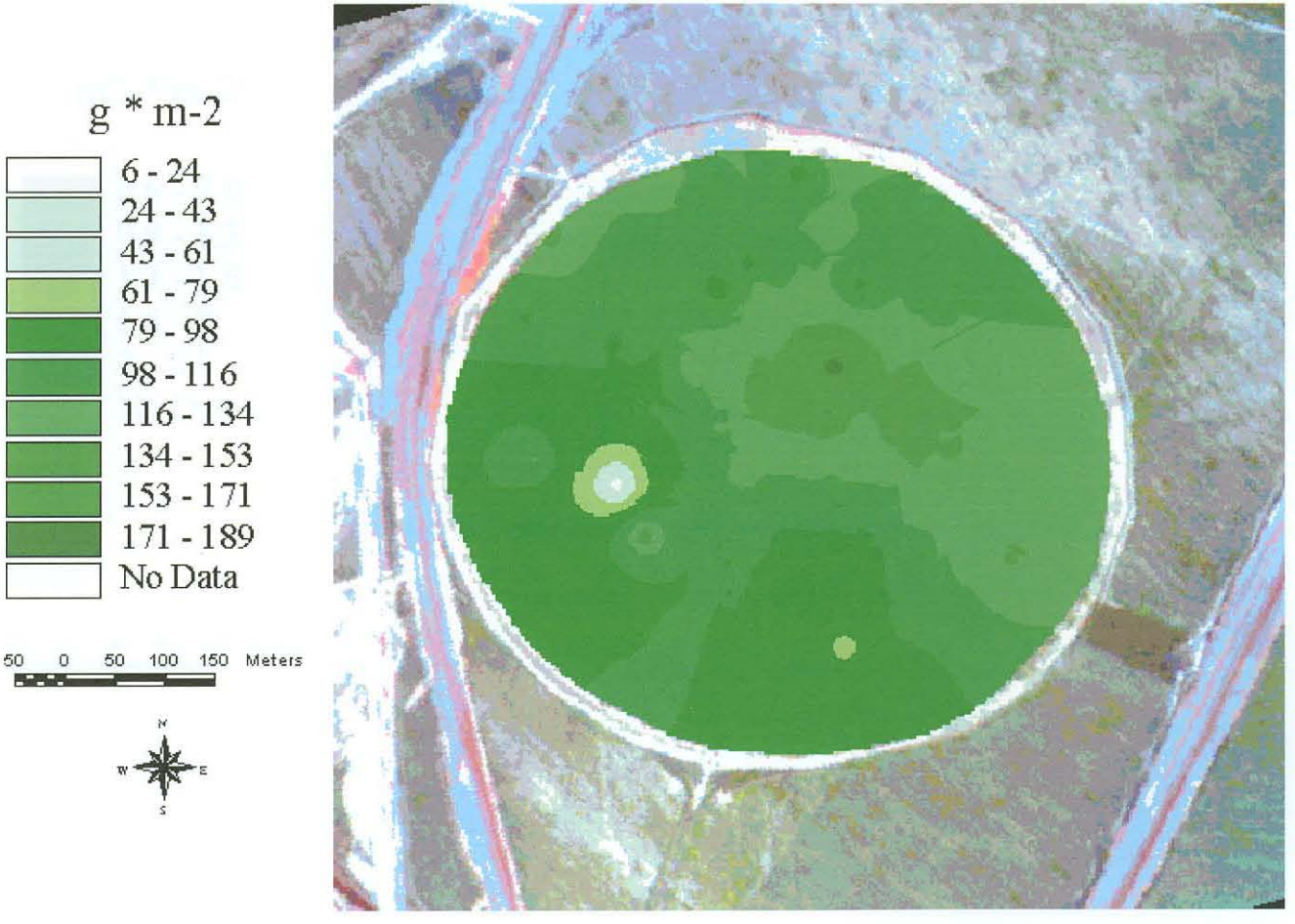

Pivot Major: LAI 08/99

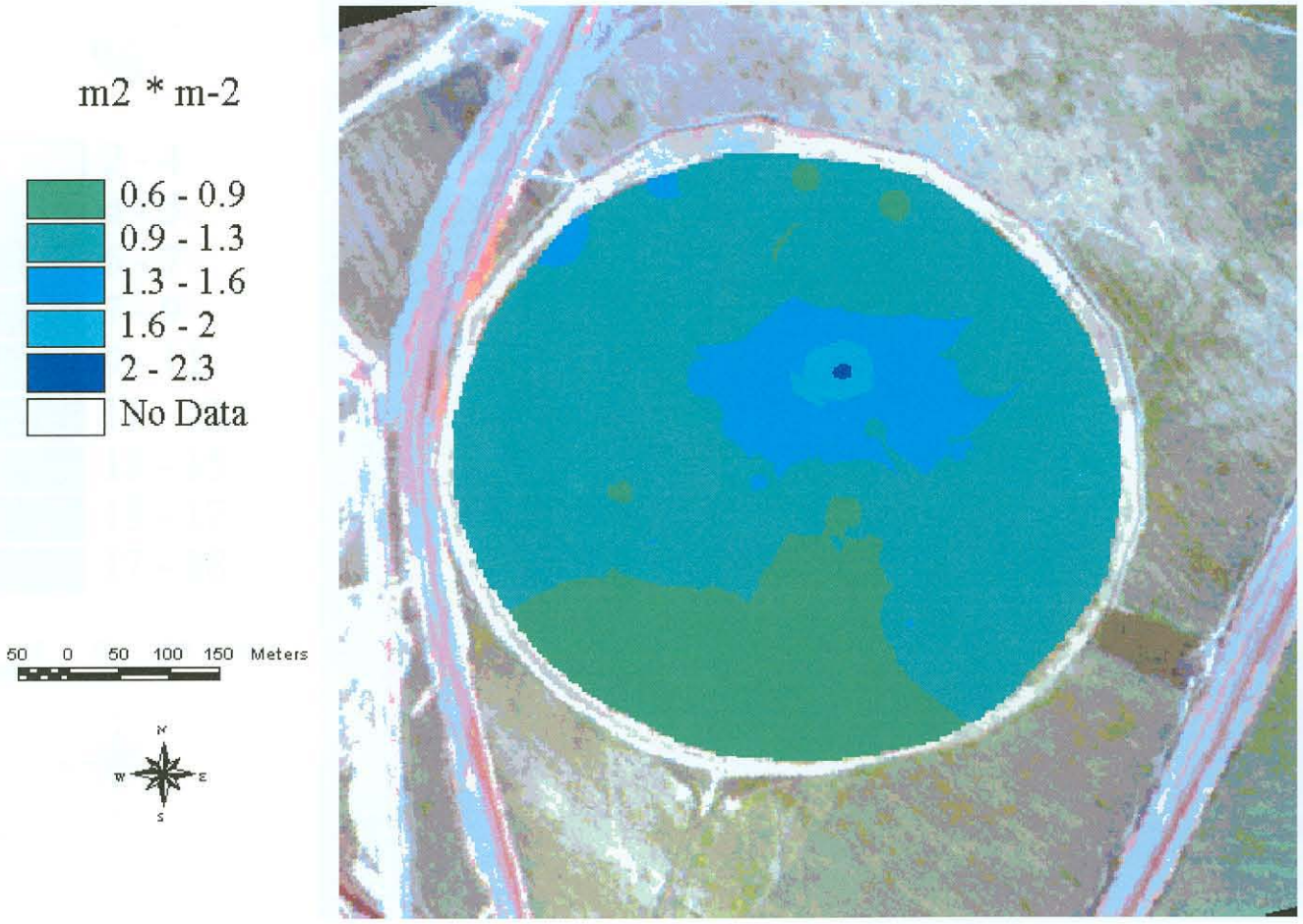

Pivot Tweefontein: AWC 0-20 cm

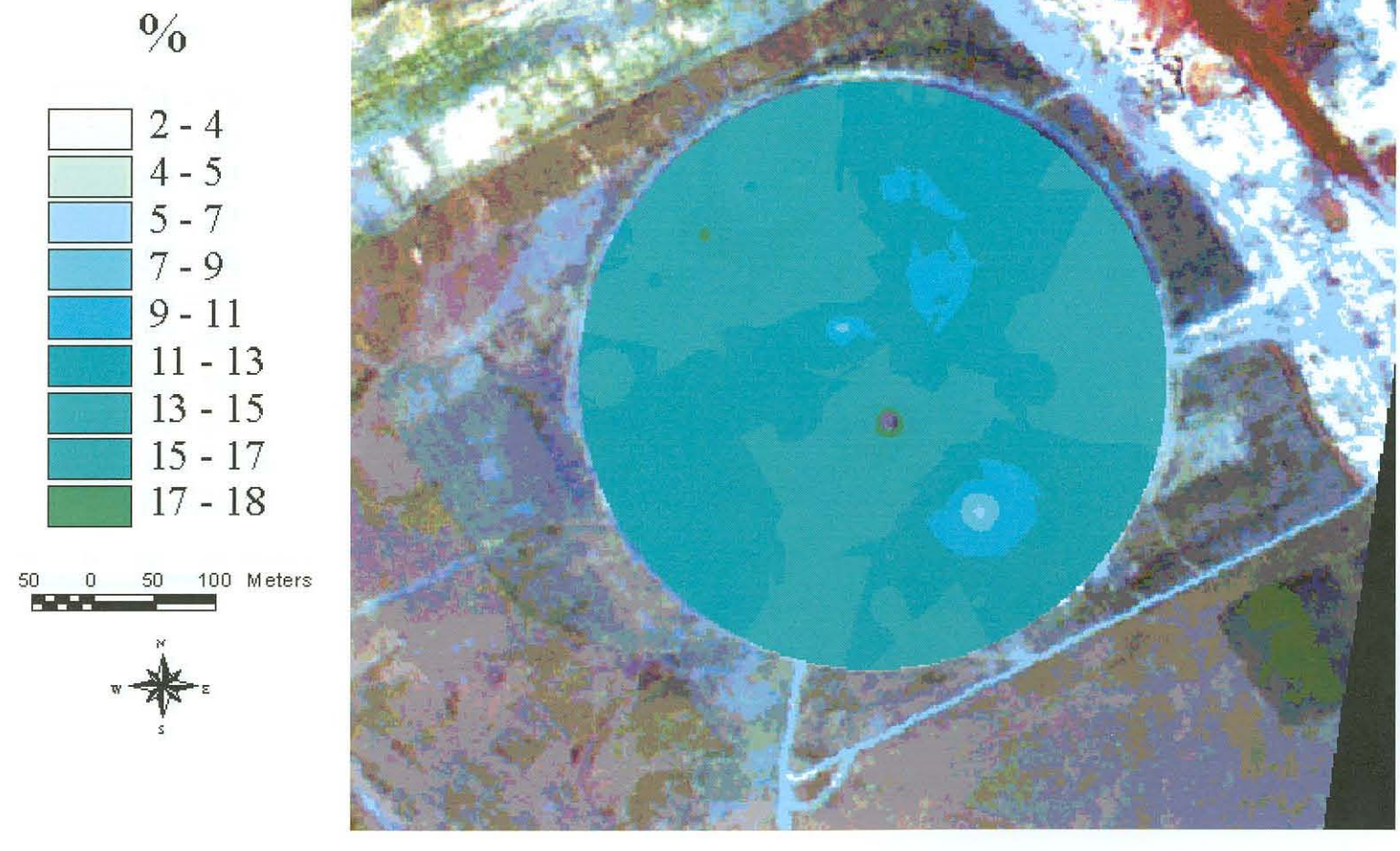

Pivot Tweefontein: AWC 20cm - Spoil/impermeable layer

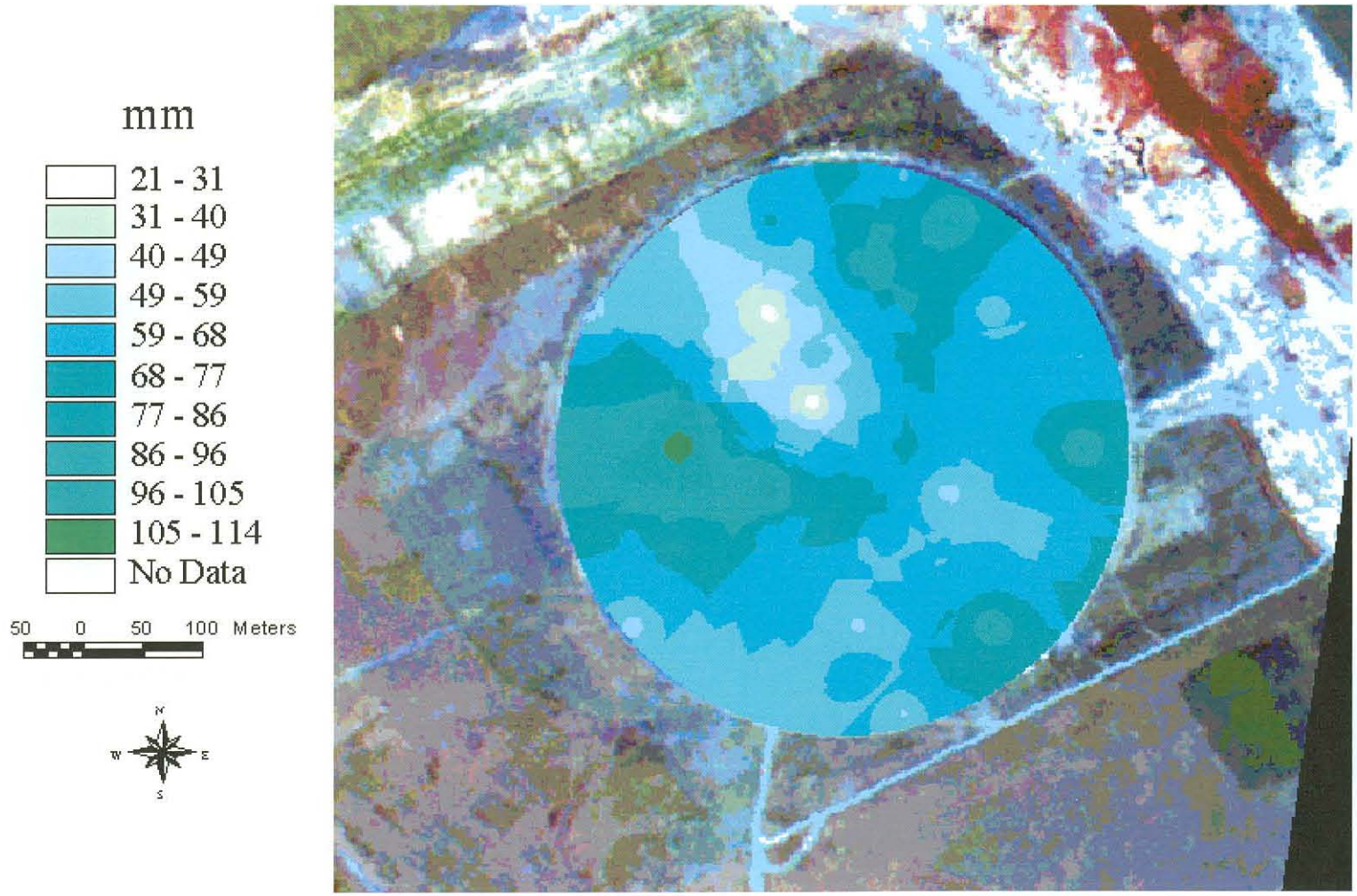

Pivot Tweefontein: AWC Total

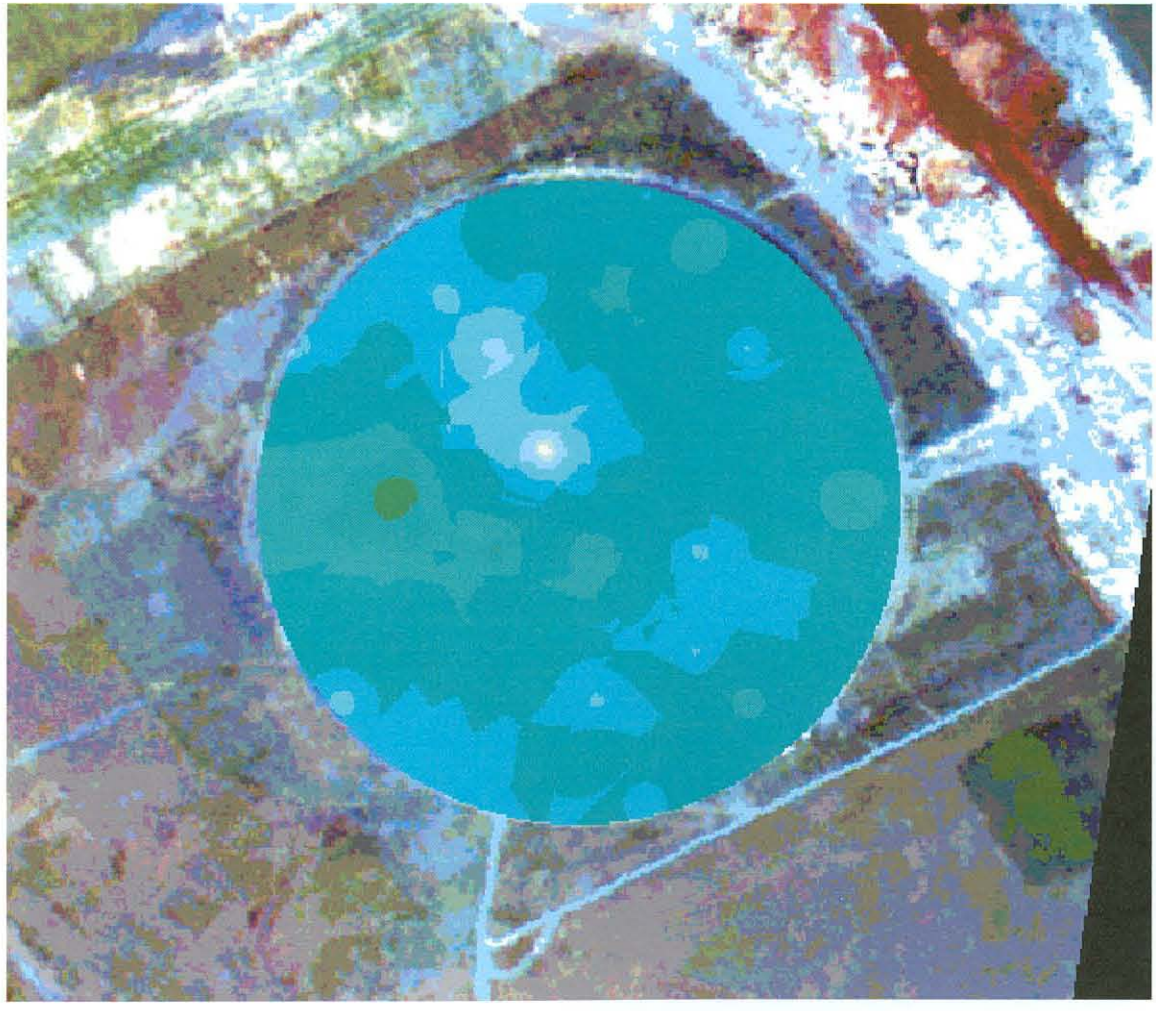

Pivot Tweefontein: Depth to Spoil/Impermeable

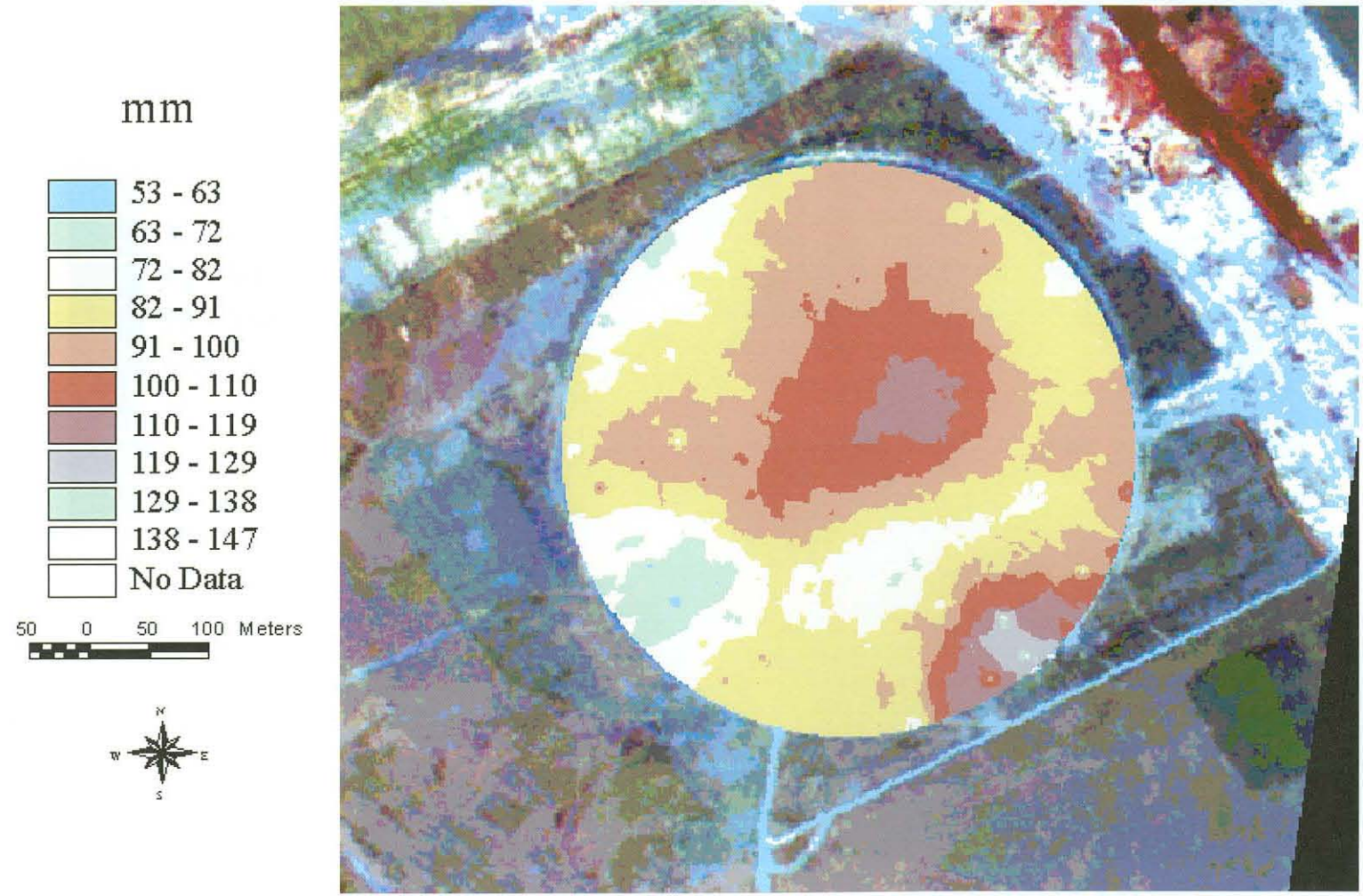

Pivot Tweefontein: Depth to Vadoze Zone

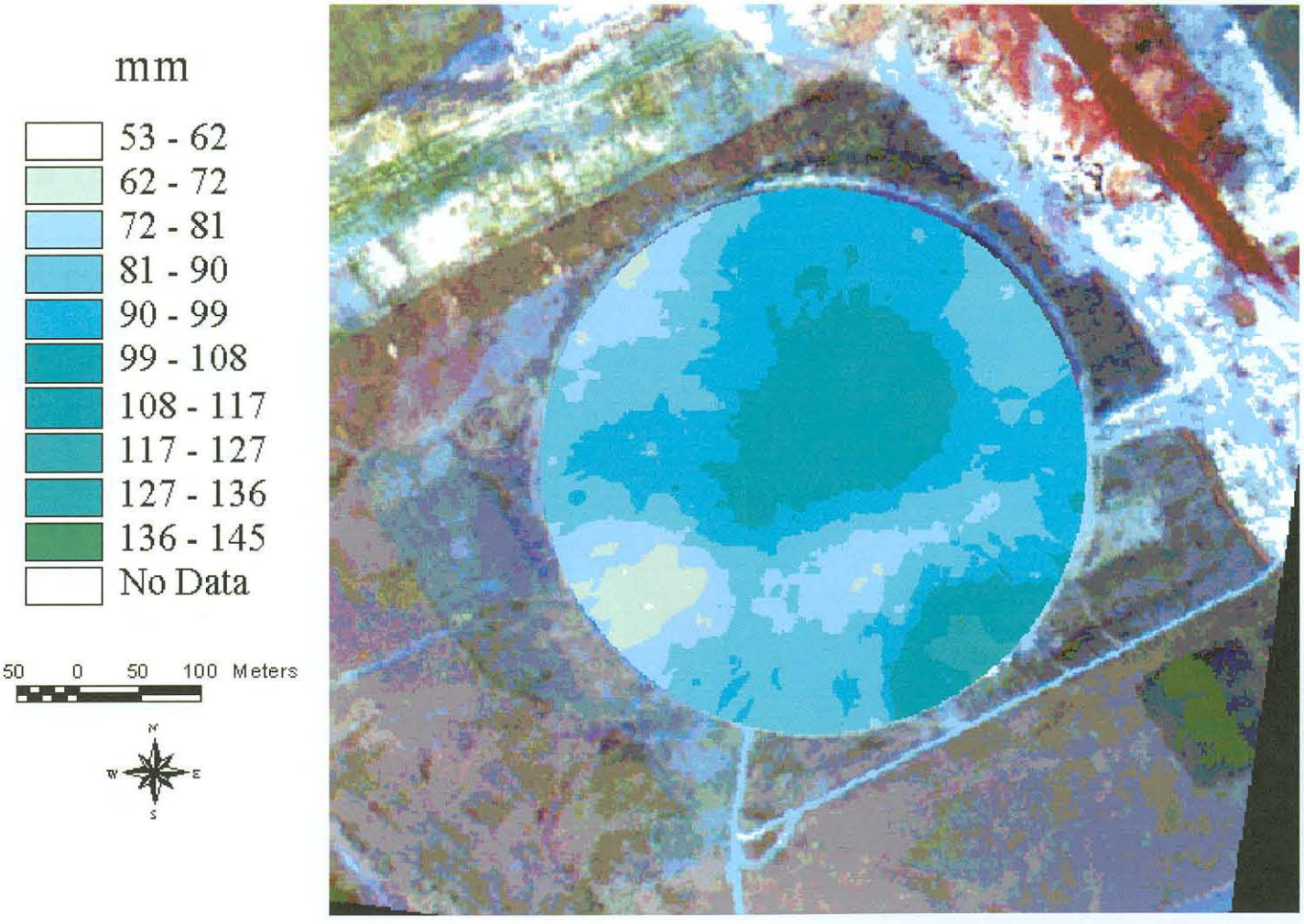

Pivot Tweefontein: Surface DEM

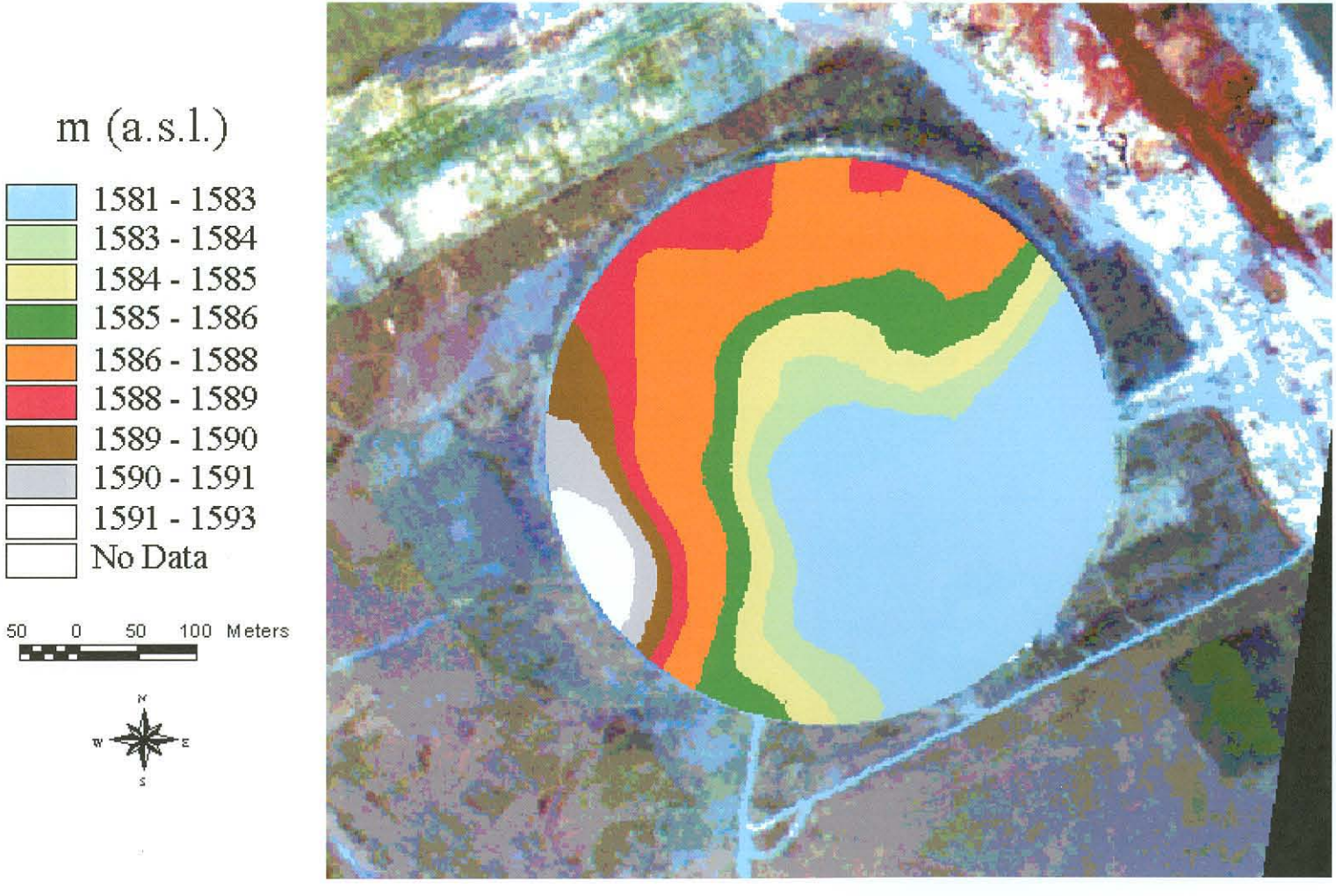

Pivot Tweefontein: Spoil DEM

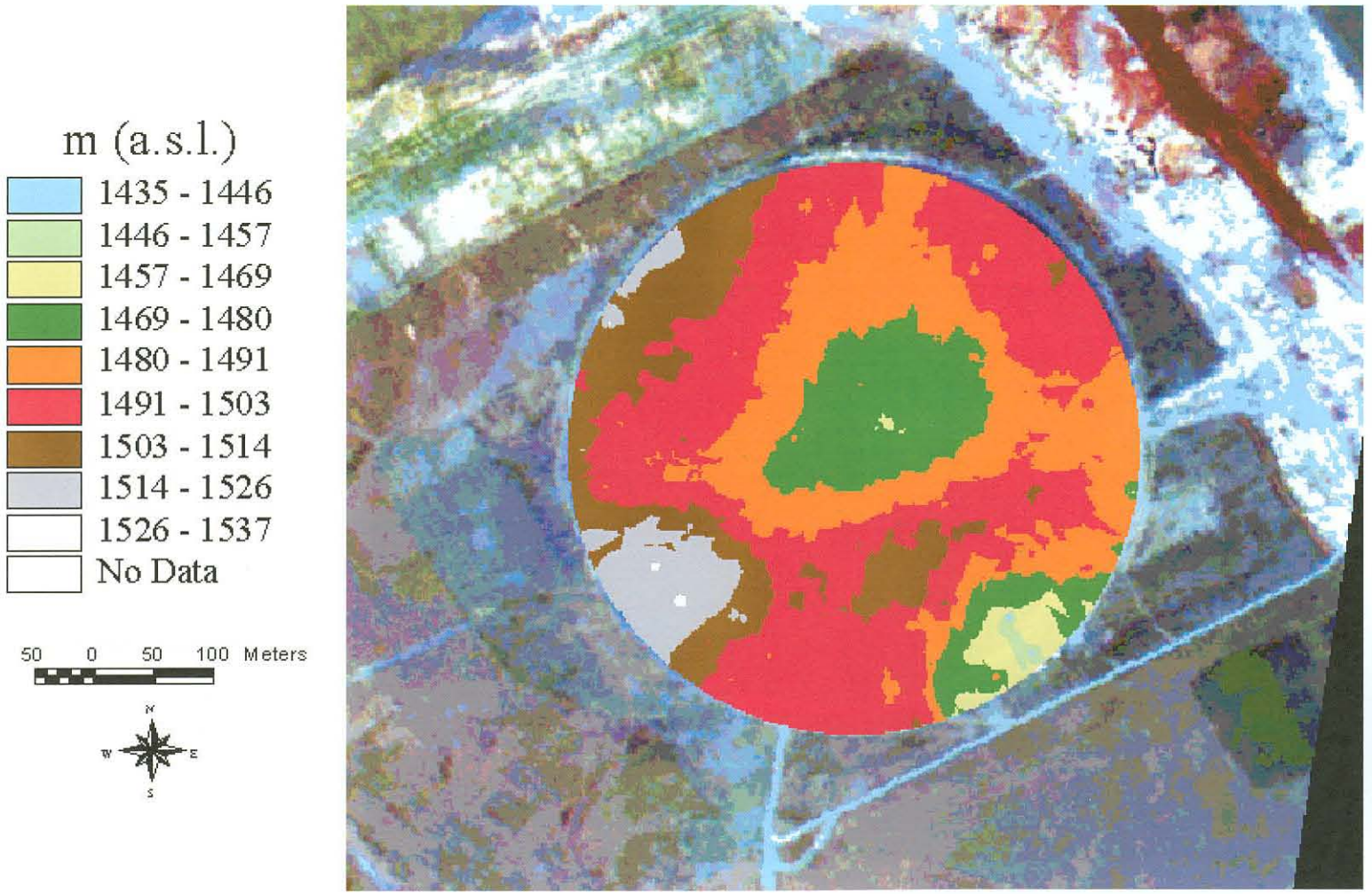

Pivot Tweefontein: 08/99 Flight

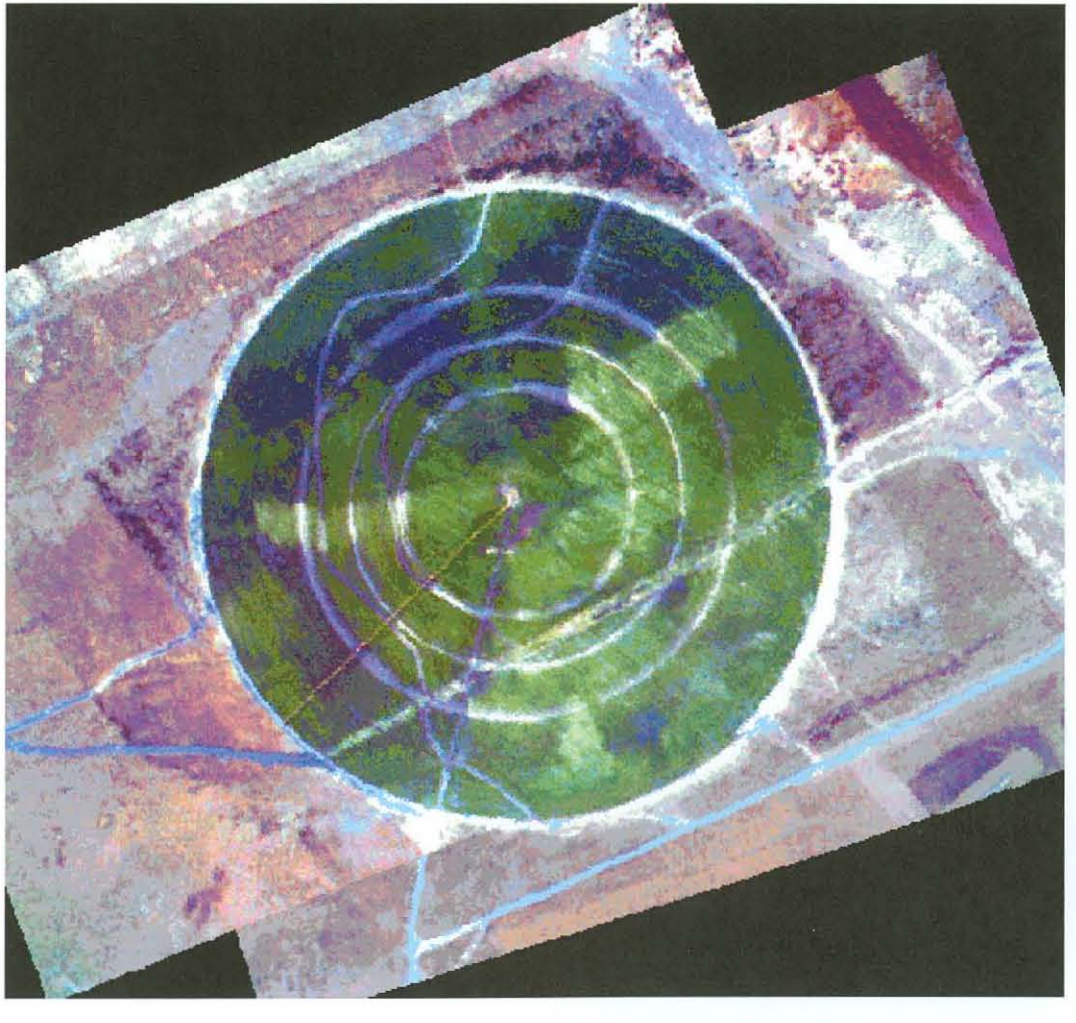

Pivot Tweefontein: 10/99 Flight

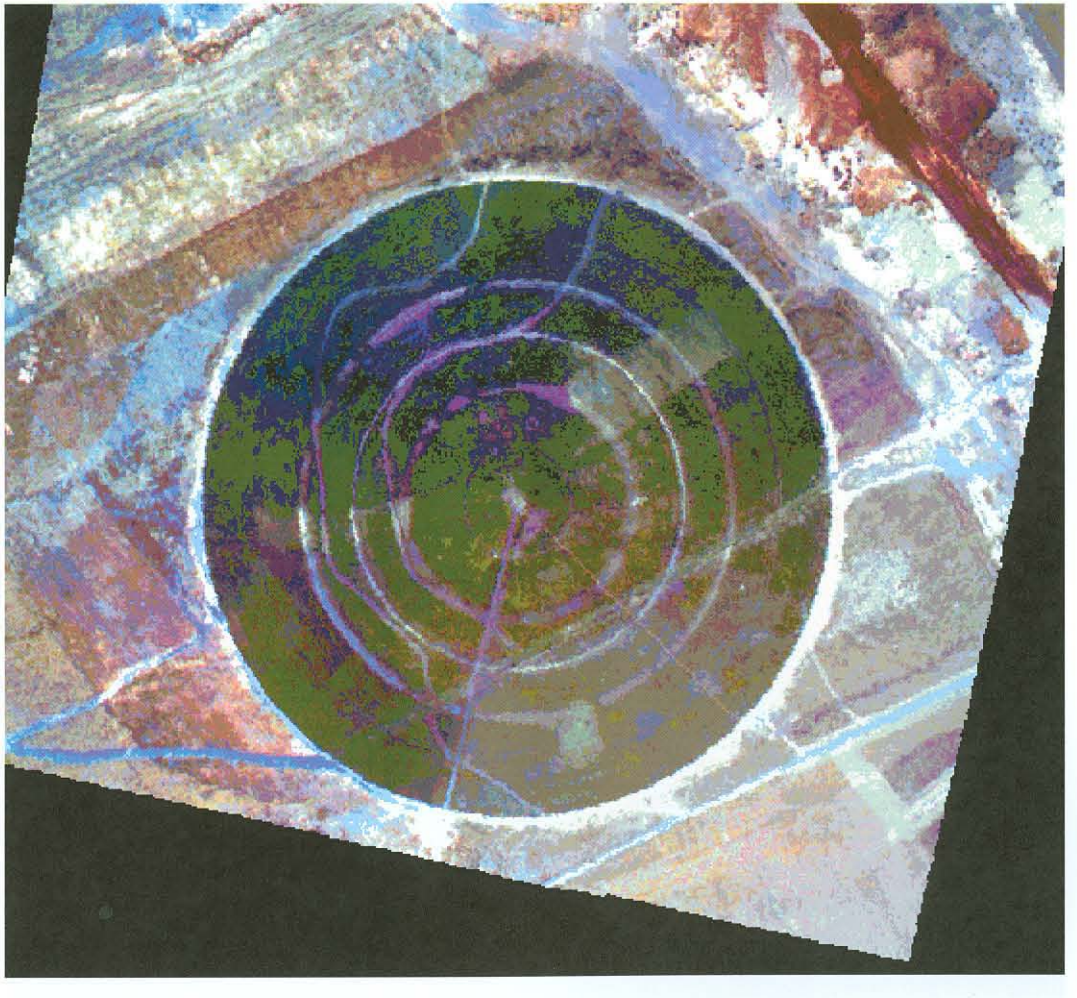

50 0 50 100 Meters

Pivot Tweefontein: TVI 08/99 Flight

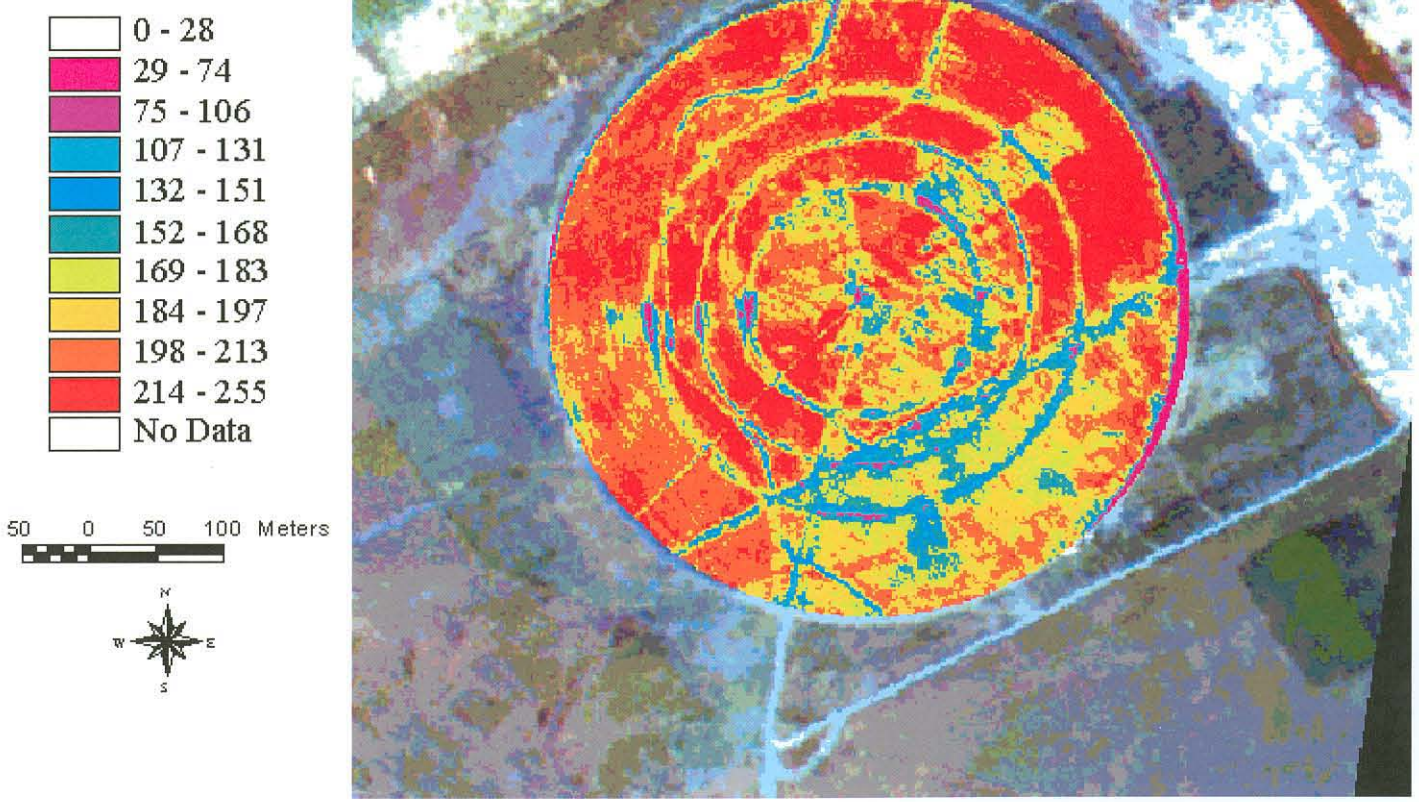

Pivot Tweefontein: TVI 10/99 Flight

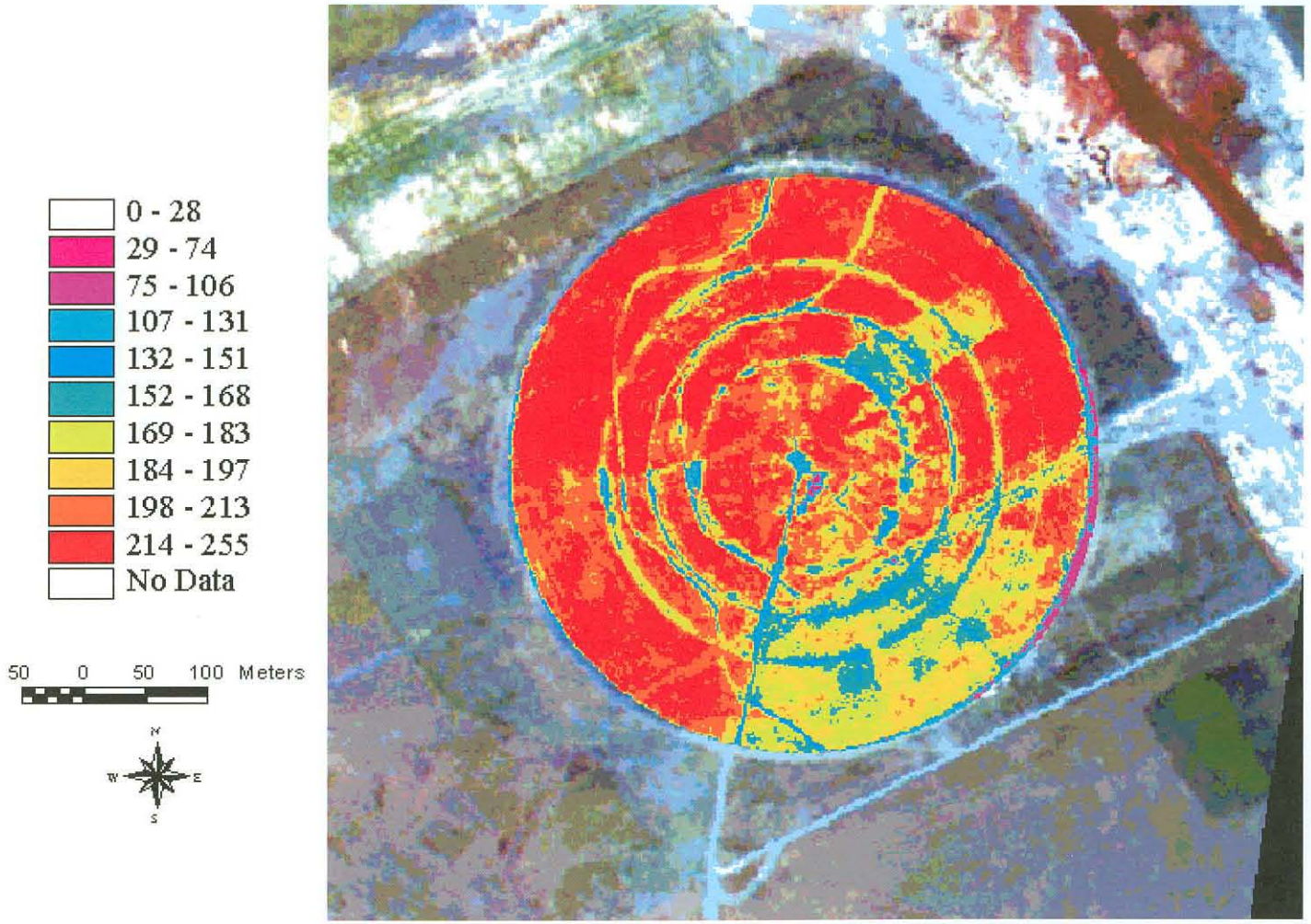

Pivot Tweefontein: PCI 08/99 Flight

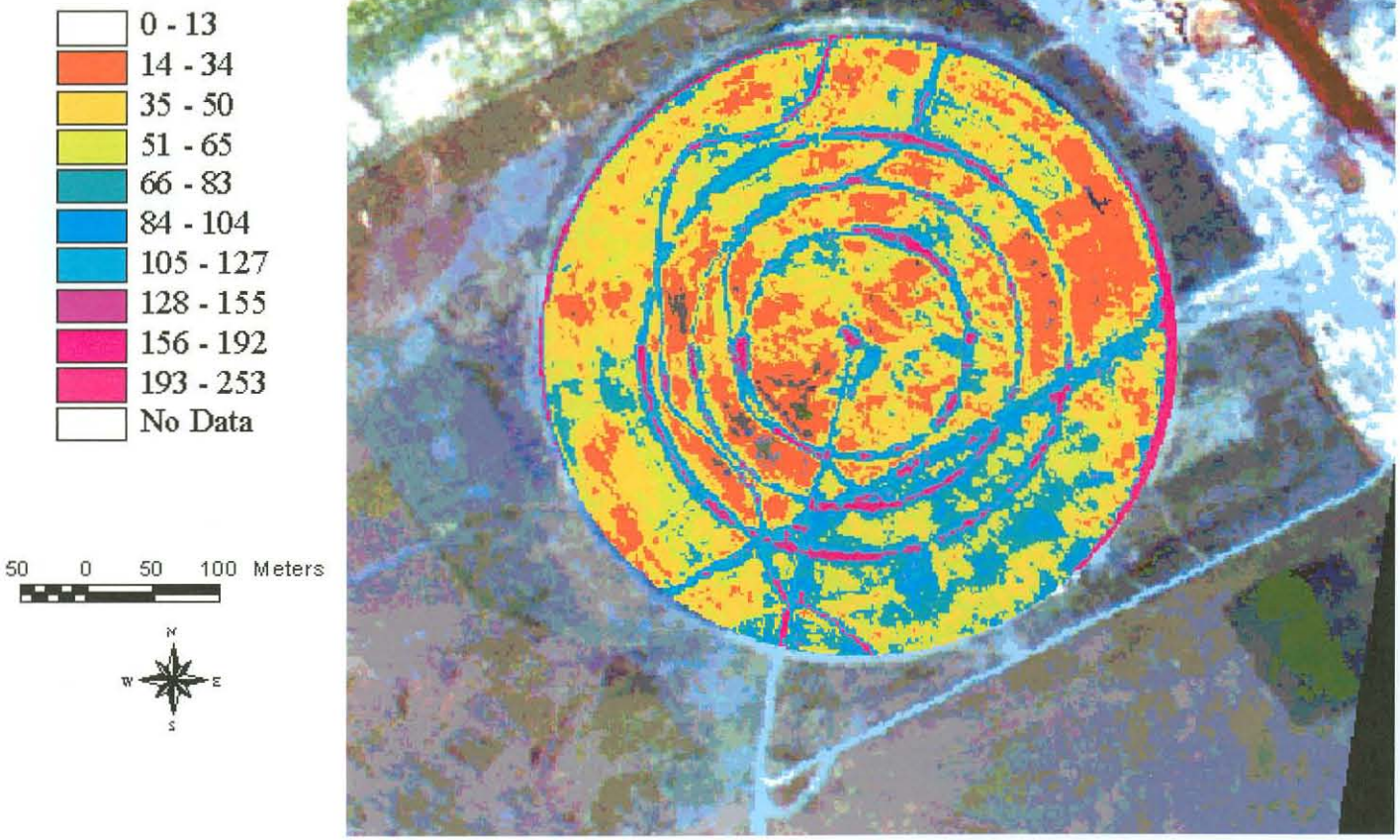

Pivot Tweefontein: PC1 10[illegible] Flight

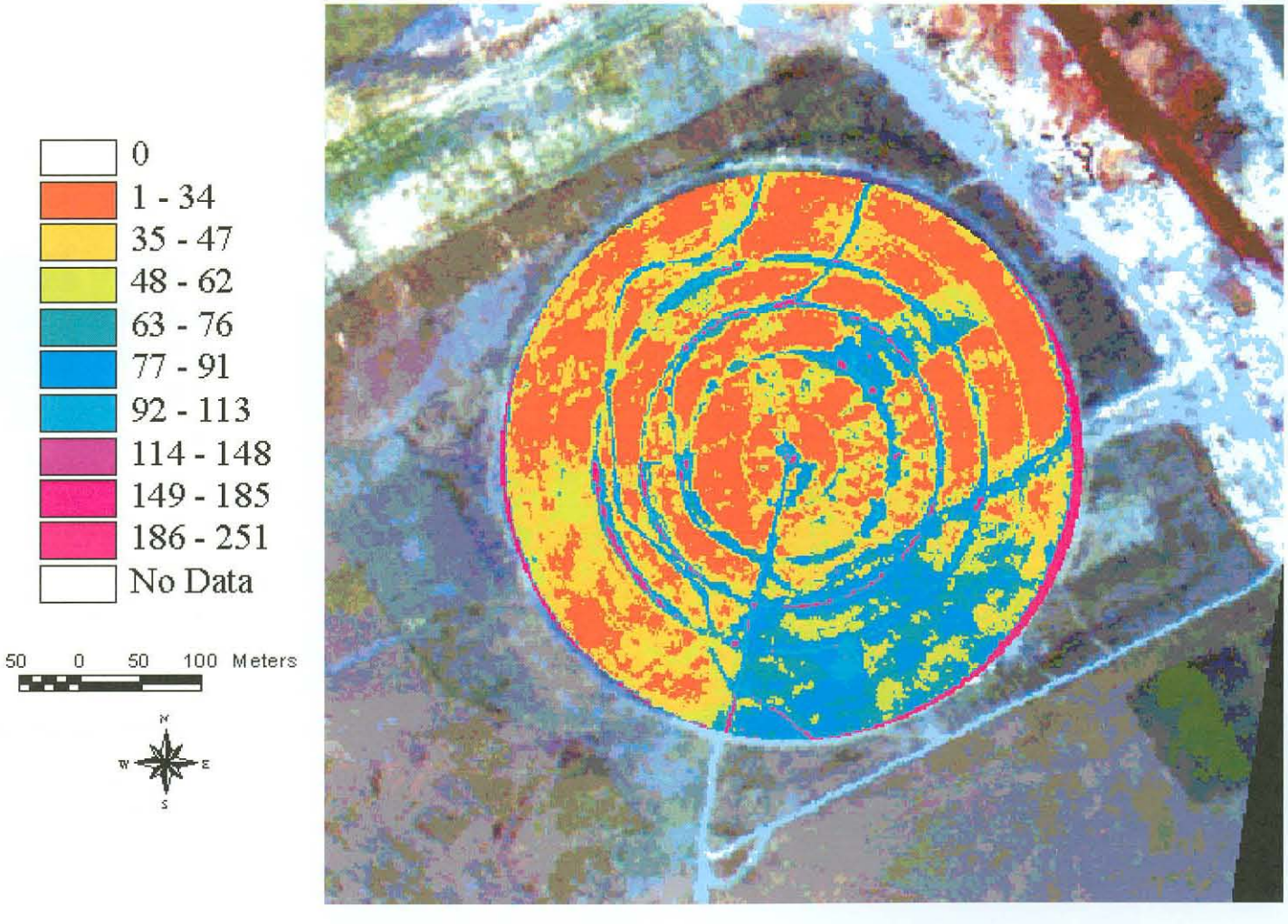

Pivot Tweefontein: Wheat yield, harvest 11/99

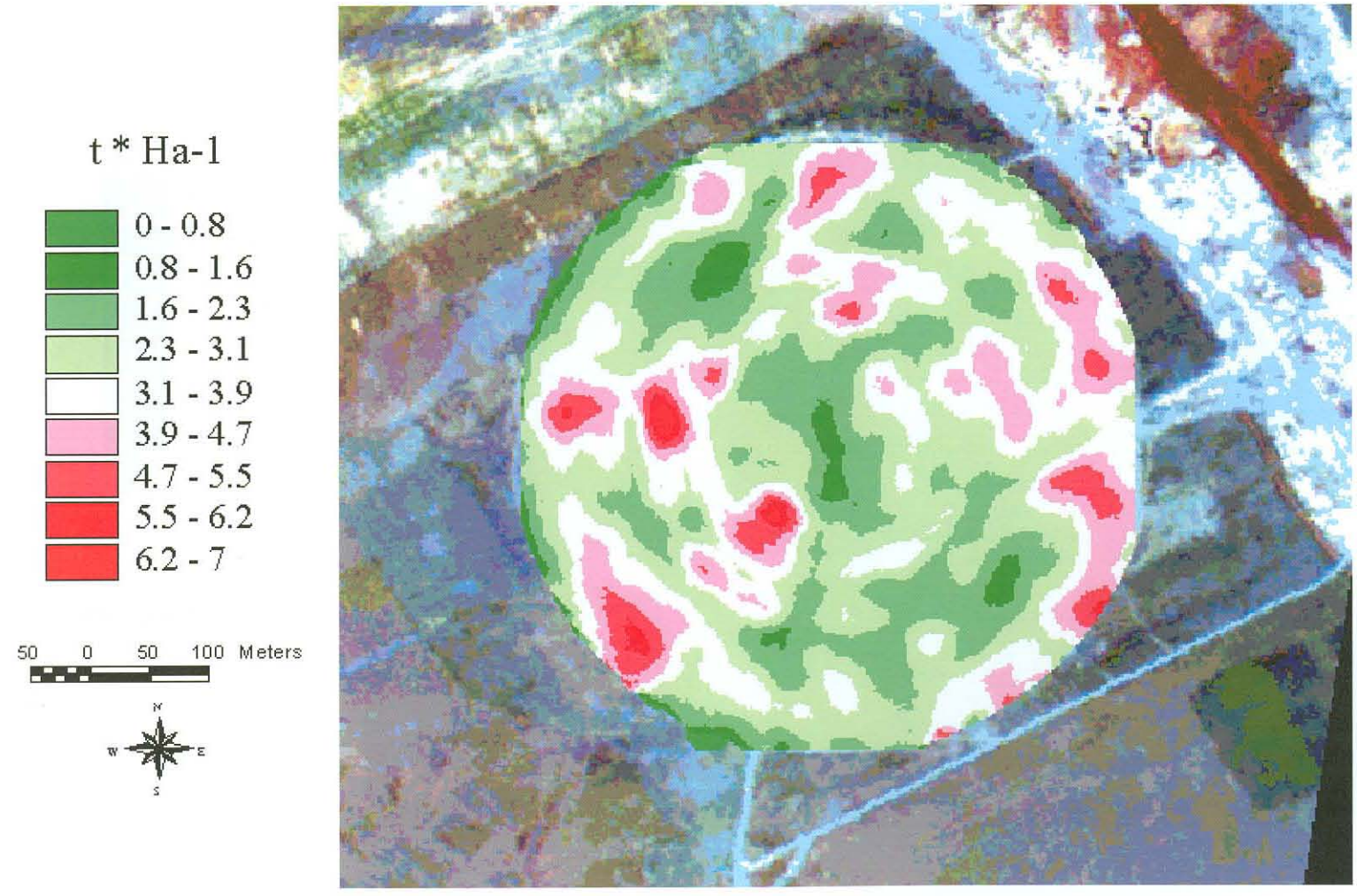

Pivot Tweefontein: Wheat moisture % at harvest

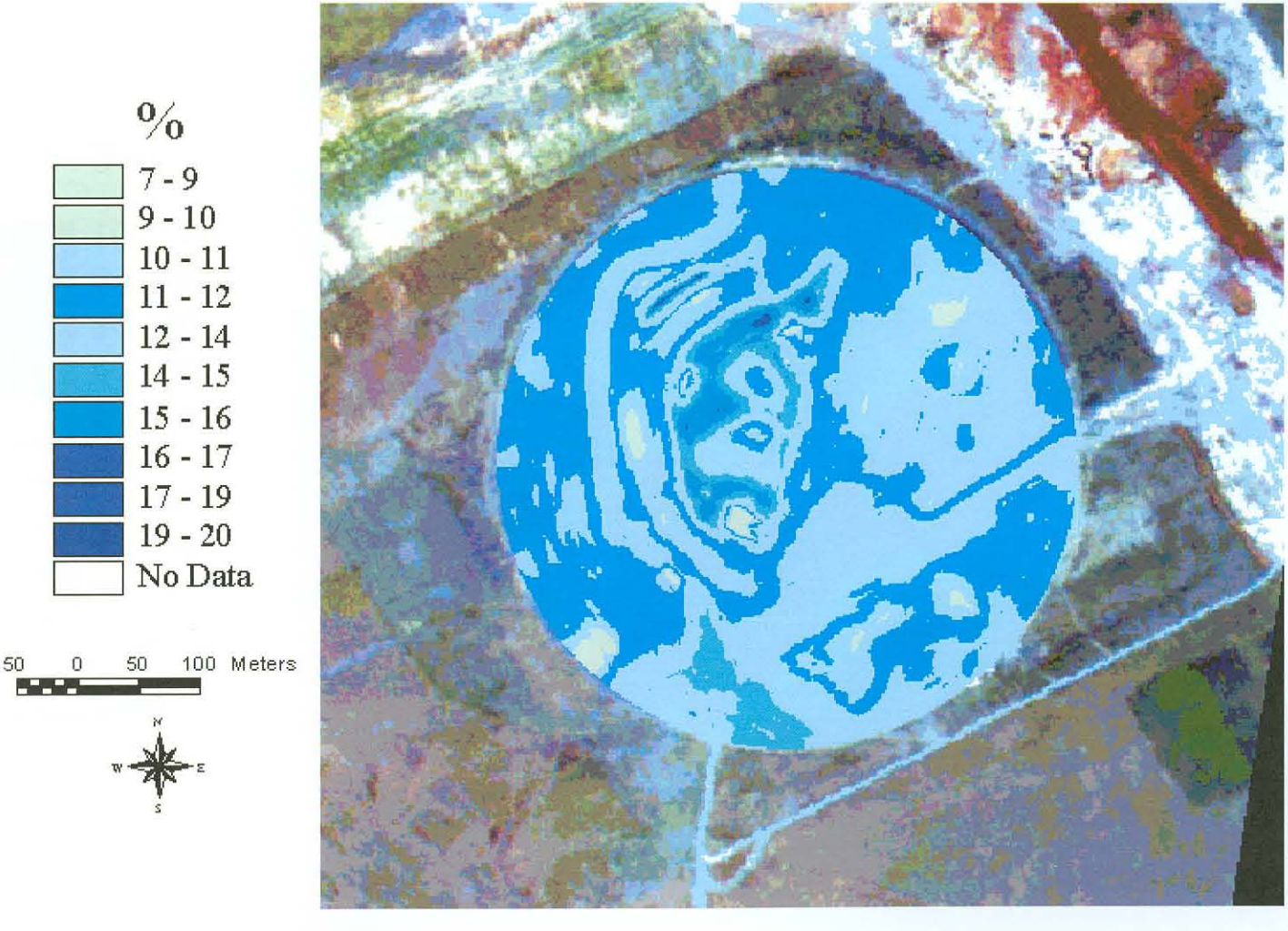

Pivot Tweefontein: Ground cover 08/99

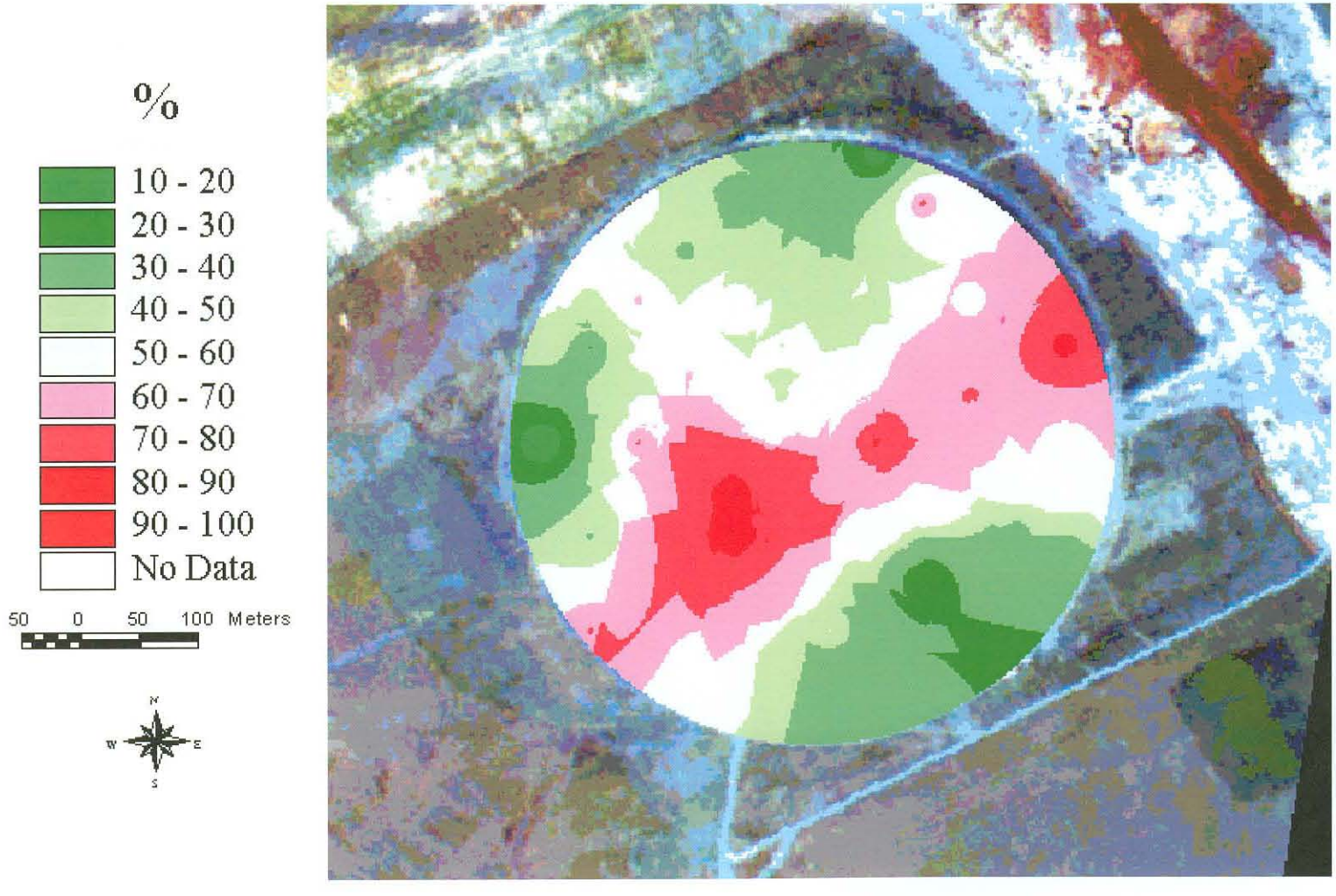

Pivot Tweefontein: Dry matter 08/99

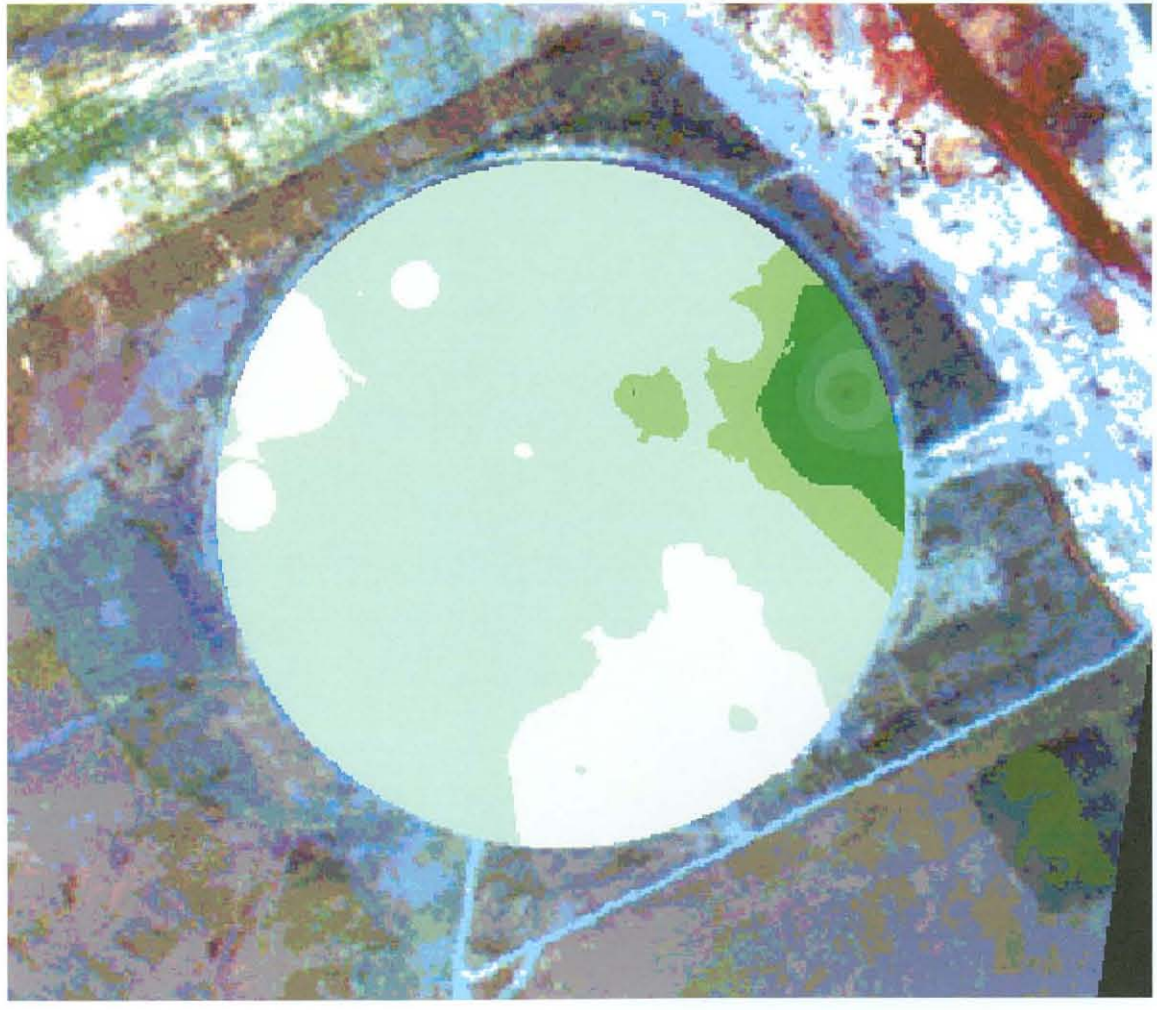

Pivot Tweefontein: LAI 08/99

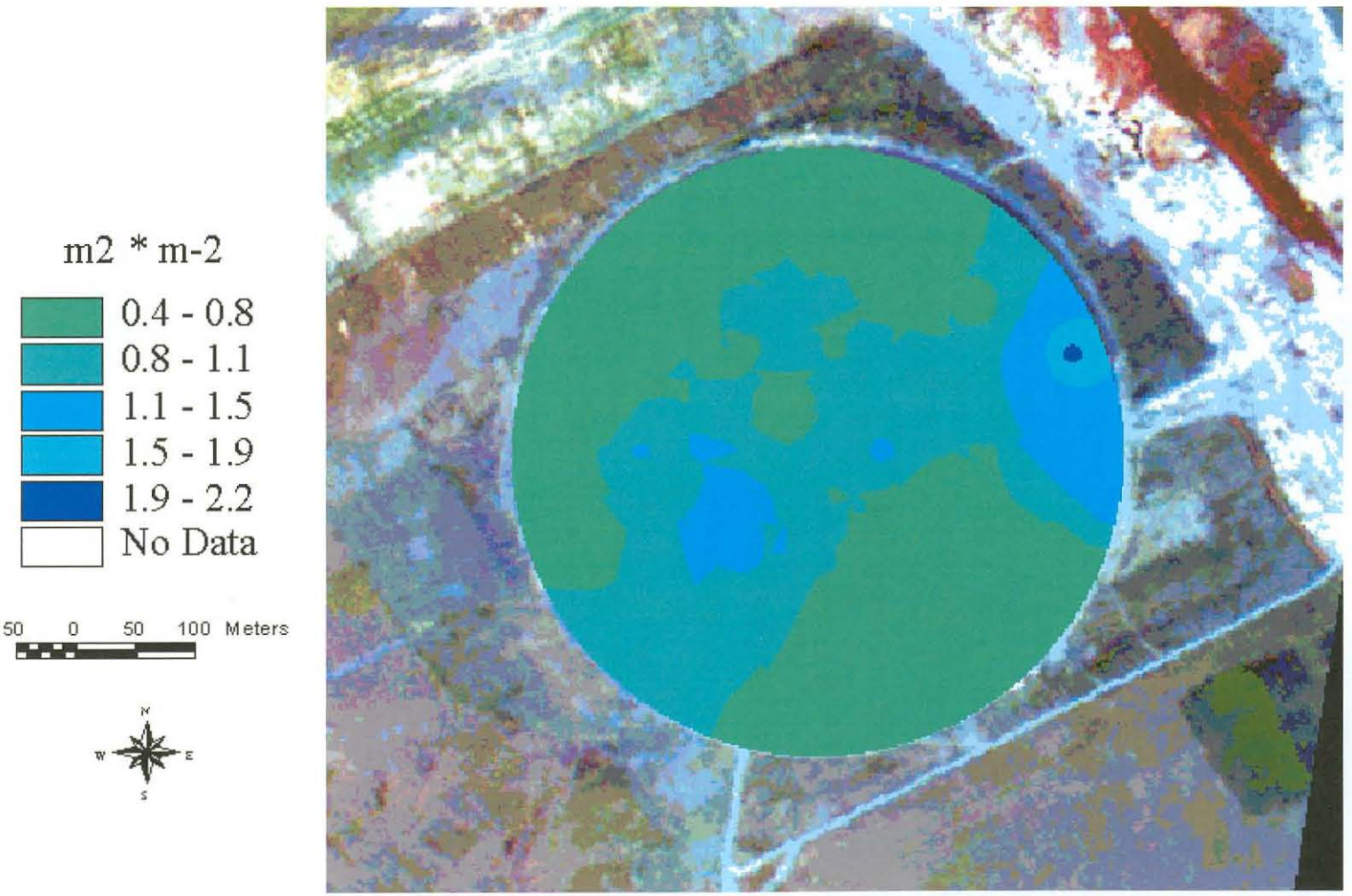

APPENDIX 2: LOCAL REGRESSION ANALYSIS MAPS

Pivot Major: Maps compared

Map 1	Map 2	Page
Top dry matter map 08/99	LAI map 08/99	132
Ground cover map 08/99	Depth of vadoze zone map7	133
Ground cover map 08/99	LAI map 08/99	134
Ground cover map 08/99	Top dry matter map 08/99	135
Total Available Water Capacity map	LAI map 08/99	136
Total Available Water Capacity map	Top dry matter map 08/99	137
Total Available Water Capacity map	Ground cover map 08/99	138
Available Water Capacity map from 20 to the spoil/ impermeable layer	LAI map 08/99	139
Available Water Capacity map from 20 to the spoil/ impermeable layer	Top dry matter map 08/99	140
Available Water Capacity map from 20 to the spoil/ impermeable layer	Ground cover map 08/99	141
Wheat yield map 11/99	Ground cover map 08/99	142
Wheat yield map 11/99	Available Water Capacity map of the first 20 cm of soil	143
Transformed Vegetation Index (TVI) map 08/99 flight	Wheat yield map 11/99	144
Transformed Vegetation Index (TVI) map 010/99 flight	Wheat yield map 11/99	145

Pivot Tweefontein: Maps compared

Map 1	Map 2	Page
LAI map 08/99	Ground cover map 08/99	146
Top dry matter map 08/99	Ground cover map 08/99	147
Wheat yield map 11/99	LAI map 08/99	148
Wheat yield map 11/99	Top dry matter map 08/99	149
Wheat yield map 11/99	Total Available Water Capacity map	150
Wheat yield map 11/99	Available Water Capacity map from 20 to the spoil/ impermeable layer	151
Wheat yield map 11/99	Transformed Vegetation Index (TVI) map 08/99 flight	152
Wheat yield map 11/99	Transformed Vegetation Index (TVI) map 10/99 flight	153

Pivot Major: Correlation map between Top Dry Matter 08/99 and LAI 08/99

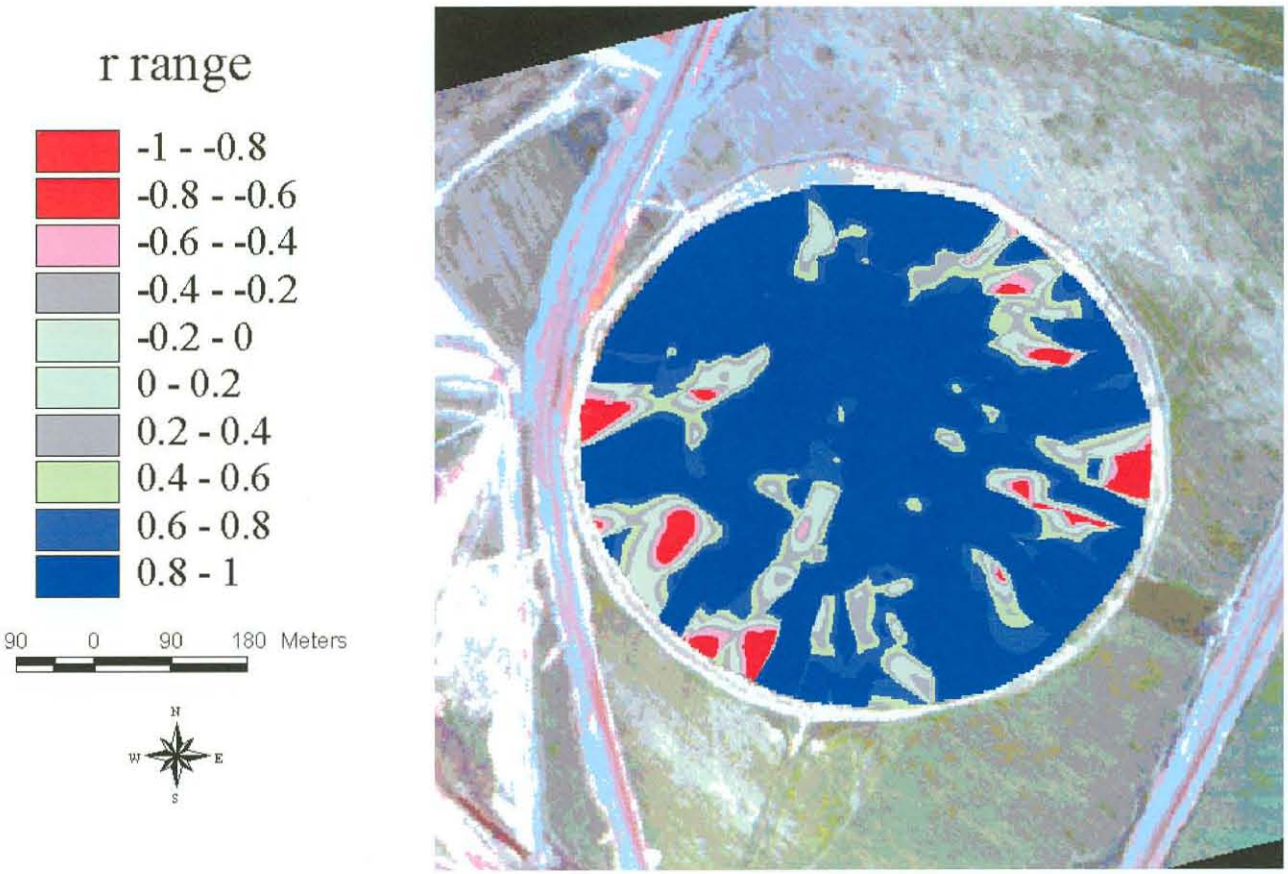

Pivot Major: Correlation map between Ground cover 08/99 and depth of the Vadoze Zone

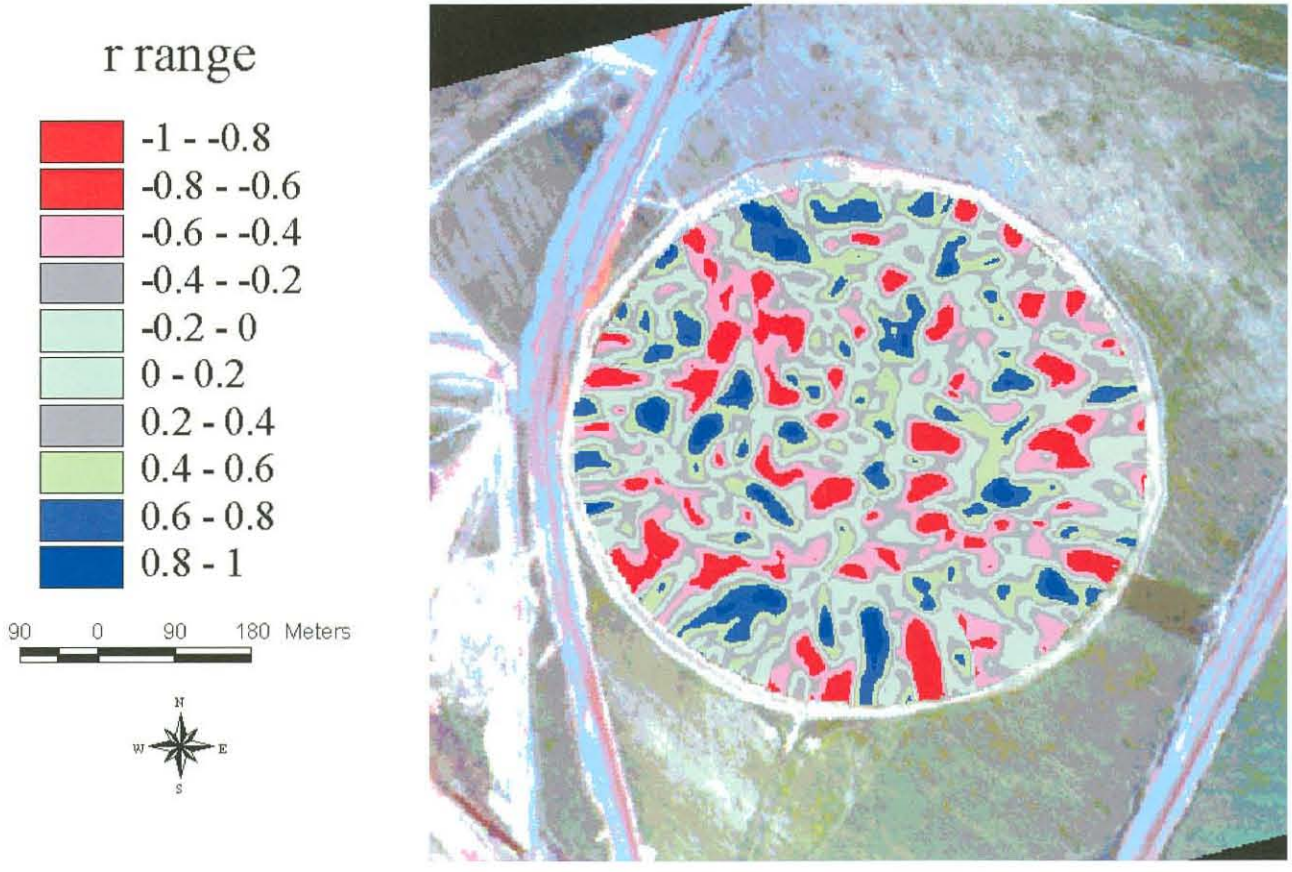

Pivot Major: Correlation map between Ground cover 08/99 and LAI 08/99

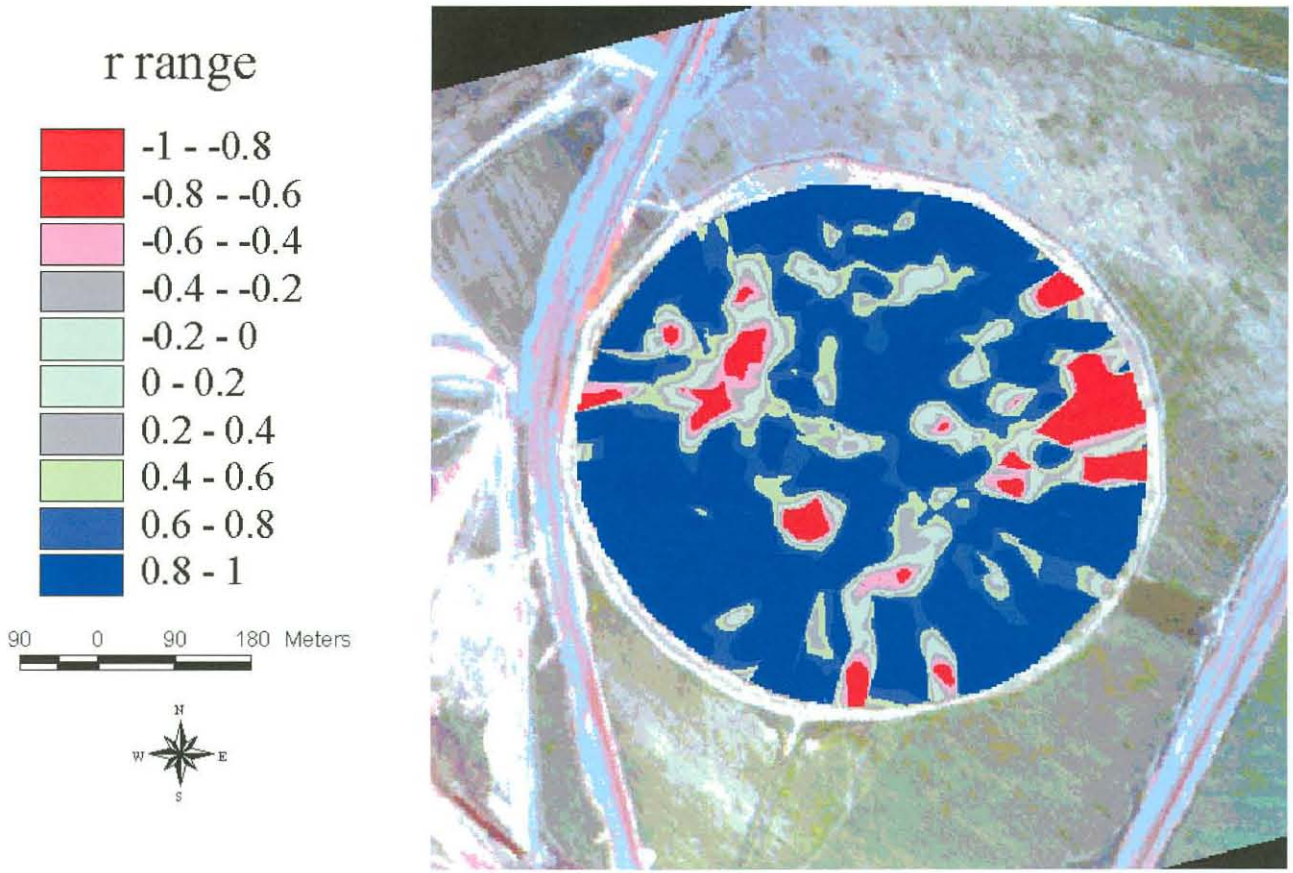

Pivot Major: Correlation map between Ground Cover 08/99 and Top Dry Matter 08/99

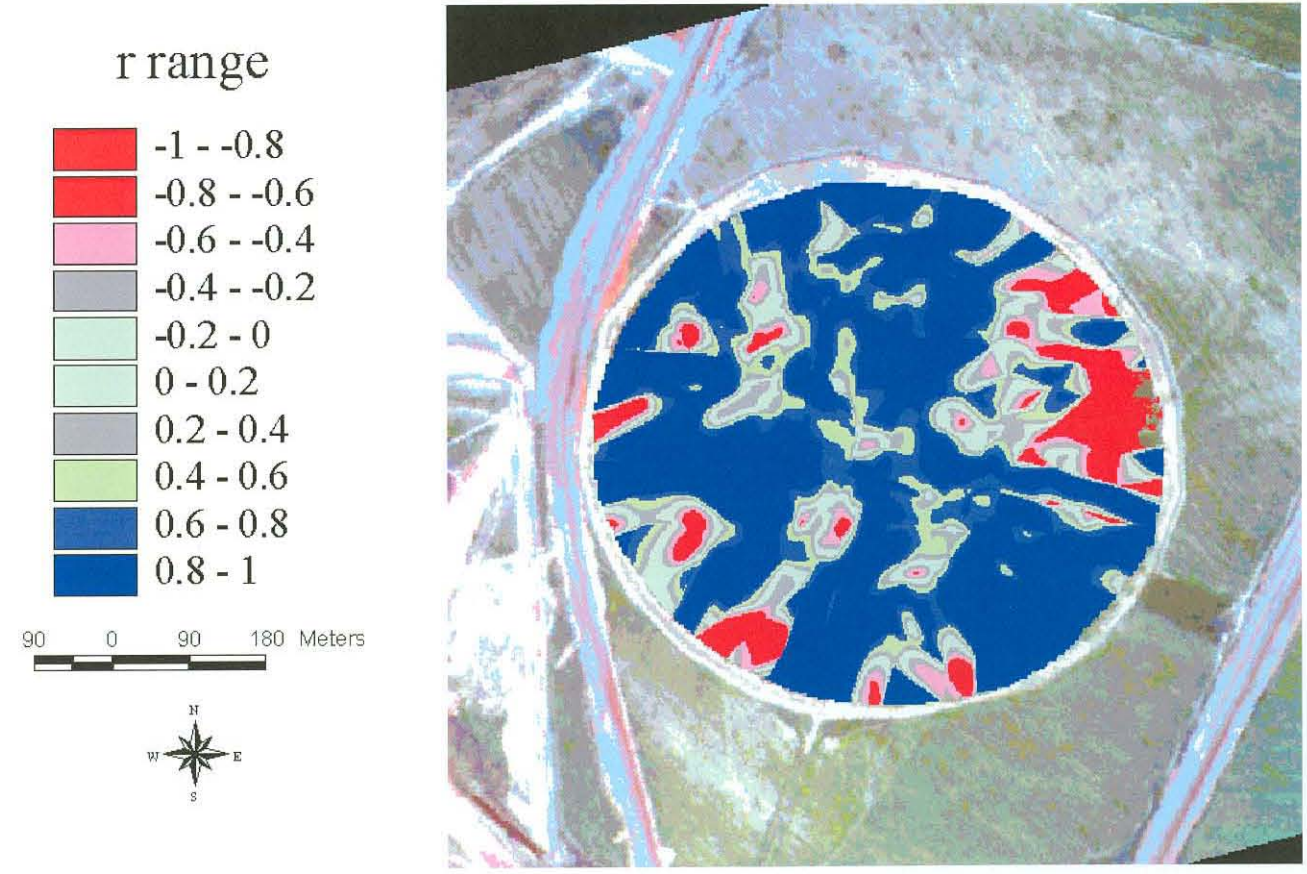

Pivot Major: Correlation map between AWC Total and LAI 08/99

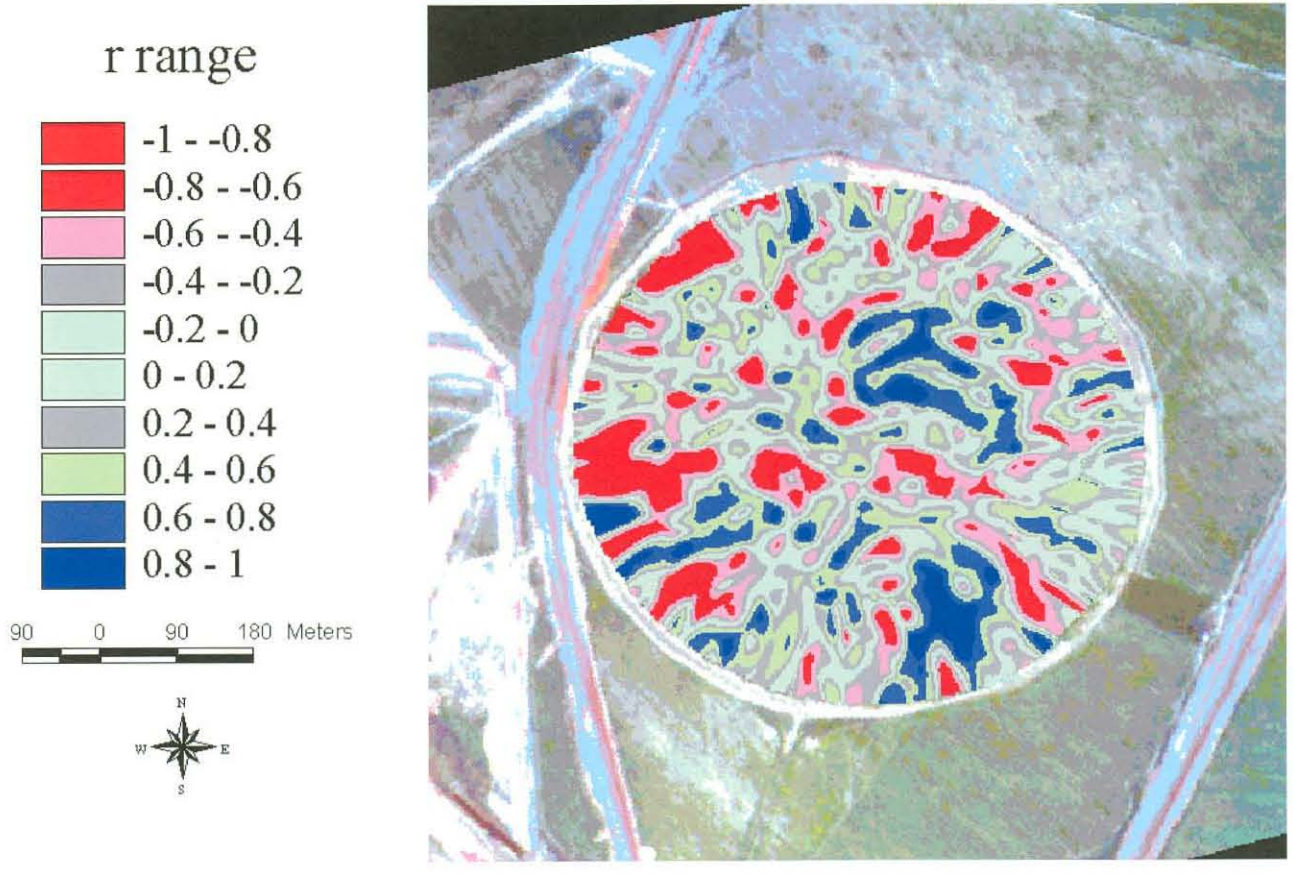

Pivot Major: Correlation map between AWC Total and Top Dry Matter 08/99

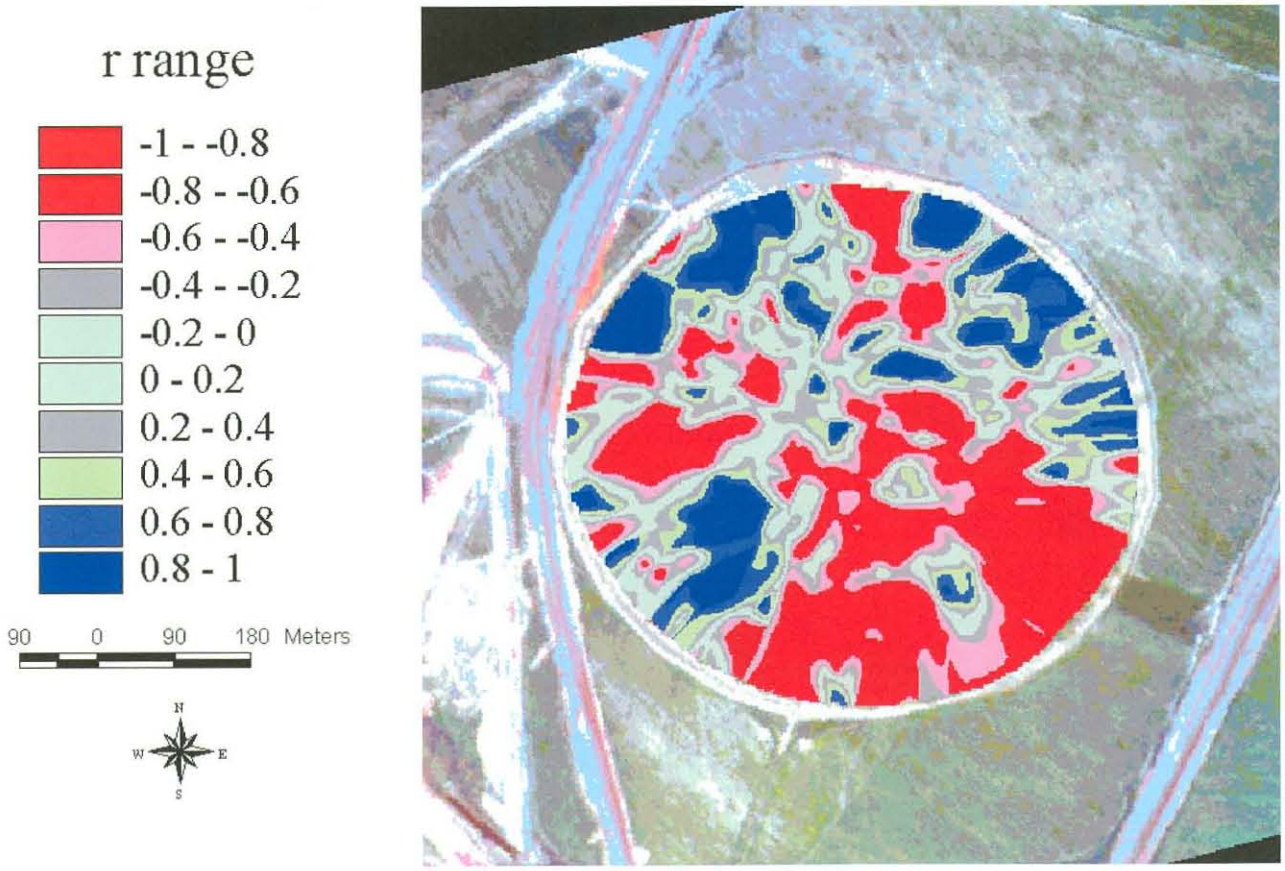

Pivot Major: Correlation map between AWC Total and Ground Cover 08/99

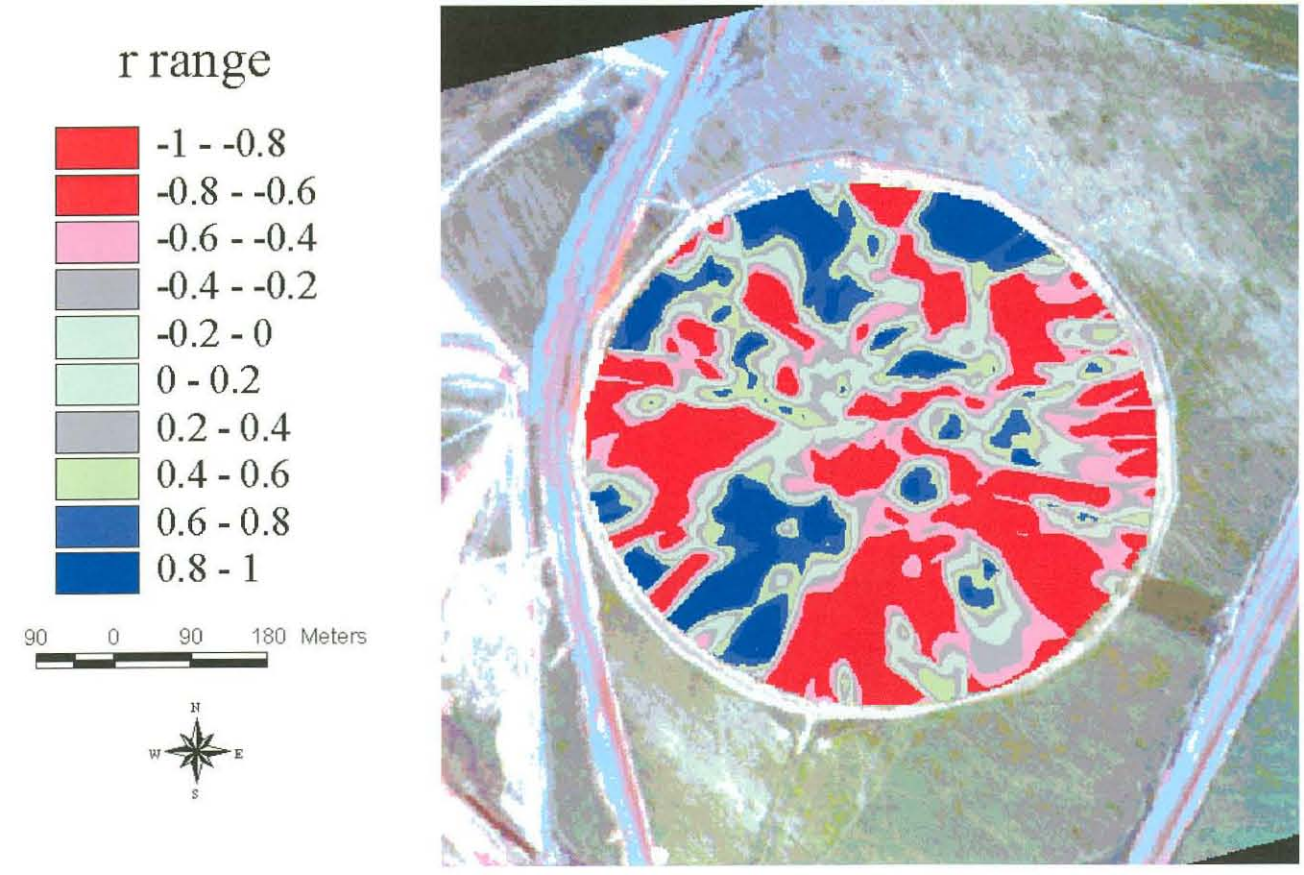

Pivot Major: Correlation map between AWC 20- spoil/impermeable and LAI 08/99

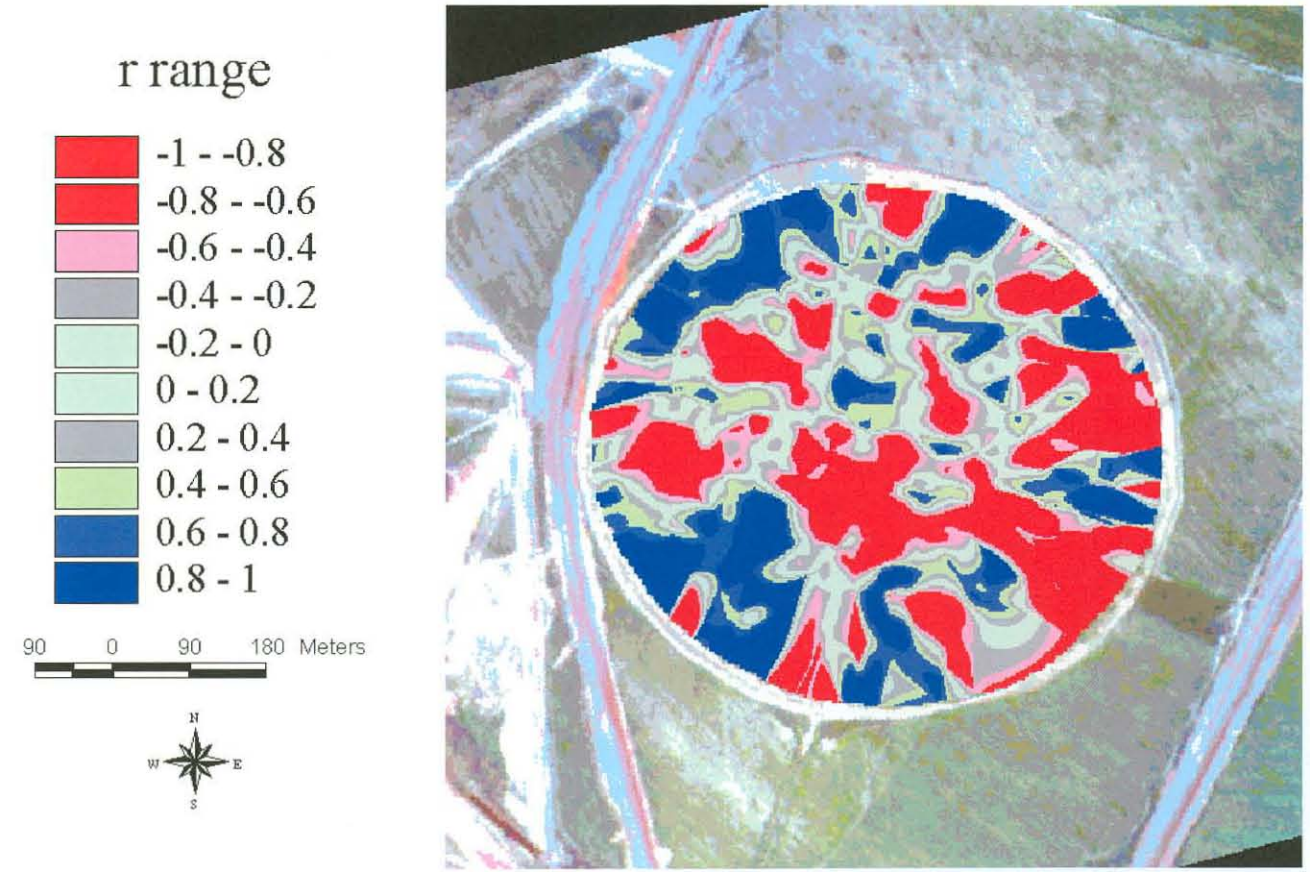

Pivot Major: Correlation map between AWC 20- spoil/impermeable and Dry Matter 08/99

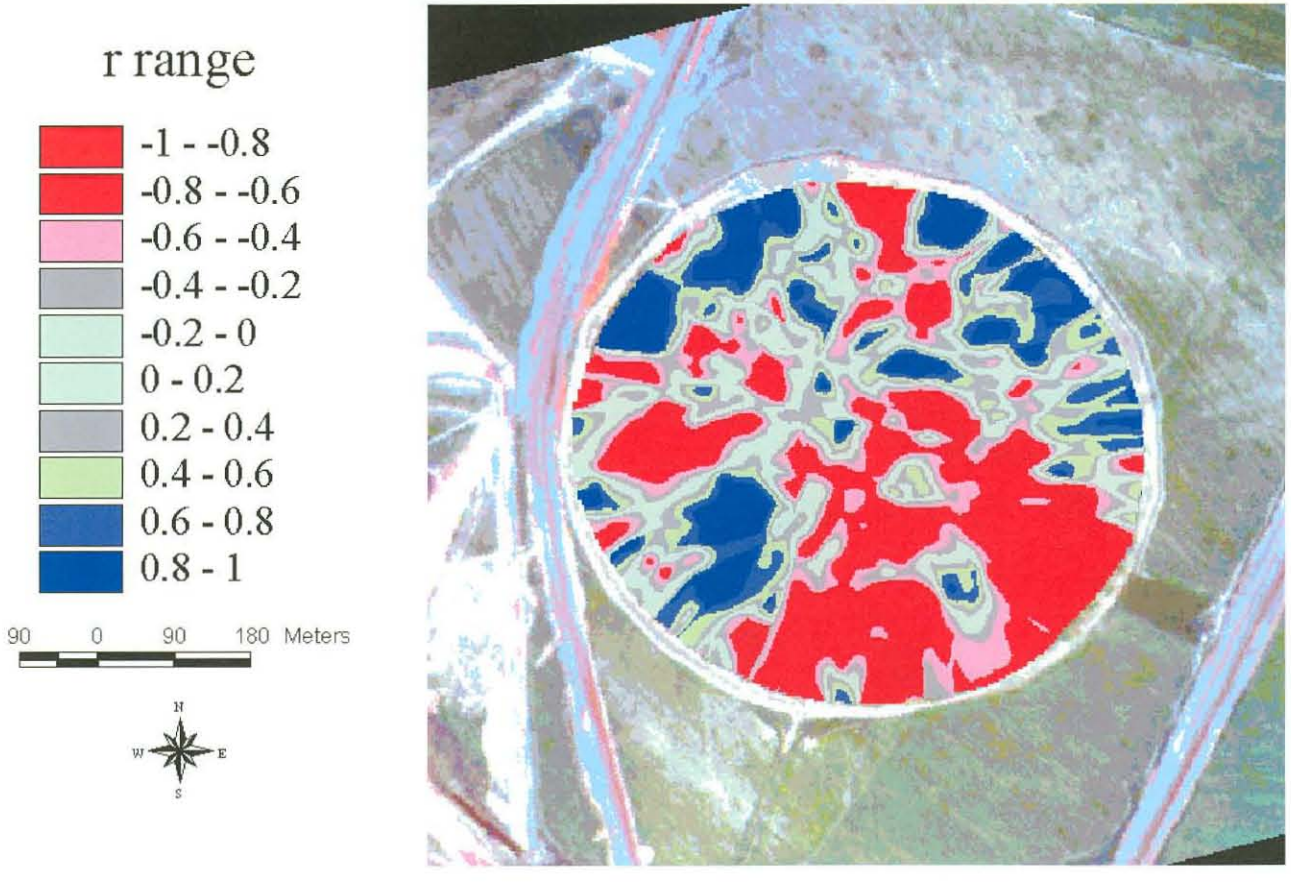

Pivot Major: Correlation map between AWC 20- spoil/impermeable and Ground Cover 08/99

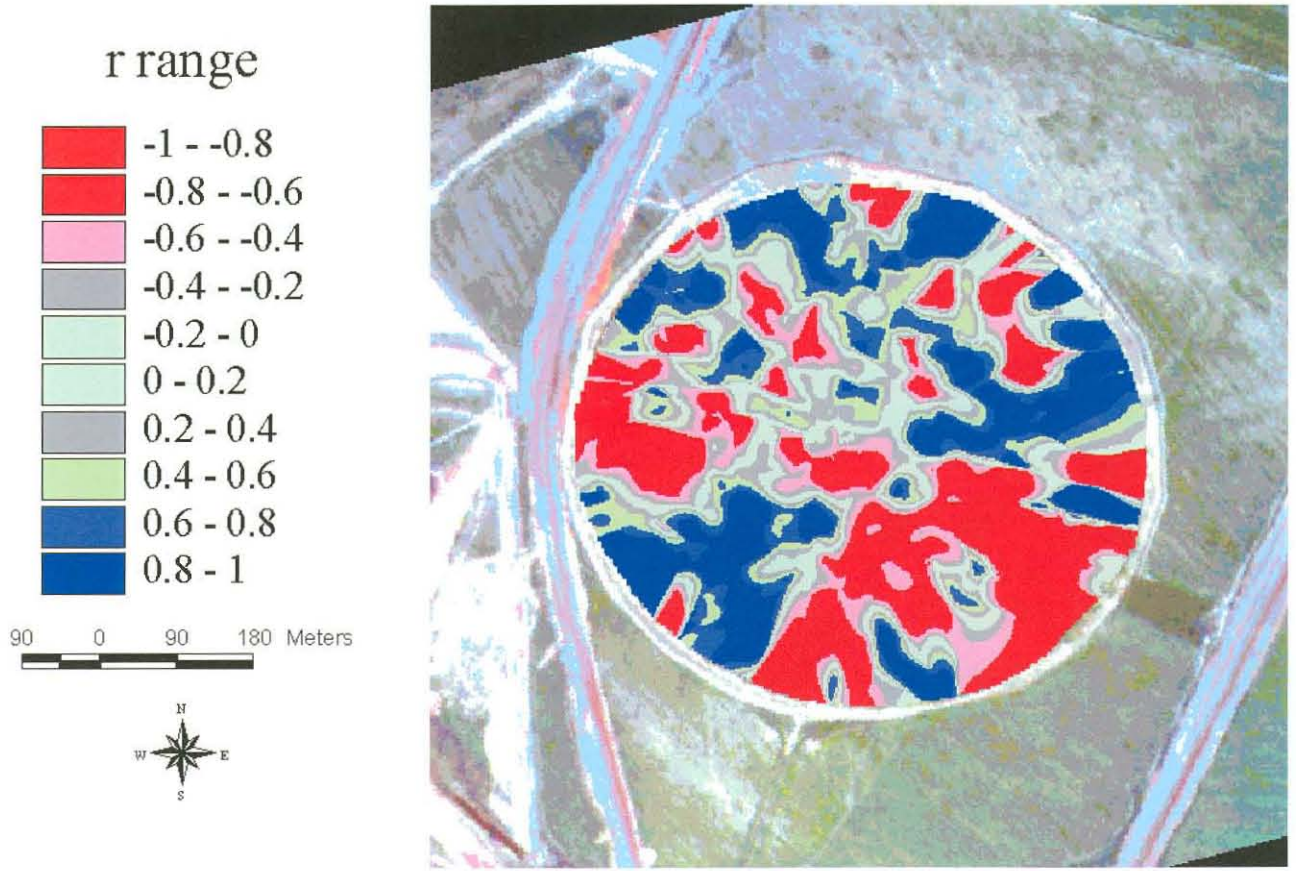

Pivot Major: Correlation map between Yield 11/99 and Ground Cover 08/99

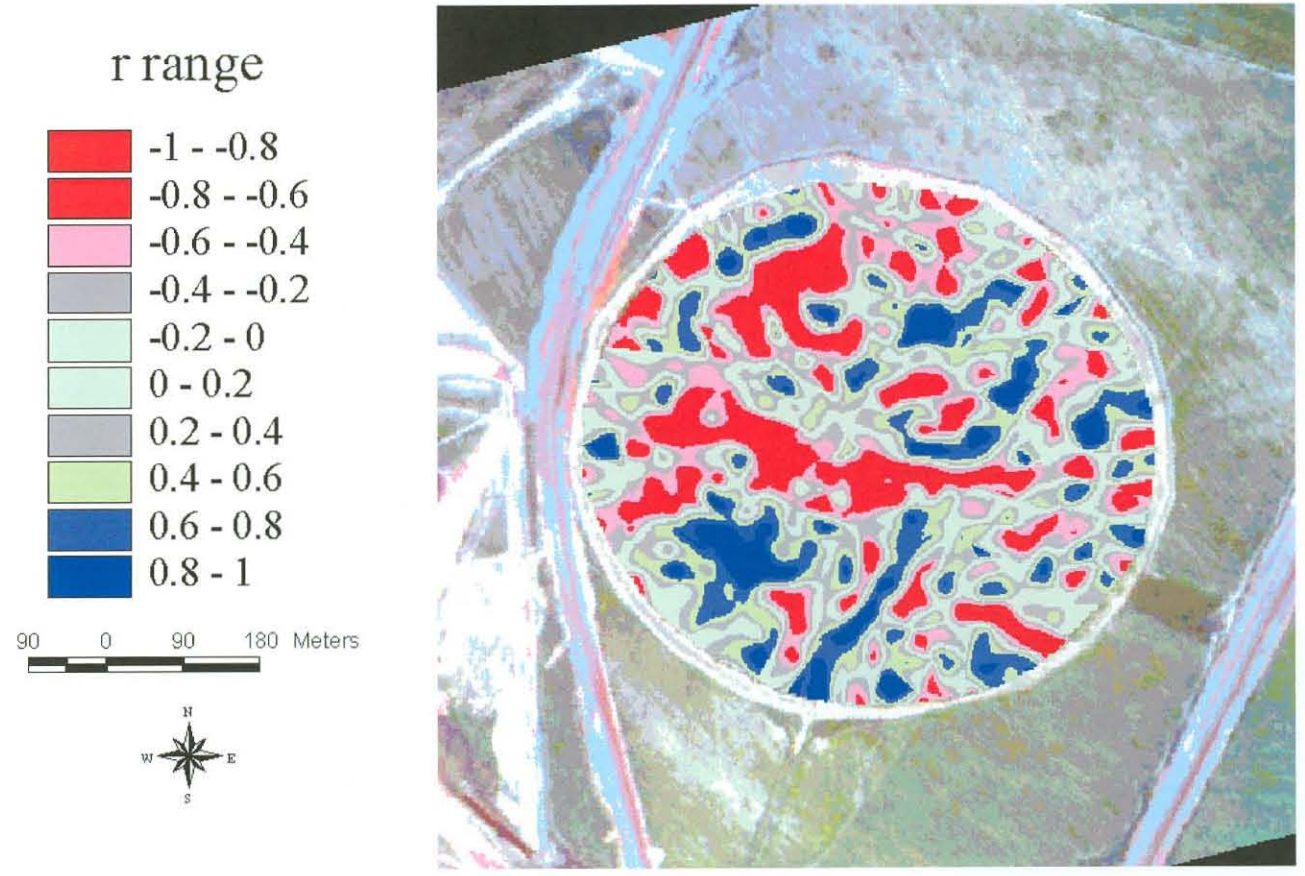

Pivot Major: Correlation map between Yield 11/99 and AWC 0-20 cm

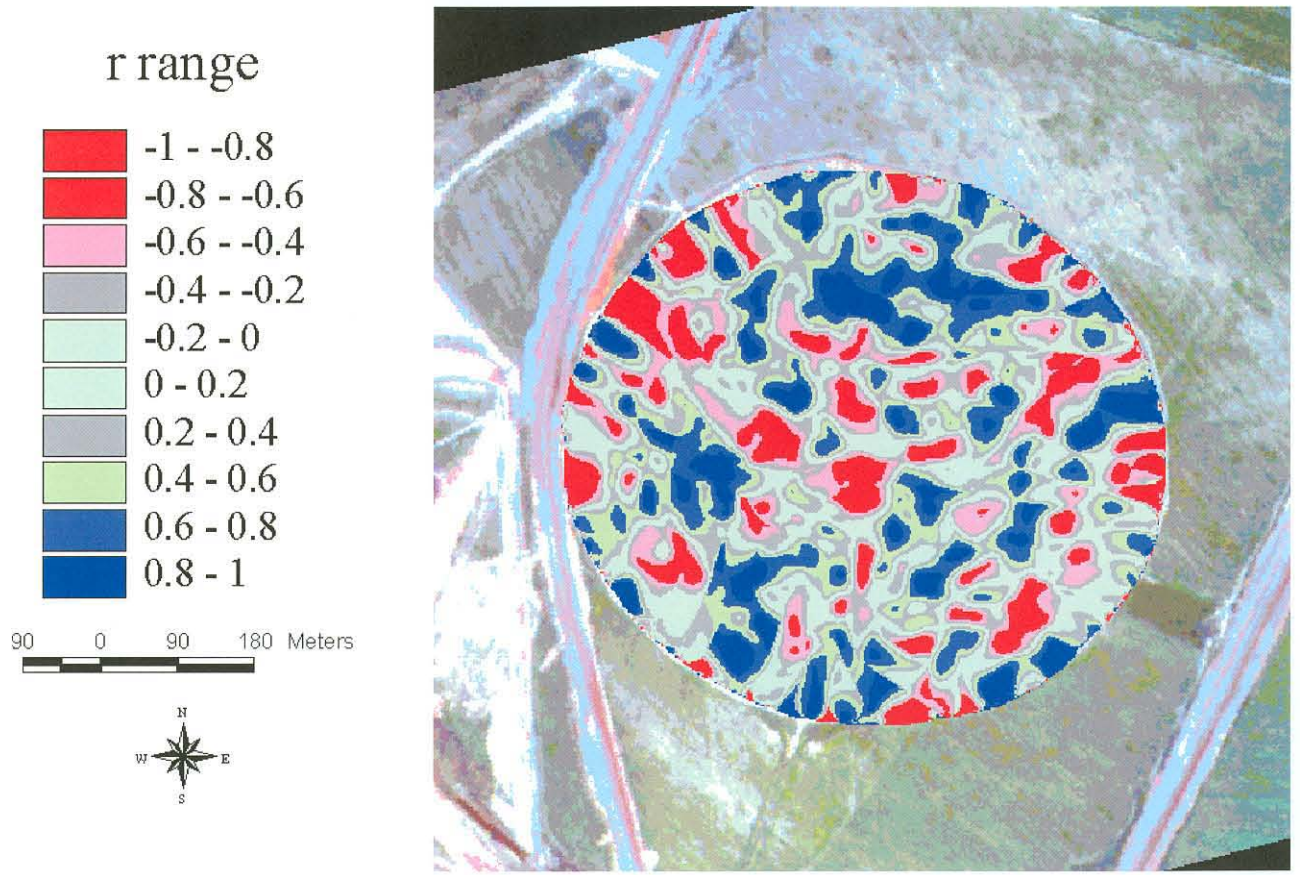

Pivot Major: Correlation map between TVI 08/99 and Yield 11/99

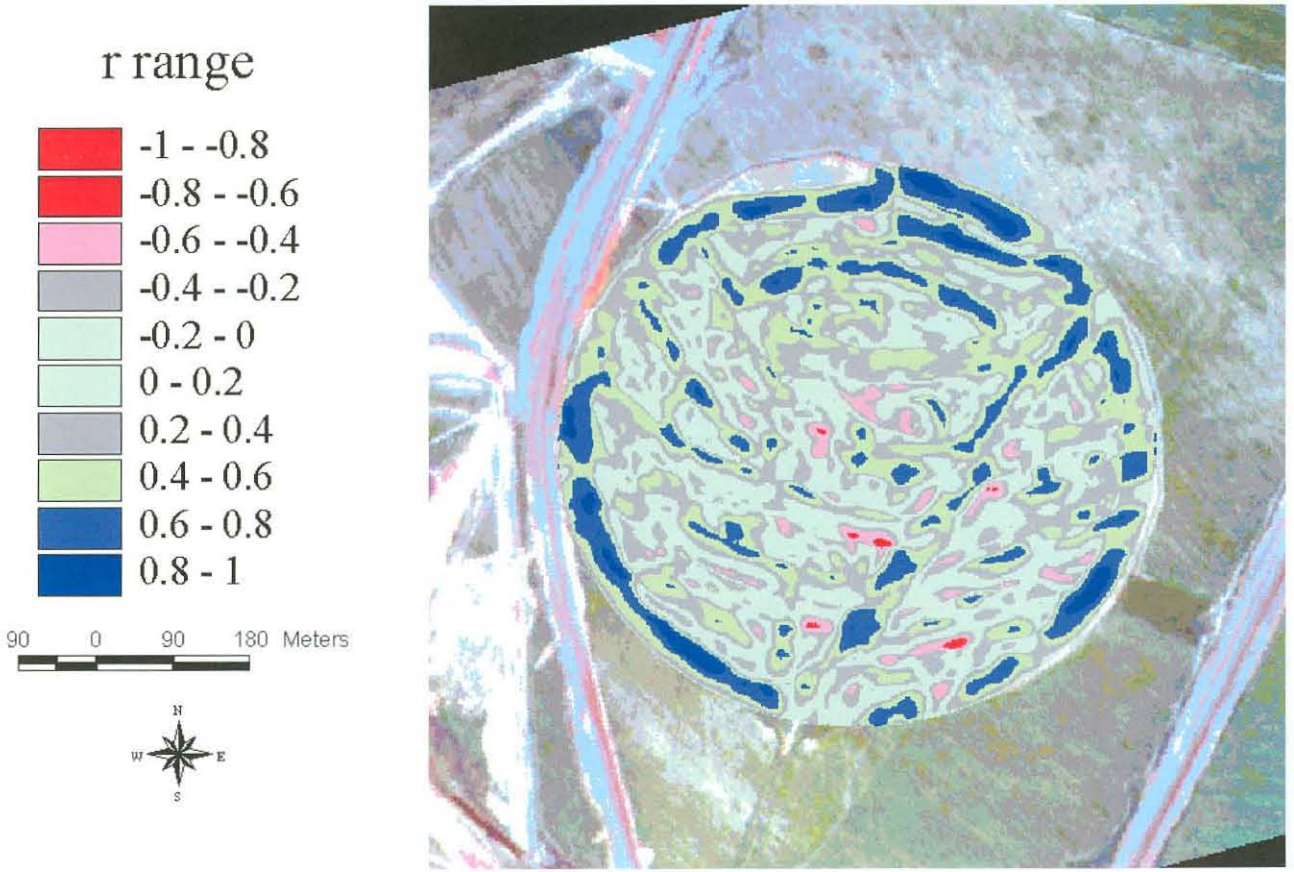

Pivot Major: Correlation map between TVI 10/99 and Yield 11/99

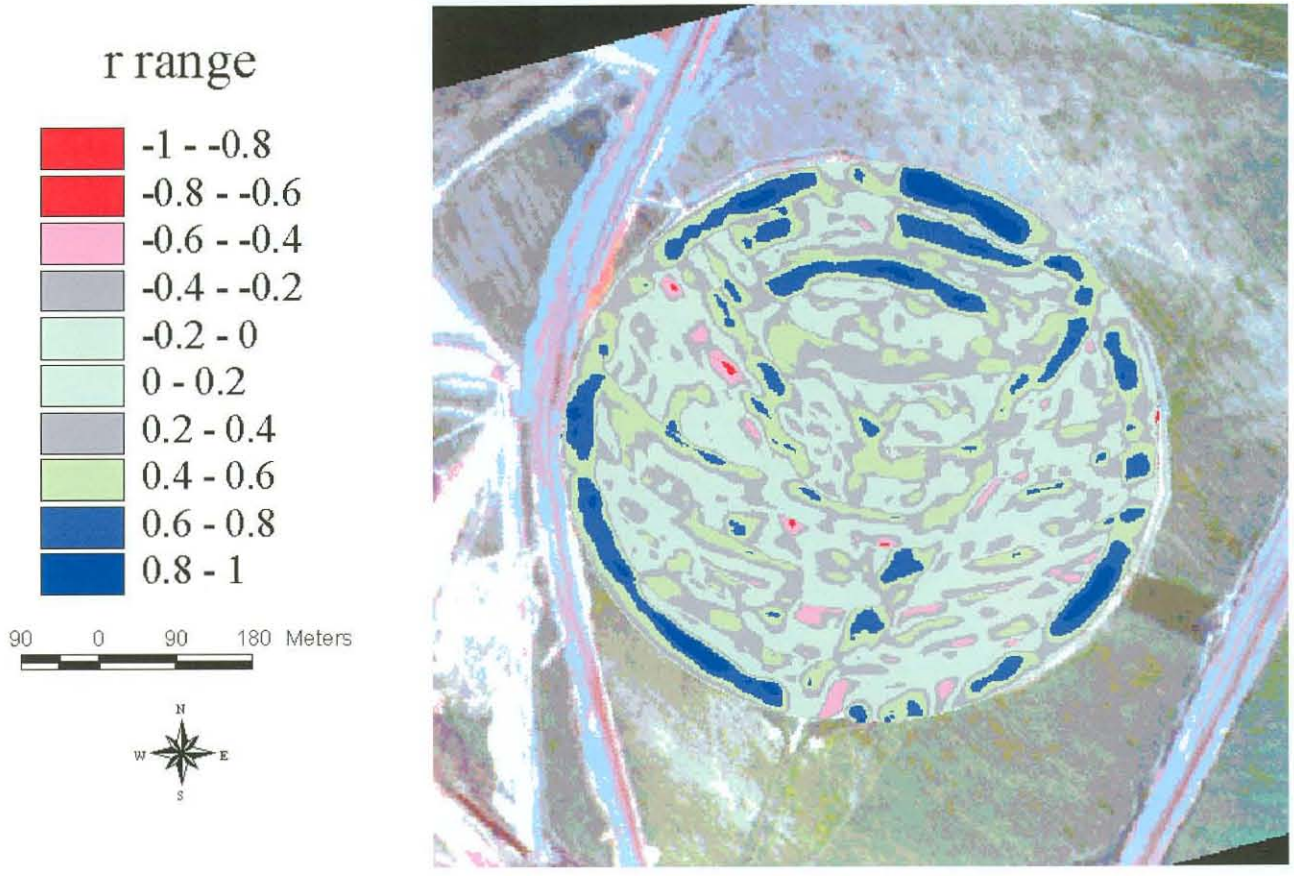

Pivot Tweefontein: Correlation map between LAI 08/99 and Ground Cover 08/99

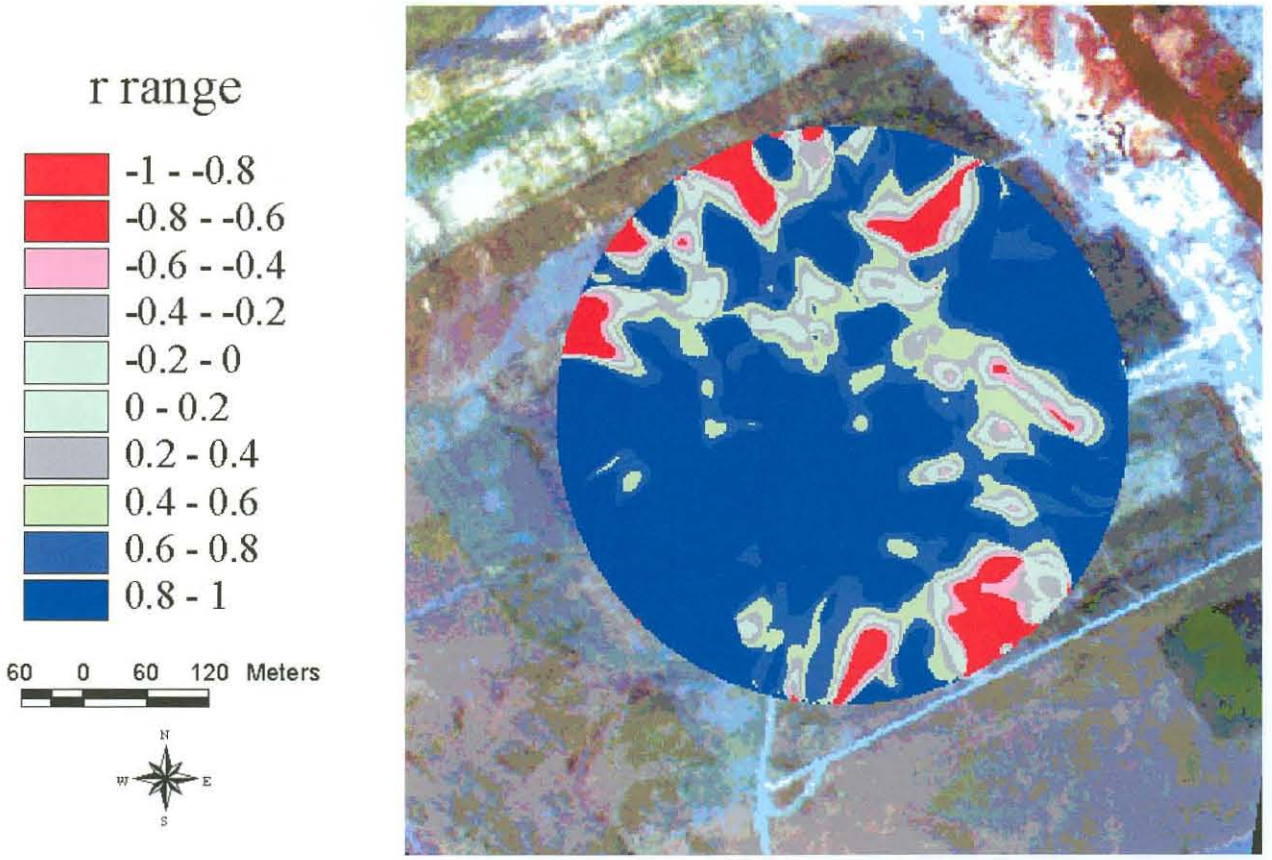

Pivot Tweefontein: Correlation map between Top Dry Matter 08/99 and Ground Cover 08/99

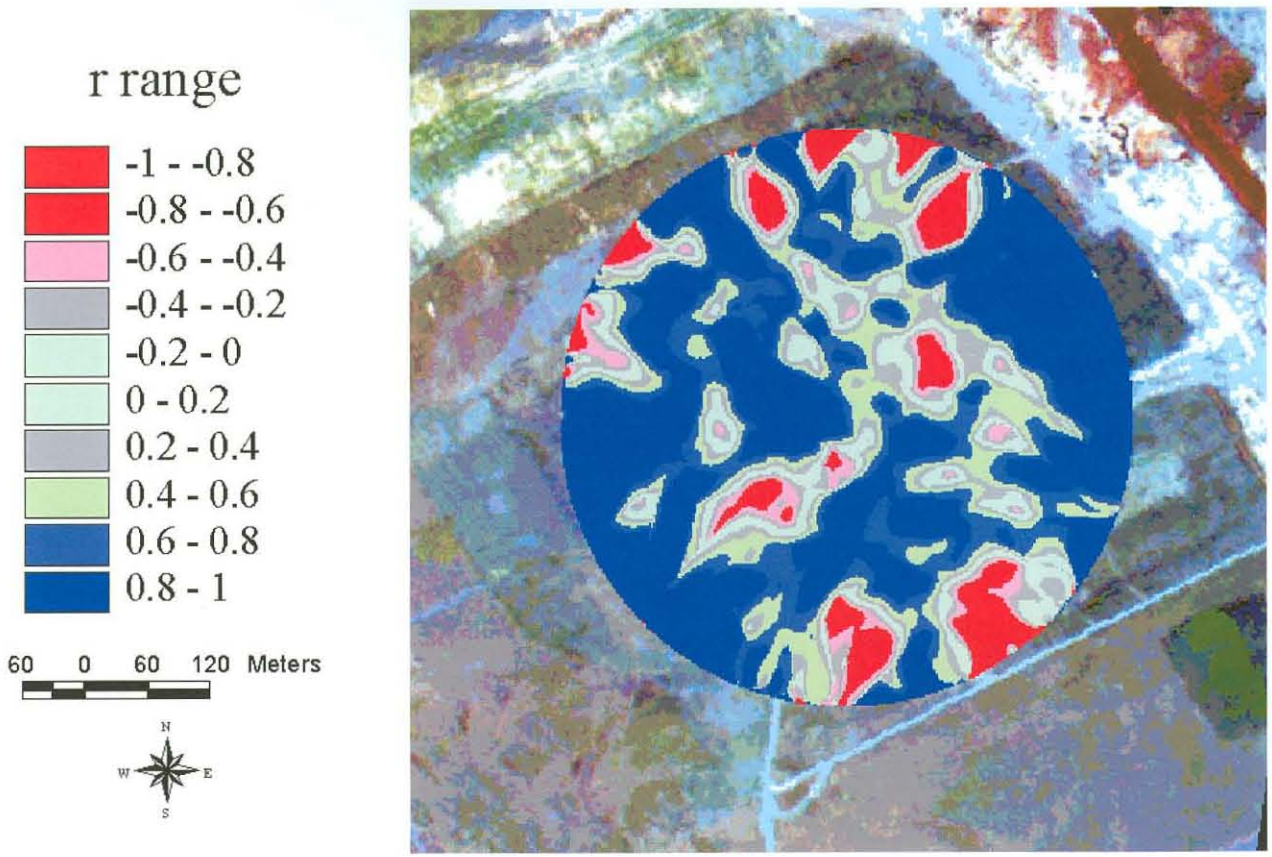

Pivot Tweefontein: Correlation map between Yield 11/99 and LAI 08/99

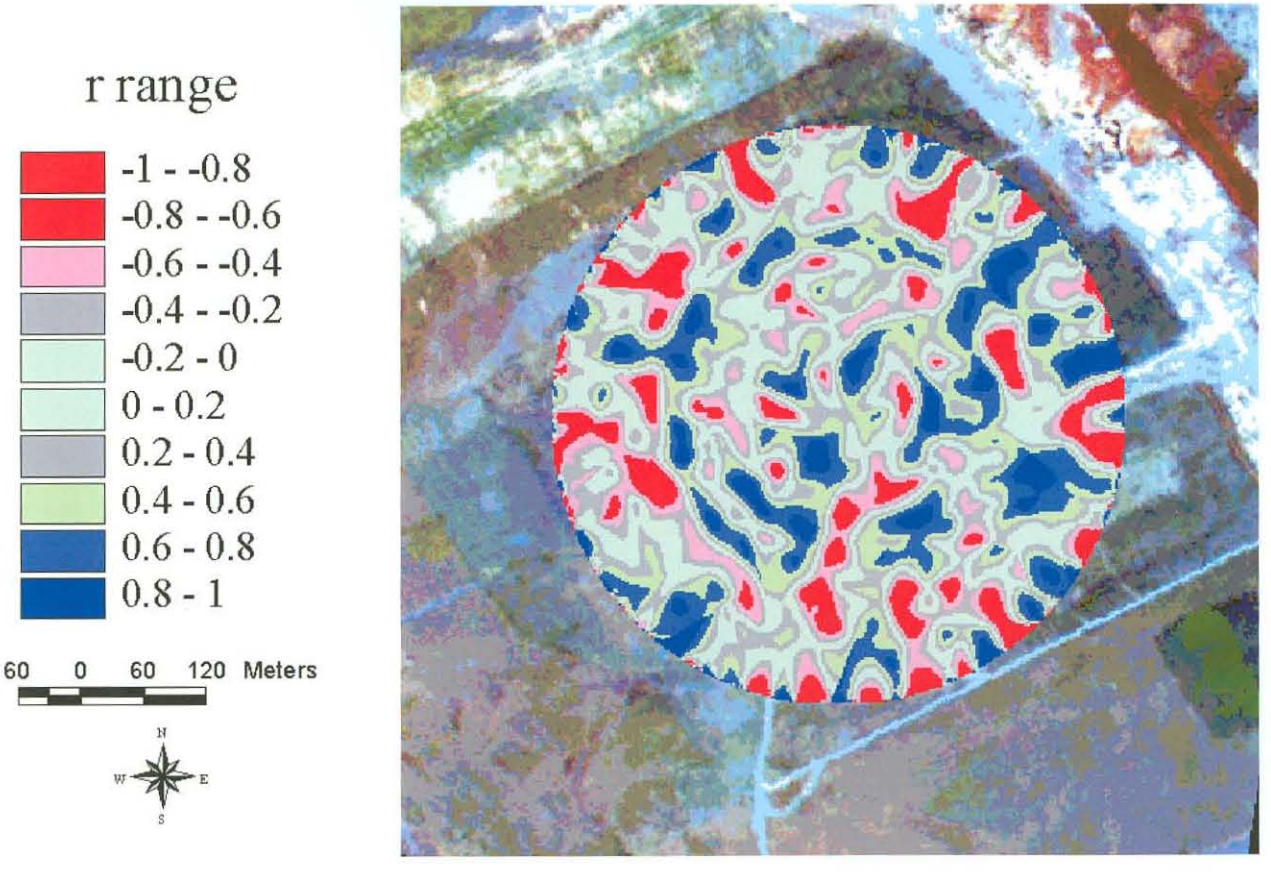

Pivot Tweefontein: Correlation map between Yield 11/99 and Top dry matter 08/99

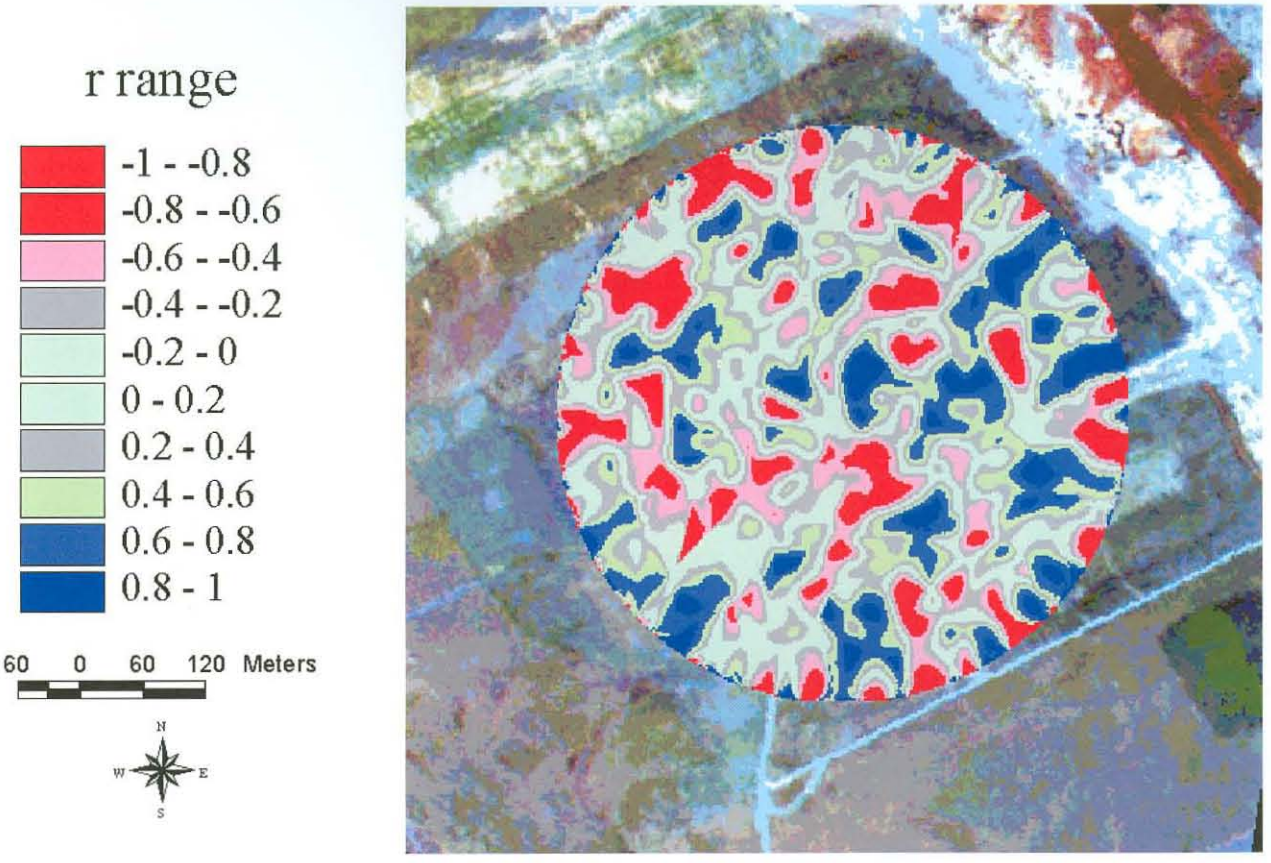

Pivot Tweefontein: Correlation map between Yield 11/99 and AWC Total

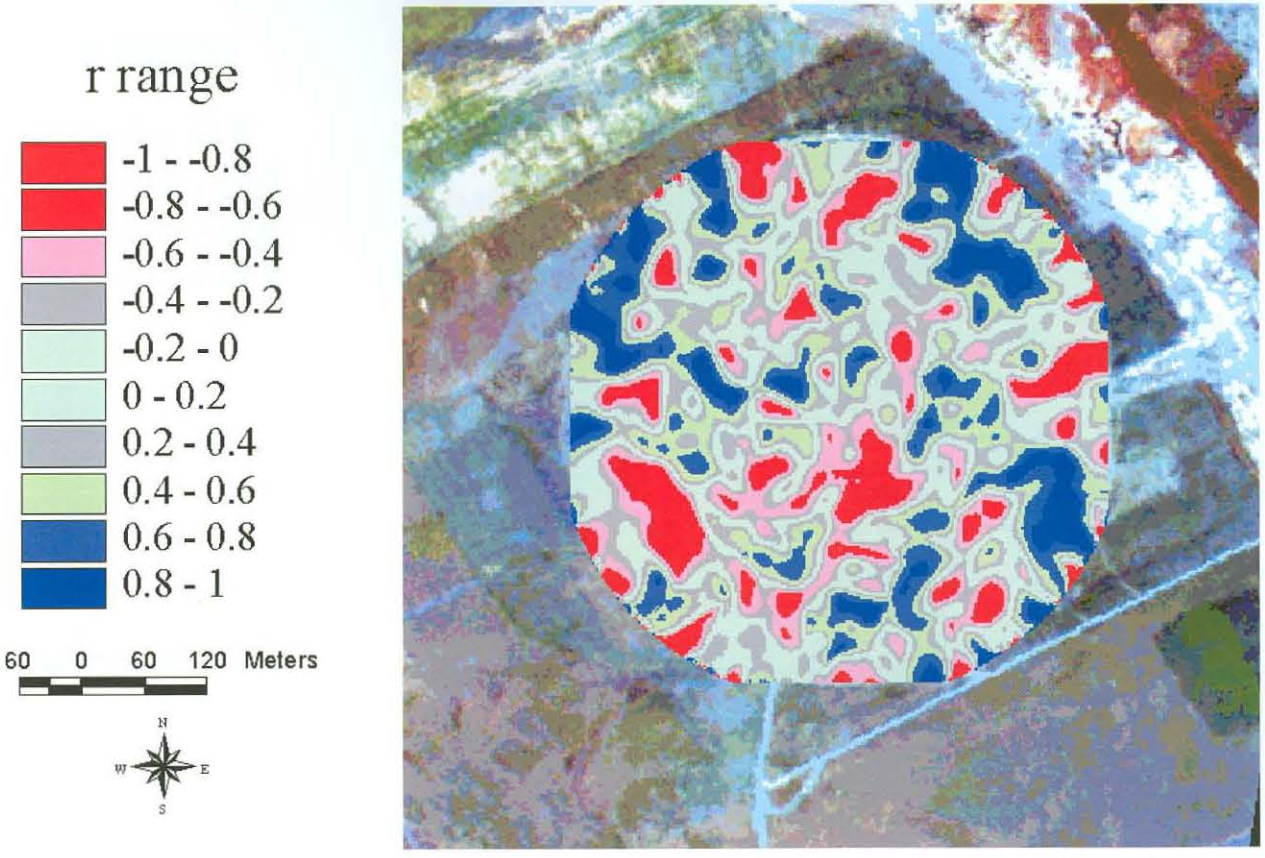

Pivot Tweefontein: Correlation map between Yield 11/99 and AWC 20- spoil/impermeable

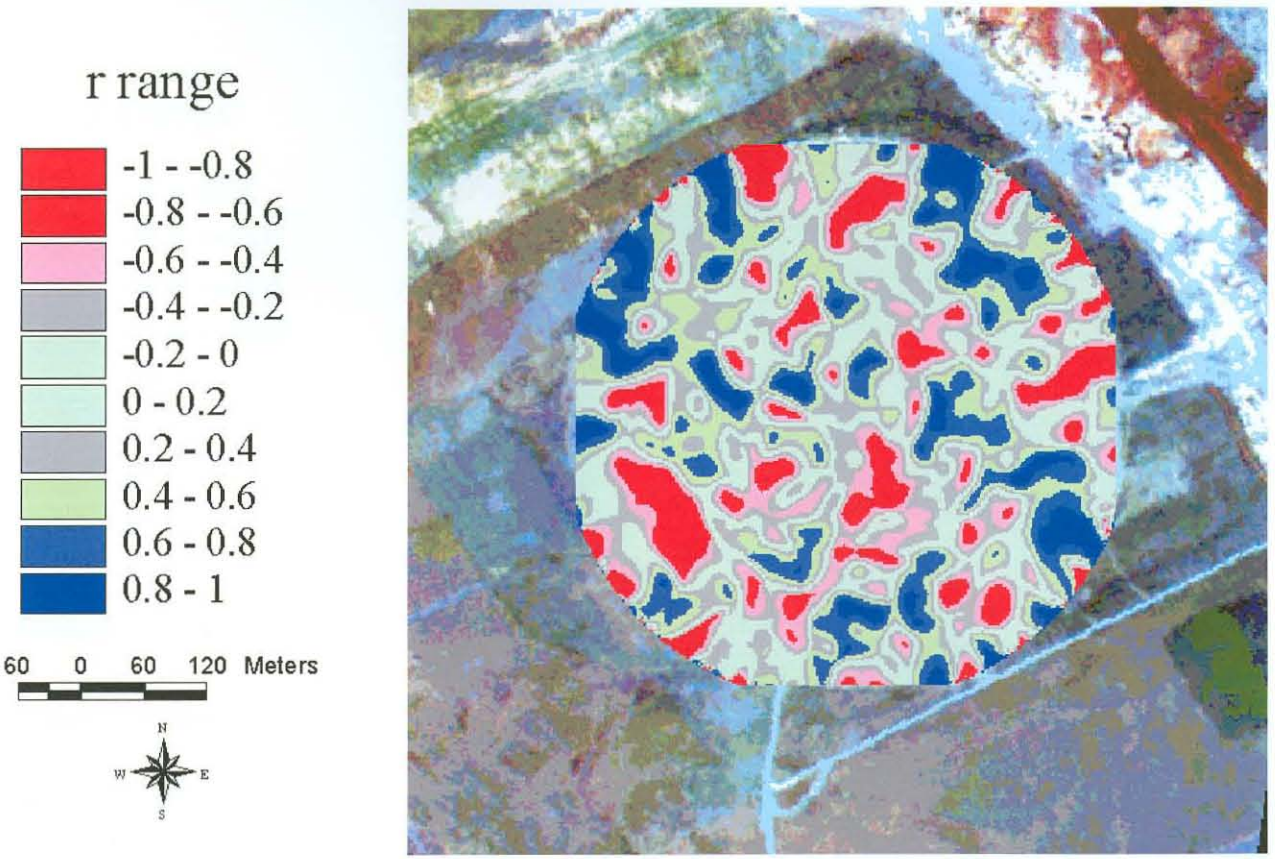

Pivot Tweefontein: Correlation map between Yield 11/99 and TVI 08/99

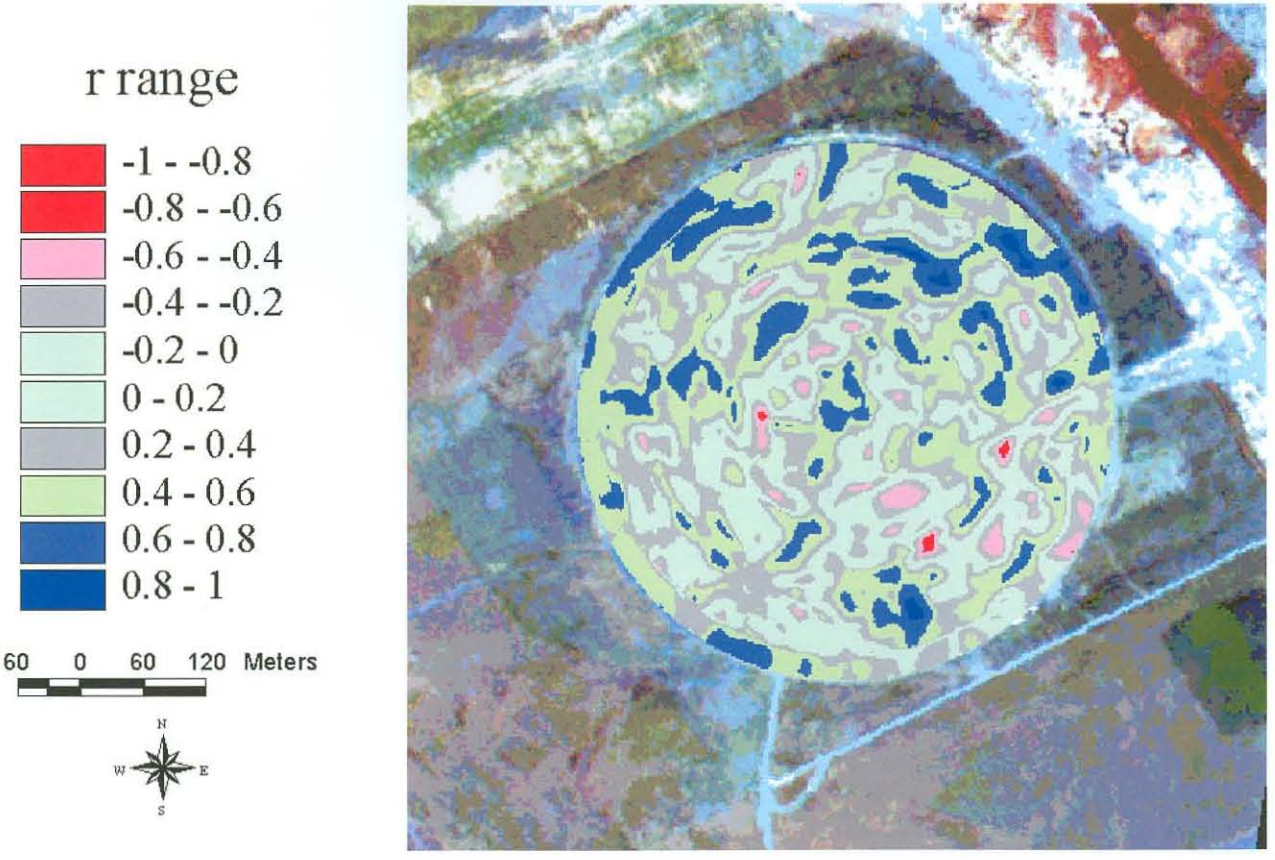

Pivot Tweefontein: Correlation map between Yield 11/99 and VI10/99

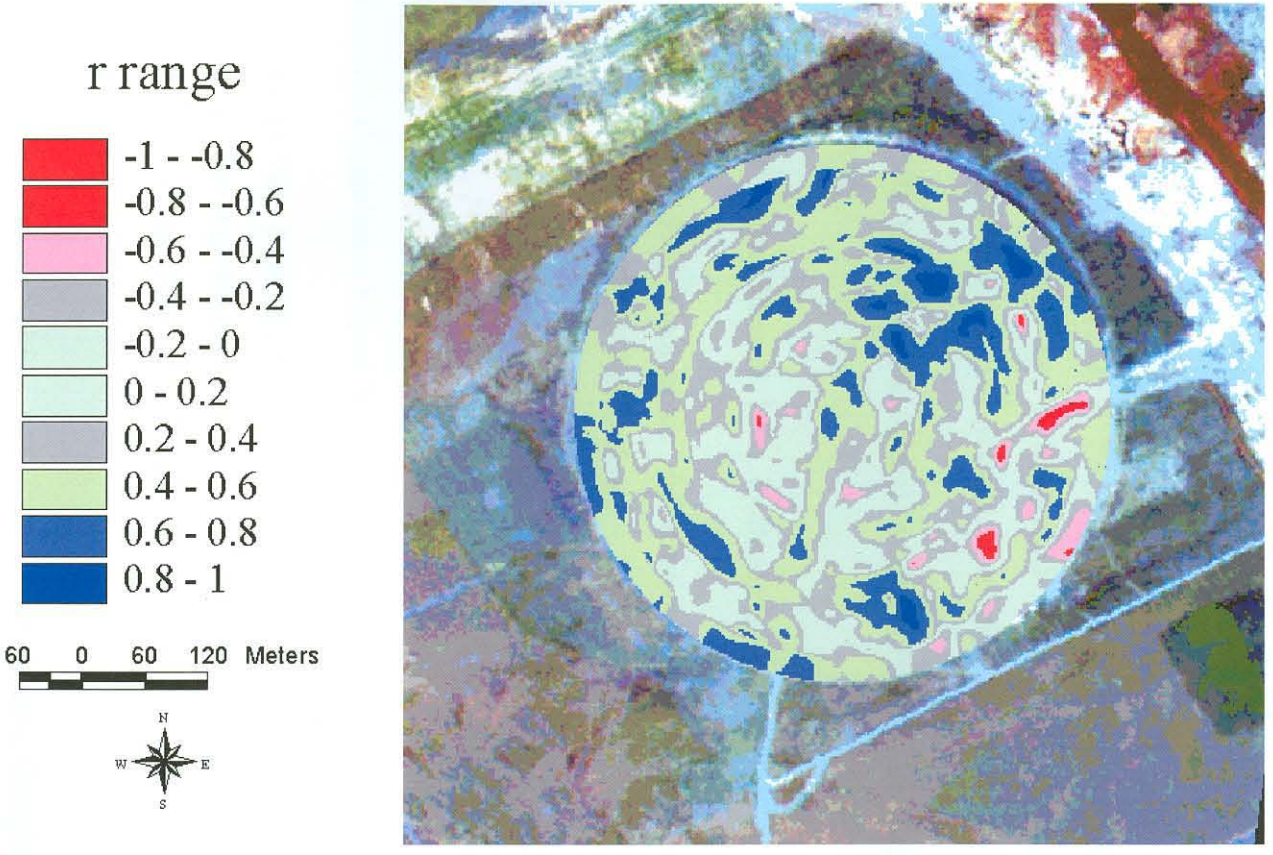

REFERENCES

ANNANDALE, J. G., BENADÉ, N., JOVANOVIC, N. Z., STEYN, J. M. & SAUTOY N., 2000. Facilitating Irrigation Scheduling By Means Of The Soil Water Balance Model. Water Research Commission Report No. K5/753, Pretoria, South Africa. In press.

ANNANDALE, J. G., JOVANOVIC, N. Z., PRETORIUS, J. J. B., LORENTZ, S. A., RETHMAN, N. F. G. & TANNER, P. D., 2000. Gypsiferous Mine Water Use In Irrigation On Rehabilitated Open Cast Mine Land. Crop Production, Soil Water And Salt Balance. Ecological Engineering.

ARABIA, G., 1993. Use Of GIS In Spatial Statistical Surveys. Int. Statist. Rev., 61, 2, pp. 339-359.

ArcView Spatial Analyst Manual. 1996. Redlands: ESRI.

ARONOFF, S., 1998. Geographic Information Systems: A Management Perspective. Ottawa: WDL Publications.

BARNARD, R. O., RETHMAN, N. F. G., ANNANDALE, J. G., MENTZ, W. & JOVANOVIC, N. Z., 1998. The Screening Of Crop, Pasture And Wetland Species For Tolerance Of Polluted Water Originating In Coal Mines. Water. Research Commission Report No. 582/1/98, Pretoria, South Africa.

DEERING, D. W., ROUSE, J. W., HAAS, R. H., & SCHELL, J. A., 1975, Measuring "For Age Production" Of Grazing Units From Landsat MSS Data; Proceedings of the 10th International Symposium on Remote Sensing of Environment, II, pp. 1169-1178.

Erdas Field Guide. Fourth Edition, 1997 ERDAS Inc, Atlanta, Georgia, U.S.A.

EVANS, R., 1990. Discrimination And Monitoring Of Soils; Applications Of Remote Sensing In Agriculture. Edited by STEVEN, M. D., CLARK, J. A. Butterworth, University Press, Cambridge, UK.

FUNG, T. LE DREW, E. (1987). Application Of Principal Components Analysis To Change Detection. *PE&RS*, 12: 1649-1658.

GIOVACCHINI, A., 1984. Crop Identification By Means Of Spectral Profiles. Proceedings of IGARSS '84 Symposium, Strasbourg 27 –30 August 1984.

GODDARD, T. W., LACHAPELLE, G., CANNON, M. E., PENNEY, D.C. & McKENZIE, R. C., 1995. The Potential Of GPS And GIS In Precision Agriculture. Proc. Dominique V: "La Route De L'Innovation". November 9-10, Montreal, P. Q., Canada

GODDARD, T., KRYZANOWSKI, L., CANNON, L., IZAURRALDE, C., MARTIN, T., 1996. Potential For Integrated GIS-Agriculture Models For Precision Farming Systems. NCGIA SANTA FE CONFERENCE, Third International Conference/Workshop on Integrating GIS and Environmental Modelling CD-ROM, January 21-25, 1996, Santa Fe, New Mexico, USA

GRIMSHAW, D., 1994. Bringing GIS Into Business. Longmans

GUYOT, G., 1990. Optical Properties Of Vegetation Canopies. Applications Of Remote Sensing In Agriculture. Edited by STEVEN, M. D., CLARK, J. A. Butterworth, University Press, Cambridge, UK.

HANEKLAUS, S., BLOEM, E. & SCHNUG, E., 1999, Precision Agriculture - New Production Technologies For An Old Crop, Proceedings of the 10th International Rapeseed Congress. Camberra Australia.

JACKSON, R. D. & HEUTE, A. R., 1991. Interpreting Vegetation Indices. Preventive Veterinary Medicine. 11:185-200.

JOVANOVIC, N. Z., ANNANDALE, J. G., TANNER, P. D. & BENADÉ, N., 1999. Modelling The Long-Term Effect Of Irrigation With Gypsiferous Water On Soil And Water Resources. Agriculture, Ecosystems and Environment 76 109-119.

JOVANOVIC, N. Z., BARNARD, R. O., RETHMAN, N. F. G. & ANNANDALE, J. G., 1998. Crops Can Be Irrigated With Lime-Treated Acid

Mine Drainage. Water SA 24(2) 113-122. MAAS EV (1986) Salt tolerance in plants. Appl. Agric. Res. 1 12-26.

LACHAPELLE, G., CANNON, M. E., GEHUE, H., GODDARD, T. & PENNEY D., 1994. GPS System Integration And Field Approaches In Precision Farming. Navigation 41(3): 323-335.

MATTER, P. M., 1990. Theoretical Problems In Image Classification. Applications Of Remote Sensing And Geographical Information Systems In Water Management. Applications Of Remote Sensing In Agriculture. Edited by STEVEN, M. D., CLARK, J. A. Butterworth, University Press, Cambridge, UK.

MORGAN, M., Ess, D., The Precision Farming Guide For Agriculturists. ISBN: 0-86691-245-2.

MOODY, A. Remote Sensing Of The Environment, Remote Sensing Resolutions. Department Of Geography, University Of North Carolina http://www.unc.edu/~aaronm/RSCC/

NIEUWENHUIS, G. J. A., MILTENBURG J. W. & THUNNISSEN, H. A. M., 1990. Applications Of Remote Sensing And Geographical Information Systems In Water Management. Applications Of Remote Sensing In Agriculture. Edited by STEVEN M. D., CLARK, J. A. Butterworth, University Press, Cambridge, UK.

PENNOCK, D. J., ZEBARTH, B. J. & De JONG E., 1987. Landform Classification And Soil Distribution In Hummocky Terrain. Saskatoon, Canada. Geoderma 40: 297-315.

PINTER Jr., P. J., ZIPOLI, G., MARACCHI, G., & REGINATO, R. J. 1987. Influence Of Topography And Sensor View Angles On NIR/Red Ratio And Greenness Vegetation Indices Of Wheat. *Int. J. Remote Sensing* 8(6): 953-957.

PRICE, J. C., 1994. How Unique Are Spectral Signatures. Remote Sensing of Environment; 49:181-186.

ROUSE, J. W., HAAS, R. H., SCHELL, J. A., DEERING, D. W., & HARLAN, J. C., 1974. Monitoring The Vernal Advancements And Retro-radiation (Greenwave Effect) Of Nature Vegetation NASA/GSFC Final Report, NASA, Greenbelt, MD, 371 pp.

SABINS, F. Jr, 1978. Remote Sensing Principles And Interpretation, W. H. Freeman and Company, San Francisco.

STARR, J. & ESTES, J. 1990. Geographic Information Systems: An Introduction. New Jersey: Prentice-Hall.

STEVEN, M. D., MALTHUS, T. J., DEMETRIADES-SHAH, T. H., DANSON, F. M. & CLARK, J. A., 1990. High Spectral Resolution Indices For Crop Stress. Applications Of Remote Sensing In Agriculture. Edited by STEVEN, M. D., CLARK, J. A. Butterworth, University Press, Cambridge, UK.

WARDLEY, N. W, MILTON, E. J., Hill C. T., 1987. Remote Sensing Of Structurally Complex Semi-Natural Vegetation. An Example From Heathland. Dep. Of Geog., Univ. Of Southampton, Southampton SO9 5NH, UK. International-Journal-of-Remote Sensing. 8: 1, 31-42; 7 fig.; 25 ref.

WATSON, D. F. & PHILIP, G. M., 1985. A Refinement Of Inverse Distance Weighted Interpolation. Geo-Processing, 2: pp 315-327.

WIEGAND, L., RHODES, J. D., ESCOBAR, D. E. & EVIRITT, J. H., 1994. Photographic And Videographic Observations For Determining And Mapping The Response Of Cotton To Soil Salinity. Remote Sensing of Environment; 49:212-223.

WIENGAND, L., RICHARDSON, A. J., ESCOBAR, D. E. & GERBERMANN, A. H., 1991. Vegetation Indices In Crop Assessment. Remote Sensing of Environment; 35:105-119.